# Multi-scale collapse of coral cover under climate change

Anna K. Cresswell[1,2,*], Vanessa Haller-Bull[3], Manuel Gonzalez-Rivero[3], James P. Gilmour[1,2], Yves-Marie Bozec[4], Arne Adam[4], Mariana Alvarez-Noriega[3], Ken Anthony[3,5], Chinenye J. Ani[3,6], Molly-Mae Baker[7,2,1], Diego R. Barneche[1,2], Deborah Burn[3], Carolina Castro-Sanguino[1], Kerryn Crossman[3], Christopher Doropoulos[8], Katharina Fabricius[3], Renata Ferrari[3], Sophie Gordon[3], Marine Lechene[3], Justin Moore[3], Peter Mumby[4], Sam Noonan[3], Pascal Omondiagbe[3], Marji Puotinen[1], Barbara J. Robson[3,6], Roberto Salguero-Gomez[9], Maren Toor[3], Juan Carlos Ortiz[3]

[1] Australian Institute of Marine Science, Perth, WA, Australia, 6009
[2] Oceans Institute, University of Western Australia, Perth, WA, Australia, 6009
[3] Australian Institute of Marine Science, Townsville, QLD, Australia, 4810
[4] School of The Environment, The University of Queensland, Brisbane, QLD, Australia, 4072
[5] Nature Assets Consulting, Brisbane, QLD, Australia, 4000
[6] AIMS@JCU, College of Science and Engineering, James Cook University, Townsville, QLD, Australia, 4811
[7] School of Biological Sciences, University of Western Australia, Perth, WA, Australia, 6009
[8] CSIRO Environment, St. Lucia, QLD, Australia, 4067
[9] Department of Biology, University of Oxford, Wellington Square, Oxford, UK, OX1 2JD

[*] Corresponding author: annacresswell@gmail.com, ORCID: 0000-0001-6740-9052

# 1 ABSTRACT

Projecting ecosystem trajectories under future climates is critical for conservation planning, yet remains constrained by uncertainty arising from limited data, ecological complexity, and biological and environmental variability. Variability, when disentangled from uncertainty, offers critical insights into population and community dynamics. For example, enhanced vital rates (growth, survival, fecundity) can enable faster population recovery, while environmental variability provides spatial refuges and ecological niches. Here, we integrated vital rate data from ~10,000 coral colonies across environmental gradients on the Great Barrier Reef (GBR) into a metacommunity model to project coral trajectories to 2100. Variability in coral-cover trajectories was explored as a function of (i) vital rates, (ii) spatial scales (from within-reefs to across regions), and (iii) future climate scenarios (represented by three Shared Socioeconomic Pathways, SSPs, informed by an ensemble of downscaled Global Climate Models, GCMs). Climate scenarios explained the greatest variance in coral-cover trajectories, with all spatial scales (across sites, reefs and regions) contributing substantial additional variance. Coral cover declined over the century under all emissions scenarios except SSP1-2.6 (warming <2°C), despite modelling increasing population thermal tolerance through natural selection. This decline was accompanied by a drastic loss of variability in coral-cover trajectories across all spatial scales, signalling reduced scope for natural adaptation, traditional management and restoration. By the end of the century, variability across GCMs also declined, leading to higher certainty about long-term reef state, i.e. coral collapse, than certainty about the near-term, should global emissions follow moderate-to-high pathways.

**Keywords:** Bayesian, coral reef, demography, ecological modelling, mechanistic modelling, metapopulation, metacommunity

# 2 INTRODUCTION

The field of ecology is increasingly asked to forecast the consequences of climate change [1–3]. Major challenges lie in projecting outside of the envelope of historical variation and

empirical observations, alongside the complexity of processes governing individuals, populations and metacommunities across spatial scales [3]. Integrative frameworks that incorporate empirical data into mechanistic process-based models are needed [4–7]. With mechanistic modelling, predictions can be understood in relation to the underlying processes that generated them [8].

Uncertainty, arising from many sources, including data limitations, incomplete understanding and simplification of complex ecological processes, is inherent in ecological forecasting [2]. Distinct from this uncertainty is variability that may be disentangled and explained by environmental gradients or biological attributes [9]. For example, linking biophysical variability across spatial [10,11] and temporal [12,13] scales to demographic variability (and uncertainty) [14,15] provides insight into expected community dynamics under future environmental conditions and management scenarios. Furthermore, differences in vital rates and genetic variation afford some individuals an advantage over others in a population [16–18], while environmental variability creates spatial refuges [19,20] that help sustain ecosystems [21].

Modelling of coral reef futures [22–25] project dramatic losses of coral cover if greenhouse gas emissions are not curbed. Such projections have been essential for illustrating the consequences of warming oceans and exploring how management or active intervention may shift the outlook for corals [26–28]. However, the complex demography underlying the dynamics of complex ecosystems remain difficult to resolve. The resilience of coral reefs depends on the growth, survival and fecundity (vital rates) of individual corals, dispersal of larvae across the wider metacommunity, and local exposure to disturbance regimes. Empirical ecological data have been limited in their capacity to capture this complexity, particularly regarding coral vital rates that depend on coral size, morphology, taxa and environmental conditions [18,29,30]. Recent technological advances—including photogrammetry [31] for quantifying vital rates [32–34], satellite-based mapping [35,36], fine-scale connectivity modelling [37,38] and downscaled global climate models [39]—have increased the resolution at which is it possible to project reef futures.

Here we integrated the largest empirical datasets on coral demography for the Great Barrier Reef [40,41] into a spatially-explicit metacommunity modelling framework, *C~scape*. Navigating the trade-offs between model generality, realism and precision [42], *C~scape* was developed to occupy a middle ground—prioritising a mechanistic representation of the coral

life cycle and the ecological processes governing disturbance dynamics to generate numerical projections of coral trajectories under different scenarios. We developed an approach to propagate colony-level vital rates (and their uncertainty) through to the population-, community- and metacommunity[43] level, projecting coral-cover trajectories across local to regional scales to the year 2100 under climate change. This included capacity for coral populations to adapt to increasing heat stress through selection of heat tolerance. We characterised and attributed variability in projected coral-cover trajectories to three sources -- (i) vital rates, (ii) spatial context (site, reef and geographic region), and (iii) future climate scenarios -- disentangling these from residual uncertainty. We illustrate the potential influence of (i) to (iii) with a simplified 'representative reef', before conducting four case studies for reefs in the offshore northern, central, and southern regions of the Great Barrier Reef. We applied ten downscaled global climate models across three greenhouse gas emissions scenarios (Shared Socioeconomic Pathways, SSPs) and used variance partitioning to investigate temporal changes in the factors underlying variability in coral-cover trajectories.

# 3 RESULTS

We developed a workflow (Figure 1) to scale information from empirical observations of vital rates at the colony level observed across environmental gradients, into site-specific trajectories of coral metacommunity dynamics across reefscapes. The *C~scape* metapopulation modelling framework presented by Cresswell et al. (2024) was further developed to incorporate demographic variability (differences in vital rates across environmental gradients) and uncertainty in estimated vital rates. Bayesian regressions of coral growth and survival data for distinct coral types as a function of colony size (planar area), local environmental conditions including wave exposure and seabed 'waterflow intensity' (root mean squared horizontal velocity amplitude [45], Table S2), and regional context. Integral Projection Models (IPMs) were then used to synthesise this information with fecundity and recruitment and acted as the engine to project annual changes in coral metacommunities in the *C~scape* framework. Acute disturbances —thermal stress, cyclones, and *Acanthaster* (COTS) outbreaks— can impact the coral populations in any given year, killing a proportion of colonies according to empirically derived disturbance-mortality functions [44]. Cross-generational heritability of thermal tolerance allowed some adaptation to increasingly frequent and intense thermal stress events under climate change (Fig. S30, S31).

In the present study we have focussed on projections of total coral cover (the most common metric used in reporting coral reef state) by converting the size frequency distribution of simulated corals to cover and summing across functional types. Future work should focus on the projections of size structure, community composition and functional diversity.

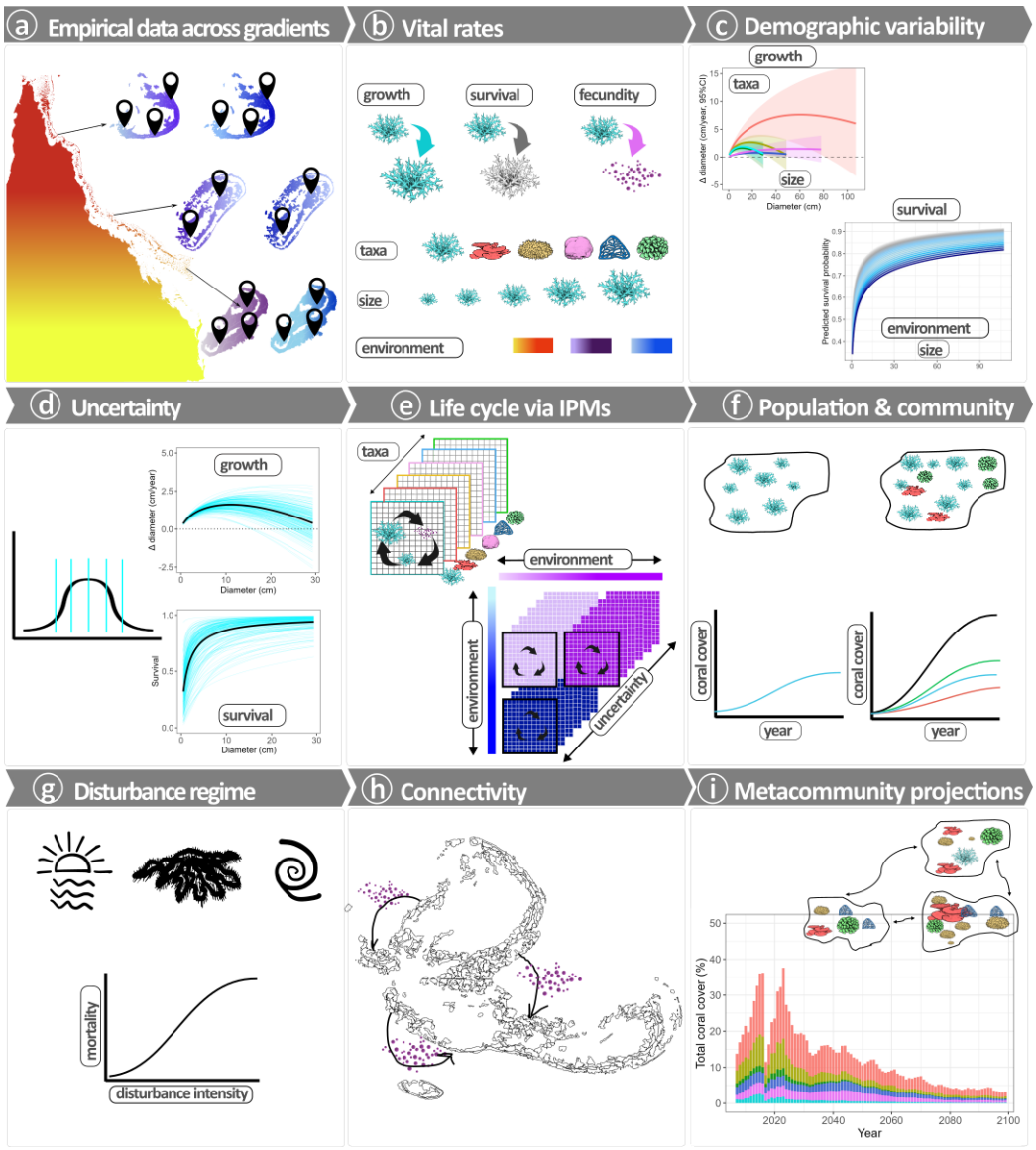


*Figure 1.* ***Schematised framework for scaling demography across spatial hierarchies into spatially explicit metacommunity projections under climate change****. The workflow involves (a) collecting or collating empirical data across environmental gradients both within and among reefs for multiple types of coral (here, six, see Table S1); (b) analysing this empirical data across coral size, taxa and environmental or spatial covariates. (c) statistical regression models predict growth and survival and (d) a Bayesian framework tracks uncertainty in estimated vital rates. (e) Predictions are integrated with information on early life history to build site-specific integral projection models through which uncertainty in estimated vital rates can be propagated to population change. (f) Coral population and community growth are projected accounting for finite coral habitat and competition for space as a resource. (g) Disturbance-mortality functions are used to simulate site-specific disturbance regimes, (h) fine-scale hydrodynamic and particle tracking modelling allows simulation of larvae dispersal and links populations to metapopulations. (i) metacommunity trajectories are projected under different disturbance scenarios or climate futures.*

## 3.1 Demographic variability and uncertainty in estimated vital rates

We identified six coral types with sufficient vital rate data to build IPMs describing growth and survival across environmental and spatial gradients: tabular *Acropora*, corymbose/digitate *Acropora*, spawning *Pocillopora*, brooding Pocilloporidae, *Goniastrea*/*Platygyra*, and massive *Porites*. Vital rates were estimated from 9,621 colonies tracked over an approximate annual periods between 2021 and 2022 across three GBR regions (north, central and south, Fig. S4). We investigated 'demographic variability', that is, differences in growth and survival across coral size, taxa, and environment (Figure 2b,c, Fig. S15), as well as the 'uncertainty in estimated vital rates' via Bayesian posterior sampling (Figure 2d, Fig. S18). Additional results and interpretation are provided in Appendix 3.

Clear differences in vital rates were evident across taxa, with initial colony size (planar area) being the primary predictor of growth and survival rates (Figure 2b, S15). The influence of depth, waterflow, and region on growth was minor compared to size, but these covariates showed taxa-dependent influences on growth and/or survival, Figure 2c, Fig. S15, S16, S17). For example, growth declined with depth for tabular *Acropora*, *Goniastrea/Platygyra*, and massive *Porites* (80% HPDI excludes zero, Fig. S15). Brooding Pocilloporidae had lower survival at greater depth (80% HPDI, Fig. S15). Demographic trade-offs were evident in some cases where depth and/or wave exposure had contrasting effects on growth and survival. Tabular *Acropora*, for instance, grew faster but had lower survival at sites with high waterflow intensity. In contrast, both growth and survival declined with depth in this group (Fig. S15). With the Bayesian framework we addressed the uncertainty in estimated vital rates across posterior draws (Figure 2d, Fig. S18).

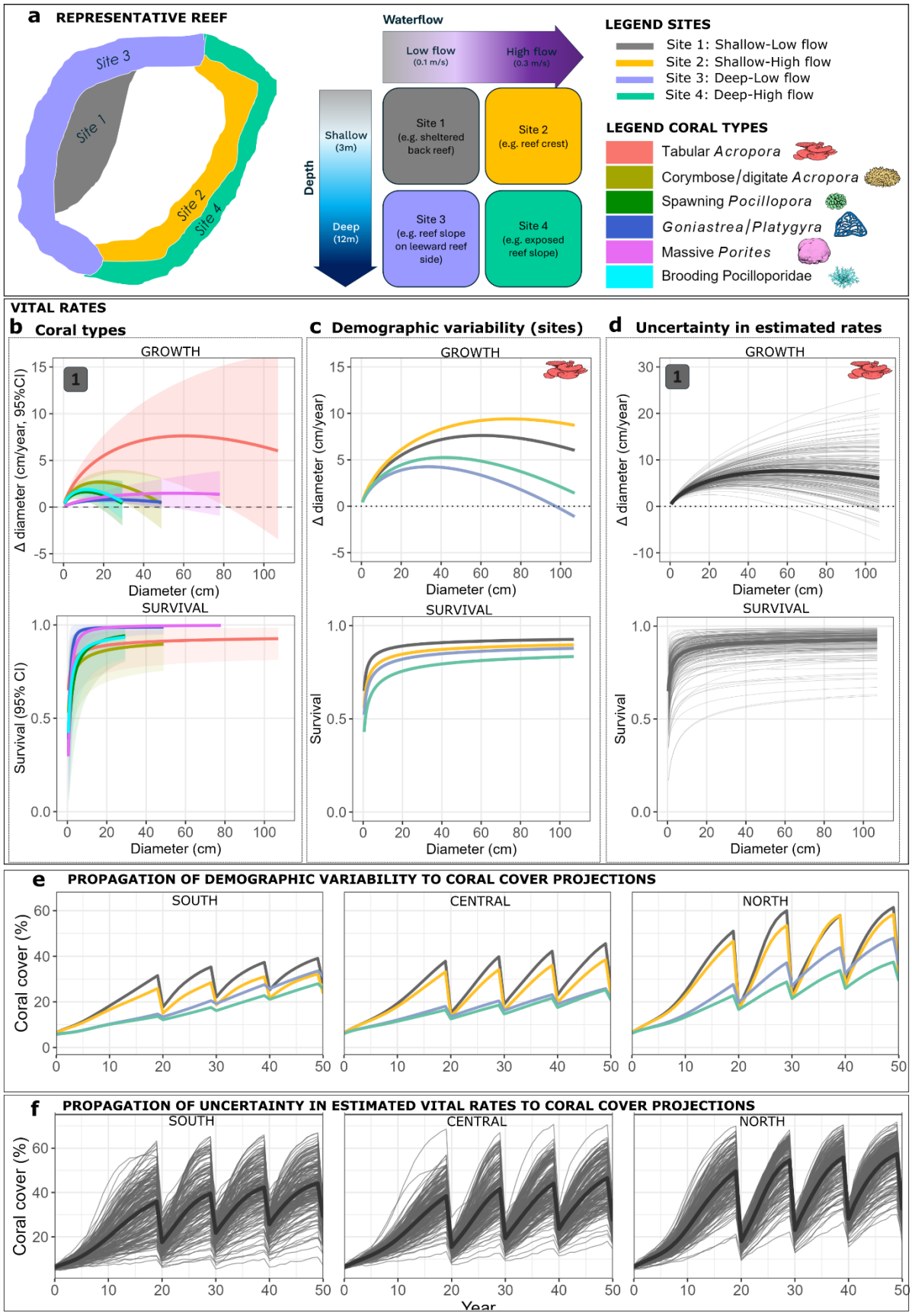
a REPRESENTATIVE REEF
Site 3
Site 1
Site 2
Site 4
Waterflow
Low flow (0.1 m/s)
High flow (0.3 m/s)
Depth
Shallow (3m)
Deep (12m)
Site 1 (e.g. sheltered back reef)
Site 2 (e.g. reef crest)
Site 3 (e.g. reef slope on leeward reef side)
Site 4 (e.g. exposed reef slope)
LEGEND SITES
Site 1: Shallow-Low flow
Site 2: Shallow-High flow
Site 3: Deep-Low flow
Site 4: Deep-High flow
LEGEND CORAL TYPES
Tabular Acropora
Corymbose/digitate Acropora
Spawning Pocillopora
Goniastrea/Platygyra
Massive Porites
Brooding Pocilloporidae
VITAL RATES
b Coral types
c Demographic variability (sites)
d Uncertainty in estimated rates
GROWTH
SURVIVAL
Δ diameter (cm/year, 95%CI)
Δ diameter (cm/year)
Survival (95% CI)
Survival
Diameter (cm)
e PROPAGATION OF DEMOGRAPHIC VARIABILITY TO CORAL COVER PROJECTIONS
SOUTH
CENTRAL
NORTH
Coral cover (%)
f PROPAGATION OF UNCERTAINTY IN ESTIMATED VITAL RATES TO CORAL COVER PROJECTIONS
Year

*Figure 2.* ***Representative reefs demonstration of vital rate propagation through coral-cover projections*** *(a) Schematic of the 'representative reefs', where four sites were characterised by contrasting depths and waterflow intensities (see Table S3). (b-d) Vital rates of growth (top row) and survival (bottom row) regression predictions marginalised across Great Barrier Reef (GBR) regions. These are plotted as a function of diameter (for ease of interpretation) but were modelled as ln(colony area). Predictions are show for (b) each coral type for site 1 'shallow-low flow', (c) tabular Acropora for each of the four sites, and (c) tabular Acropora for site 1, including 200 posterior draws. (e–f) show C~scape model trajectories over a 50-year period, for the case when the representative reef was simulated for the southern, central, and northern GBR regions (columns) under an artificial disturbance regime (see Table S3). (e) Coral-cover trajectories for the four sites informed by the median of 8000 posterior draws (i.e. excluding uncertainty in estimated vital rates). (f) Coral-cover trajectories for site 1 only (grey line in e), where each of 200 narrow lines is a separate simulation in C~scape, where each sampled an individual posterior draw from the Bayesian regressions for growth and survival.*

## 3.2 Propagating vital rates to coral-cover trajectories across local and regional scales: representative reefs

Integrating these taxa-, size- and environment-dependent vital rates into the *C~scape* framework allowed synthesis of the interacting factors that influence coral-cover trajectories. In these artificial scenarios, the goal was to isolate the effects of demographic variability (size-, taxa-, or environment-driven differences) and uncertainty in estimated vital rates on coral-cover projections. Therefore, other parameters were kept constant, i.e., coral habitat z

Projections of coral-cover trajectories over a 50-year period for the representative reef simulated in each of the north, central and southern regions of the GBR with intermittent acute thermal stress events (Table S3) showed emergent differences in the coral-cover trajectories.

The trajectories of coral cover differed with region and sites (columns and coloured lines, Figure 4e). The fastest increases in coral cover were predicted in the north GBR scenario, followed by the central and south regions. In the initial undisturbed decades, coral cover after 20 years in the shallow sites of the northern region reached ~50%, while in the south it reached ~30% (Figure 2e). Deep sites exhibited slower rates of increasing coral cover than shallow sites but were returned to similar coral cover by the disturbances. The deep sites registered less disturbance impact, likely reflecting a combination of differing community composition and coral-type susceptibility, and their depth affording some mitigation of temperature stress (as governed by the bleaching mortality function, Fig. S29).

By running replicate scenarios (200 times), each time sampling an individual posterior draw from each of the growth and survival regressions, we propagated uncertainty through the coral-cover projections. Figure 2f shows the resulting trajectories, while Figure 2e used the

198 median vital rates. Substantial uncertainty in coral cover emerged, even within individual
199 sites, and increased with time since disturbance for all regions and sites (Figure 2e).

200

201 ### 3.3 Coral-cover trajectories across local and regional scales: GBR case studies

202 Investigations with the representative reefs established that substantial variability in total
203 coral-cover projections can theoretically arise from demographic variability across
204 environmental gradients and uncertainty in estimated vital rates. Further complexities exist on
205 real reefs, including heterogeneity in reef terrain and habitat availability, connectivity
206 between populations, environmental gradients, and the timing and intensity of acute
207 disturbances [44]. With four case studies, 'clusters' comprising 5-9 reefs each, we investigated
208 whether the patterns identified in the representative reefs would also emerge in real reefs.
209 Two case studies were conducted in the northern GBR (Lizard Island Cluster and Moore Reef
210 Cluster), and one in each of the central (Davies Reef Cluster) and southern (Heron Island
211 Cluster) regions. Each cluster was partitioned into 272-583 sites utilising high-resolution
212 geomorphic and benthic composition habitat maps to define the reef extent and the habitat
213 availability for corals [35,44] (Fig. S4, S5).

214 The primary goal of this work was not to precisely replicate every historical data point, but
215 rather to represent the emergent system processes and behavioural dynamics underpinning
216 ecosystem dynamics [42,46]. We compared empirical observations from the Australian Institute
217 of Marine Science Long-term Monitoring Program [AIMS LTMP, 47] from both fixed-position
218 phototransect sites and reef perimeter manta-tow surveys against hindcast model trajectories
219 (2008-2024) (14 reefs with monitoring data available, Figure 3, Fig. S20). Visual assessment
220 suggested that simulations reasonably reproduced observed patterns of impact and recovery
221 from acute (Figure 3, Fig. S20). Quantitative assessment corroborated this assessment; the
222 global pooled Spearman's rank correlations of 0.50 (manta-tow) and 0.49 (phototransects)
223 indicated that the model on average captured the timing of downturns and recovery phases.
224 Trend alignment was strongest within the Davies and Heron clusters, where pooled
225 Spearman's correlations reached 0.77 and 0.66 respectively (phototransects), while the
226 Moore cluster exhibited the poorest alignment (pooled Spearman's $< 0.20$; phototransects).
227 This varied further at the reef level, with some correlations high, i.e. $>0.90$ for No Name,
228 North Direction, Carter, and Macgillivray reefs and others poor, for example Moore and
229 Yonge reefs. Absolute deviation was relatively low, with a global Root Mean Square Error of

approximately 13.5%, although this also varied between the clusters and reefs, the lowest absolute deviation was observed in the Moore and Davies clusters (pooled RMSE < 10%), whereas the Heron cluster showed the highest deviation (pooled RMSE > 23%). The pooled Percent Bias was low for manta-tow data (-2.3%), while that for the phototransects (-17.3%) suggested an underestimation by the model, which would be expected given the phototransects target the northern leeward reef slope where coral cover is generally high relative to other habitats. Model projections underestimated peak coral cover values obtained on southern reefs due to extremely fast recovery trajectories in recent years (e.g., One Tree Reef and Wreck Island reef) (Figure 3).

The model simulates a larger spatial area and numerous sites relative to the scope of the empirical surveys. Therefore, these monitoring data provide a spatially restricted benchmark to verify the integrity of simulated site-scale hindcasts. We deemed model performance acceptable in capturing the system sensitivity to acute disturbances and the subsequent rate of recovery dictated by the mechanisms in the *C~scape* model.

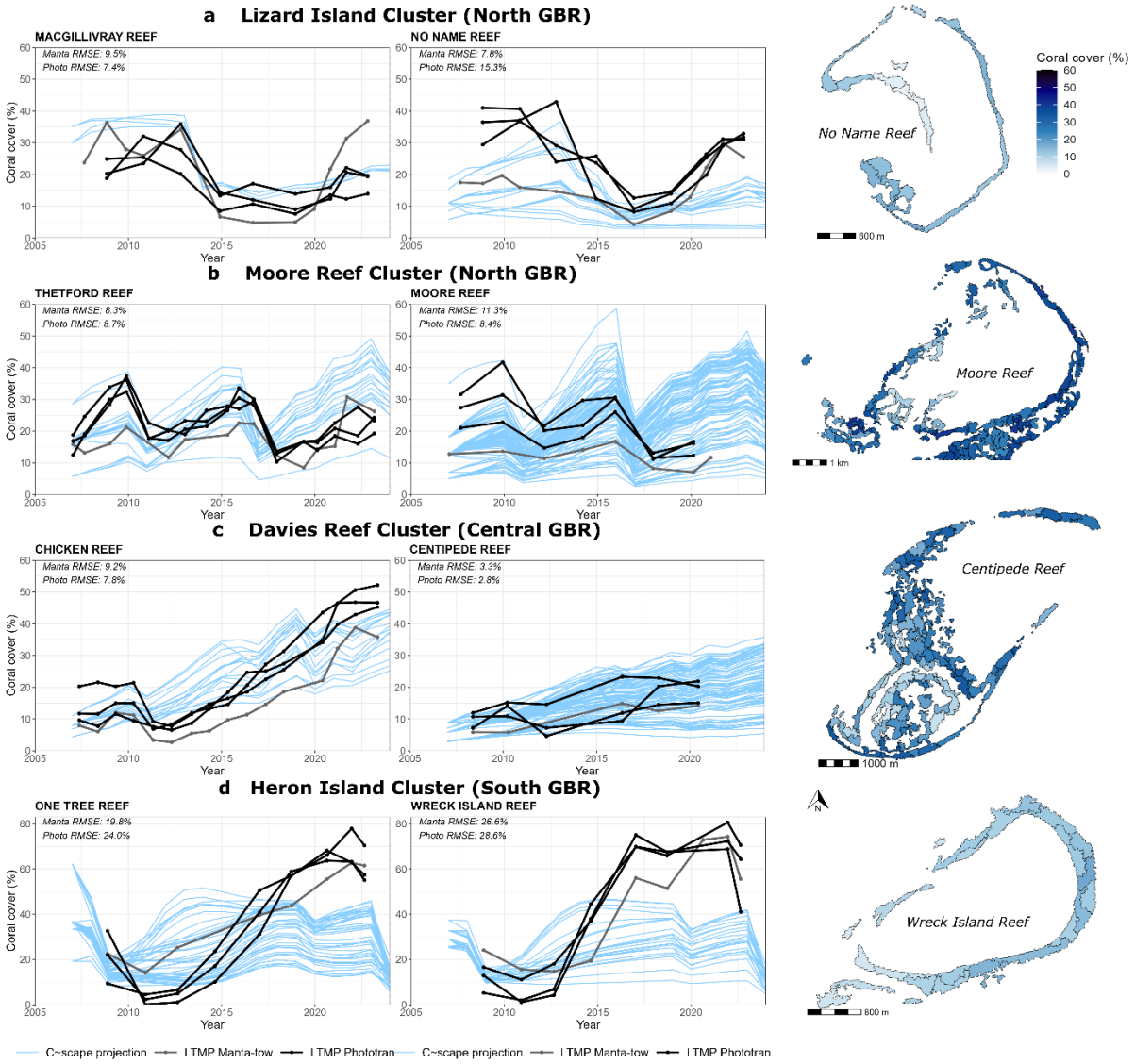


*Figure 3.* ***Evaluation of C~scape hindcast trajectories of total coral cover (%) against empirical monitoring data.*** *Trajectories from C~scape are shown for individual sites (blue lines) for two reefs within the four case study clusters that had data from the Australian Institute of Marine Science Long-Term Monitoring Program (AIMS LTMP) available for comparison, subset for those sites in the 'slope' or 'sheltered slope' geomorphic zones. Lizard Island Cluster and Davies Reef Cluster had additional LTMP reefs shown in Fig. S20. The right-hand panel shows an example map of one of the reefs in the year 2024 with the colour gradient showing total coral cover. Data from the AIMS LTMP are shown from fixed-position phototransects (black lines) and manta tow surveys (grey lines). LTMP fixed-position photo transect data are from three sites on the leeward north-east slope of the reefs. In contrast, LTMP manta tow surveys provide estimates from around the reef perimeters, targeting the reef slope. While manta tow surveys are less accurate than fixed-position phototransects, they offer broader spatial information across the reef. The Root Mean Square Error (RMSE) is shown for the comparison of model trajectories to manta tow and phototransects in the top left of each panel, see Appendix 3.3 for further quantitative evaluation.*

## 3.4 Projecting reef futures under climate change

We used Shared Socioeconomic Pathways [SSPs, 48] to represent different greenhouse-gas emissions pathways. To characterise the thermal stress associated with these pathways, we selected 10 Global Climate Models (GCMs) [see 25] and investigated the resulting variability in projected coral cover across SSPs and GCMs to 2100 (Table S4). Each GCM provided a deterministic thermal-stress trajectory (input to *C~scape* as annual maximum Degree Heating Weeks, DHW). Stochasticity in thermal stress timing was introduced by shuffling decadal DHW sequences to generate 20 disturbance 'realisations' for each GCM [see 25]. This resulted in 600 simulations for each of the four case studies and a hierarchy of climate, spatial and demographic influences (Figure 4a).

The projections, when averaged for each SSP scenario, showed ocean warming to reduce coral cover to varying extents. By the end of the century, an average of ~10% coral cover remained under the most optimistic emissions pathway (SSP1-2.6), whereas coral cover was <5% under SSP2-4.5, and zero under the high-emissions pathway (SSP3-7.0) (Figure 4a, Fig. S22). The *C~scape* framework accounts for natural selection of thermal tolerance and we found that the recurring heat stress events led to an increase in the heat stress that the coral community would survive (Fig, S24), but not enough to halt the decline of coral cover, in line with findings by [24,25].

The magnitude of the projected reduction in coral cover varied across case studies (Figure 4b, Fig. S23). The Moore Reef Cluster (northern GBR) exhibited the greatest capacity to maintain coral cover towards the end of the century, and Davies (central) and Heron Reef Cluster (southern) the least (although these differences did not persist under the high emissions pathway (SSP3-7.0), where coral cover was near zero for all clusters, Fig. S22).

Variability in coral-cover trajectories was also evident across the 200 future climate scenarios (10 GCMs and 20 disturbance realisations) per SSP (Moore Reef Cluster, SSP2-4.5: Figure 4c; all clusters: Fig. S23). High site-scale variability in coral trajectories also emerged (Figure 4d, 1/200 trajectories shown in Figure 4c) from the demographic variability across local site conditions alongside other influences such as connectivity and coral habitat availability [44].

Running numerous posterior draws from the vital rate posteriors was computationally intensive, so this was carried out under a single GCM realisation; Figure 4e and Fig S23

291 showed that substantial variability in projected coral cover arose from uncertainty in
292 estimated vital rates.

293

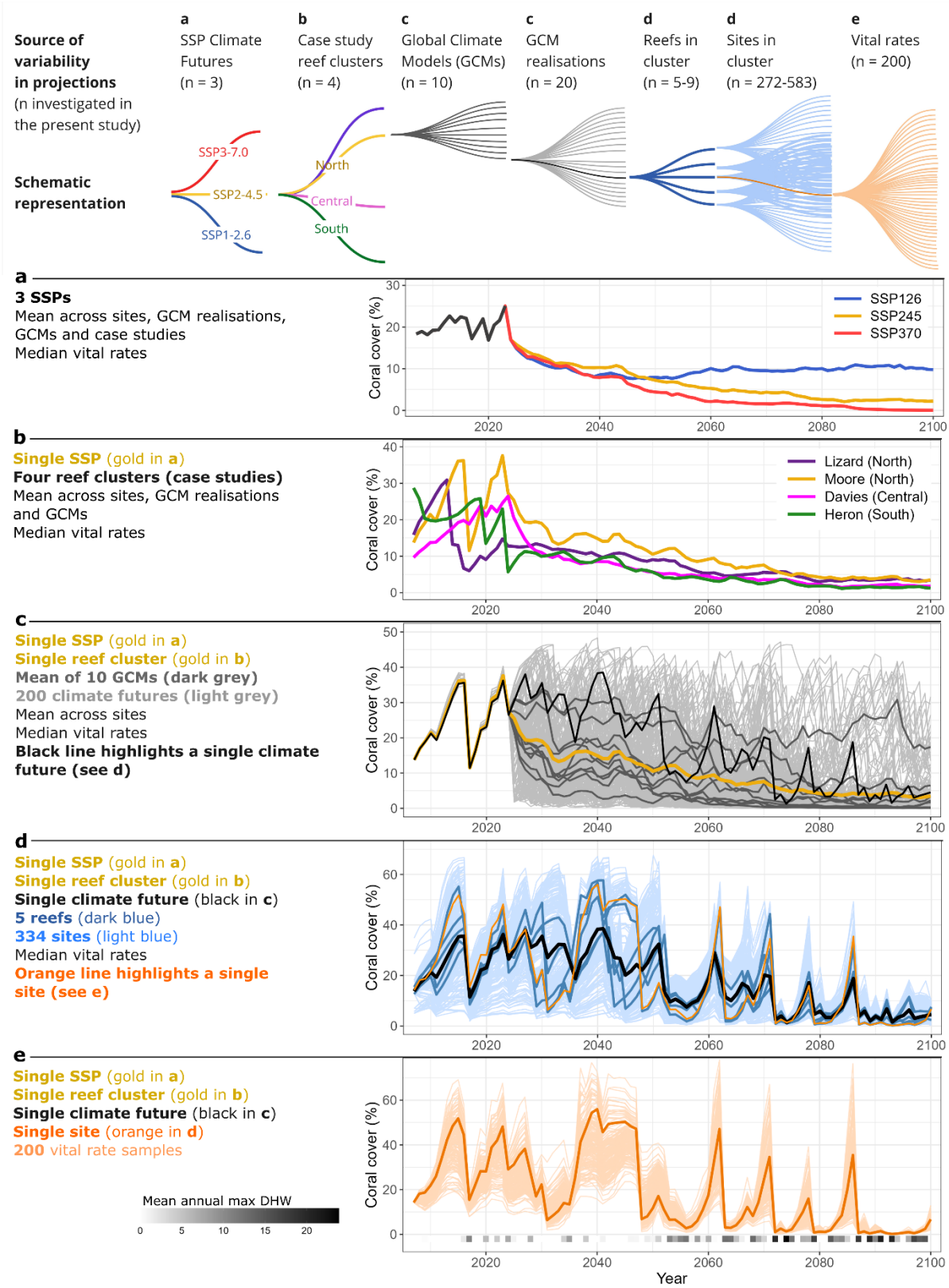


*Figure 4. Hierarchical decomposition of coral-cover projections and associated variability across spatial and climate scales. The top panel illustrates the sources of variability and uncertainty assessed in this study, with numbers indicating the levels considered and letters linking to panels (a)–(e), which present simulated total coral-cover trajectories from 2008 to 2100 as projected by the C~scape modelling framework. (a) Coral cover for three Shared Socioeconomic Pathways (SSPs), averaged across all sites, case studies, Global Climate Models (GCMs) and GCM realisations. (b) Coral cover for SSP2-4.5 across the four case studies. (c) Moore*

*Reef Cluster (North GBR) under SSP2-4.5 showing 200 future climate trajectories (light grey lines; 10 GCMs × 20 realisations). Dark grey lines show the mean trajectory for each GCM, gold shows the grand mean, and the black line highlights a single realisation from MRI-ESM2-0 selected for further examination. (d) The MRI-ESM2-0 realisation decomposed across spatial scales: black shows the overall case study mean (334 sites), light blue shows each site, dark blue shows reef-level means, and orange highlights a representative (median) site. (e) Trajectories for that representative site based on 200 replicate simulations (light orange lines), each sampling a posterior draw (out of 8000) from the Bayesian regressions describing coral vital rates. Dark orange line is the projection run using the median of the Bayesian posterior draws. Greyscale tiles show the magnitude of the mean annual maximum degree heating week (DHW) in the climate scenario of d) and e).*

## 3.5 Variability in coral cover is eroded under climate change

Variance partitioning analysis using linear mixed-effects models allowed identification of the influence of spatial context (site, reef and geographic region), future climate scenarios and uncertainty in estimated vital rates on coral-cover trajectories. A pooled analysis of data from the full forecast simulation period (2025–2100) indicated that after the residual (unexplained) variance, GCM explained the most variance, followed closely by SSP (Figure 5a). Region and site identity also explained relatively high proportions of variance, with slightly less at the reef level (Figure 5a).

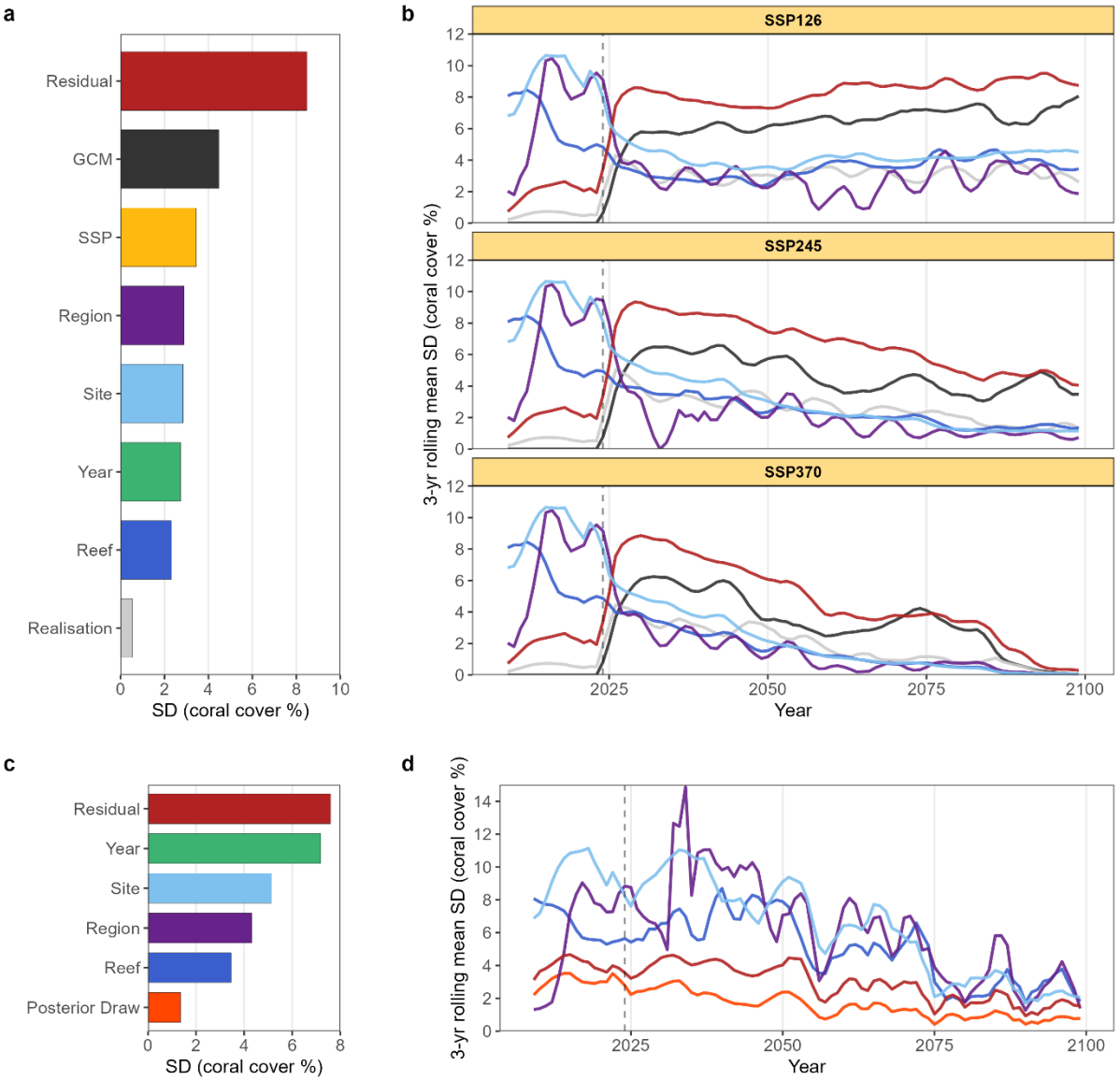


*Figure 5.* ***Variance partitioning of coral-cover projections****. (a) Variance partitioning (pooled analysis) for the full forecast simulation period (2025–2100) and all Shared Socioeconomic Pathways (SSPs). Bars represent the Standard Deviation (SD) in coral cover attributed to each component, ordered by magnitude. The residual represents unexplained variance not captured by the random effects. (c) Pooled analysis of variance targeting the inclusion of uncertainty in estimated vital rates (conducted for SSP4.5, GCM MRI-ESM2-0, single realisation). The posterior draw component represents the variance in coral-cover projections resulting from uncertainty in the estimated growth and survival vital rates, compared against the spatial hierarchy (Region, Reef, Site). (b) and (d) show temporal trajectories of variance obtained by fitting independent mixed-effects models to each SSP x year subset of the same data in (a) and (c) respectively. To facilitate the interpretation of multi-year trends, trajectories are presented as a 3-year central rolling mean of the annual SD (coral cover %). The vertical dashed line at 2024 indicates the transition from the hindcast to the forecast.*

Temporal variance partitioning analysis showed that the magnitude of these variance components shifted as the century progressed (Figure 5b). The major differences between SSPs emerged in the second half of the century (Figure 5a). As expected, variance associated with GCMs emerged immediately in the transition from hindcast to forecast (Figure 4c, Figure 5b). Under the low-emissions pathway (SSP1-2.6) GCM variance remained high, indicating uncertainty in the projections of coral cover across the climate model ensemble. Variance associated with spatial factors also remained elevated or increased in the final decades under SSP1-2.6, reflecting divergent recovery trajectories in the second half of the century (Figure 5, Fig. S22). However, under the high-emissions pathway (SSP3-7.0), and to a lesser extent under the middle-of-the-road scenario (SSP2-4.5), variance was compressed towards zero, tracking the convergence of coral-cover trajectories towards zero coral cover (Figure 5) and suggesting higher certainty in a collapsed reef state.

Uncertainty in estimated vital rates was not included in the main variance partitioning analysis due to computational constraints; instead, we processed 200 posterior draws for one climate trajectory (SSP4.5, MRI-ESM2-0, single realisation) across the four case studies (Figure 5c,d). Variability in coral-cover trajectories across posterior draws was reduced towards the end of the century (Figure 5d), particularly when high disturbance frequency prevented coral cover from diverging (Figure 4e, Fig. S23). However, some posterior draws retained potential for rapid recovery in the final decades (Figure 4e, Fig. S23). Variance attributed to posterior draws (Figure 5c,d) was relatively low compared to spatial factors.

# 4 DISCUSSION

Making informed ecosystem projections under future climates, for which ecosystem responses are uncharted territory, is a complex challenge. By integrating empirical measurements of vital rates through the *C~scape* mechanistic modelling framework, we scaled demography into spatially explicit metacommunity projections under climate change. Demographic variability, uncertainty in vital rates, spatial and environmental context and future climate scenarios all drove variability in the projections of coral-cover trajectories. Seemingly minor differences in vital rates propagated through coral-cover trajectories, generating ecologically meaningful shifts in trajectories and producing spatial variability both within and among reefs and regions, pointing to the potential for demographic buffering [49,50]. Some sites and regions consistently maintained higher cover, exhibited faster population growth, or experienced lower disturbance impacts, which has also been observed empirically [18,51–53].

Across 600 simulations spanning three Shared Socioeconomic Pathways (SSPs), there was high variability in coral-cover trajectories for the GBR case studies. The choice of GCM used to inform projections created substantial variability in coral-cover trajectories, representing the largest source of variance in the forecasts (Figure 5). This highlights both the uncertainty in projections due to climate uncertainty, and the strong role of thermal stress in shaping coral reef futures. However, under the higher-emissions pathways (SSP2-4.5 and 3-7.0), the intensity and frequency of thermal stress narrowed the variance in coral cover towards zero across GCMs in the late century. This occurred despite incorporating the capacity for increasing thermal tolerance in the coral populations via natural selection (Fig. S24, S31). Both average coral cover, and variability in coral-cover trajectories across simulations, were compressed toward zero as the century progressed, consistent with recent GBR-wide modelling [25]. This indicates high confidence in a major loss of coral cover by the end of the century under all but the lowest emissions pathway (SSP1-2.6, warming <2°C). In other words, our results fall within a rare space where there is greater certainty about long-term states (i.e. collapse) than near-term trajectories, should global emissions follow moderate-to-high pathways. However, these findings must be interpreted within the bounds of our modelling framework (see assumptions and limitations Appendix 5).

Crucially, the contraction of variability in coral-cover trajectories permeated multiple levels of the hierarchy (Figure 4a). Under the high-emissions scenarios, the temporal reduction in

variance attributed to vital rates, spatial scales, and climate scenarios can be explained by the increasing frequency and intensity of marine heatwaves and associated bleaching mortality toward the end of the century. High intensity bleaching events repeatedly 'reset' the community to low coral cover, while high frequency leaves insufficient time for environment-driven demographic differences to manifest during recovery [54,55]. When disturbances were less frequent (e.g. in the representative reefs investigations and under SSP1-2.6), substantial variability in coral-cover trajectories emerged from small differences in vital rates. This supports findings that even small differences in coral growth rates can translate into large differences in population recovery trajectories (fig. 3, [56]). Although we did not explicitly disentangle intra-population variability from uncertainty in the estimated vital rates, genetic and physiological differences among individuals might have contributed to the observed posterior uncertainty. If so, it would be plausible to expect that some traits are likely to persist longer or contribute to more rapid recovery under repeated disturbances, offering avenues for management, restoration, and adaptive responses [17,57]. Partitioning such individual-level effects from measurement or model uncertainty would require multi-year demographic datasets with repeated measures of identical colonies to isolate persistent individual traits from interannual variability. This would help guide the choice of taxa and traits for restoration initiatives. While we captured uncertainty in coral growth and survival, the complex roles of early life history of biophysical connectivity processes are not fully resolved due to data limitations (Appendix 5) and better characterisation of coral early life history processes is urgent [16].

Further implications for conservation and management lie in the spatial variability explored in this study. We found high variance in the projections of coral cover explained by region (north, central, south GBR), reef and site identity (Figure 5). Such spatial variability (across 100s m to 100s km) represents a combination of vital rates and coral community composition varying with local conditions, larval supply connectivity, available habitat and exposure to thermal stress. These factors collectively shape population resilience through both resistance and recovery potential [49]. The spatial variability we identified in the near-term decades, and that persisting under SSP1-2.6, is generally consistent with previous regional-scale studies identifying thermal refugia under moderate warming scenarios [20,59–62] which are eroded under high emissions scenarios. Under the low-emissions scenario, we projected high variability in coral-cover trajectories in the near term across spatial scales and found the loss of variability in coral cover was not spatially uniform, with the northern GBR retaining higher variability

for longer. Such refugia can retain taxonomic and genetic diversity important for future recovery [25,63]. Our results show a cross-scale contraction of spatial variability as the century progressed, which would limit the capacity for natural recovery, natural or assisted adaptation, and options for management and restoration approaches that depend on remnant healthy populations as larval sources [64,65].

Interpreting future ecosystem projections requires confronting uncertainty in both climate trajectories and biological responses. Disentangling variability from uncertainty, and attributing it to factors such as demographic variability and spatial context [9], helps identify where opportunities exist to improve ecosystem outlooks and target management effort. Here we have demonstrated a framework for propagating information from individuals to populations and communities, with a strong multi-scale spatial component central to both the approach and its management implications. While this study focused on total coral cover, future applications should investigate coral composition and size structure to inform on the relative roles of different taxa, sizes and life stages. Disentangling the effects of demographic variability across environments on population and metacommunity performance is foundational to identifying what properties characterise resilient reef locations. Our findings support the need for a strong spatial component in all management and restoration efforts including at the sometimes overlooked 'site' scale. However, the spatial variability underpinning opportunities for management and intervention collapsed under high-emissions scenarios towards the end of the century. While future coral reef state remains uncertain due to processes not captured here (Appendix 5), our projections occupy a rare space where certainty about long-term state exceeds certainty about near-term trajectories in the case global emissions follow moderate-to-high pathways, with the variance across the global climate model ensemble reducing to zero under SSP3-7.0. Management efforts to curtail global coral loss towards the end of the century will be largely ineffective unless emissions are kept within the bounds of the increasingly unlikely SSP1-2.6 pathway.

# 5 METHODS

## 5.1 Overview

This study advanced the *C~scape* metacommunity modelling framework [44], which combines coral demography with heterogenous environmental conditions within and between reefs to simulate spatially explicit coral metacommunity dynamics (Fig. S27). Key developments include expanding to six distinct coral types informed by GBR demographic data, the incorporation of environmental covariates to predict site-specific vital rates, methodology to propagate individual-level uncertainty through projections, and projections of coral-cover trajectories under future climate considering the capacity of corals to show some adaptation to thermal stress via natural selection.

*C~scape* partitions reefs into numerous spatial units which form a mosaic of 'site' polygons. This partitioning is informed by high resolution maps of reef geomorphic zonation and bathymetry. Conditions are assumed to be homogeneous within each site, but variable between sites. A community composed of six distinct coral types is simulated at each site, with each represented as a population structured across 100 size classes and three discrete life stages (eggs, larvae, and settlers). Population growth is modelled using Integral Projection Models (IPMs), which capture size-specific vital rates (growth, survival and fecundity). Growth and survival were derived from Bayesian regressions informed by ~10,000 annual measurements of coral colony growth and survival across gradients of the Great Barrier Reef (GBR). Depth, seabed 'waterflow intensity', and geographic region were included as covariates in these regressions, allowing growth and survival to vary according to site-specific characteristics rather than remaining uniform across reefs.

To simulate community-level interactions, density dependence is integrated using ordinary differential equations, such that as space becomes limiting, the growth rate of all coral types decreases [44]. Each site is modelled independently, but sites are linked into a broader metacommunity via the dispersal of larvae. This larval transport is governed by connectivity matrices.

Acute disturbances —thermal stress, cyclones, and *Acanthaster* (COTS) outbreaks— occur in any given year, killing a proportion of colonies according to empirically derived disturbance-mortality functions [44]. Cross-generational heritability of thermal tolerance was incorporated using phenotypic variance, where an individual's thermal tolerance is defined as its deviation

from the population's mean response. This term acts as an offset within the thermal stress-mortality function, such that individuals experience more or less mortality as a function of their relative thermal tolerance. Individual corals retain their assigned tolerance class from settlement to maturity and multigenerational transmission of this trait is modelled using a modification of the Breeder's equation.

Simulations and analyses were conducted under two primary avenues. First, simple representative reefs scenarios were used to investigate the community-level consequences of demographic variation due to regional and local site conditions. Second, the *C~scape* framework was applied to four GBR case studies, to evaluate hindcast accuracy against long-term monitoring data, to project future coral cover under climate change scenarios and to evaluate the sources of variability underlying these projections.

## 5.2 Coral types and input datasets

Previous application of the *C~scape* model captured two coral types [44]; here we expanded to a total of six coral types. The choice of coral types and the key taxa used to parameterise the demography of these coral types was shaped by both data availability and the goal to represent distinct common coral types on the GBR. We selected six coral types distinct in growth form, life-history traits and susceptibility to disturbance: tabular *Acropora*, corymbose/digitate *Acropora*, spawning *Pocillopora*, brooding Pocilloporidae, *Goniastrea/ Platygyra* and massive *Porites* [66–68], Table S1).

Different datasets were used to determine the growth, survival and early life history parameters for each coral type. The taxonomic resolution varied between datasets; for example, data relating to settler or juvenile corals was not possible to obtain at the taxonomic resolution matching selected coral types, in which case samples from genera or families were selected for the six coral types (Table S1).

Growth and survival were investigated by synthesising two datasets collected at the same locations but using different survey methodologies: the 'photogrammetry dataset' [31,33,34] and the 'juvenile coral dataset' [40]. Both datasets are part of a strategic program targeting key gaps in ecological knowledge and represents one of the largest demographic sampling efforts for coral reefs. The sampling design is nested with juvenile quadrats (0.5 x 0.5 m) within survey plots (12 x 6 m), within sites (distributed across habitats with different levels of seabed

512 waterflow intensity and different depths), nested within reefs and regions [31]. Data was
513 selected for seven reefs within three offshore regions of the GBR (north, central and south,
514 Fig. S4) from the 2021-2022 monitoring period, a year during which no known major acute
515 disturbances (bleaching, cyclones or crown-of-thorns outbreaks) were recorded at the study
516 reefs.

517 The photogrammetry dataset was built from high-resolution large-area orthomosaics (~72 $m^2$)
518 obtained with in-water photogrammetry surveys that were conducted at two time points
519 approximately 12 months apart, such that individual coral colonies and their 2D planar area
520 could be tracked across consecutive orthomosaics (for detailed methods see [31–34]. The
521 juvenile coral dataset was generated from sampling within 0.5 x 0. 5m fixed-position
522 quadrats which were selectively placed on areas with ≥1 juvenile coral (<5cm) when
523 deployed to increase sample size [40]. Corals within the quadrats were mapped in situ, taxon (to
524 genera where possible) identified, and longest diameter measured. The quadrats were
525 initiated and resurveyed at the same time as the photogrammetry.

526 The photogrammetry and the juvenile coral demography datasets were synthesised to build a
527 combined growth and survival dataset across the size range of the different coral types. The
528 diameter measurements in the juvenile coral dataset were transformed to an estimate of 2D
529 planar area, assuming the colonies were circles. Taxa for the six coral types were selected for
530 analysis. Corals from the juvenile dataset were generally <5 cm diameter, while corals from
531 the photogrammetry dataset were generally >5cm diameter.

532 A fecundity dataset was used from [68,69] to parameterise the production of eggs from the two
533 *Acropora* and the *Goniastrea/ Platygyra* coral groups. Data from the literature were used for
534 parameterising fecundity for the other three coral groups (Table S1, Appendix 1.3).

535 Density dependent processes influence the growth and survival of small corals such that there
536 are limits to the total observed coral juveniles of reefs [70]. Data from belt transect surveys
537 conducted at the same locations from which the growth and survival data were obtained was
538 used to quantify the density of juvenile corals (<5 cm) per available space (not covered by
539 other organisms or unsuitable substrates like sand) at each surveyed site from which a cap of
540 the maximum number of juveniles was calculated.

541 Alongside coral type and coral size, additional environmental and spatial covariates were
542 incorporated into the Integral Projection Models. The depth of each photogrammetry site was

determined by averaging substrate depth measurements taken at 20 points (five measurements per each of four plots) and correcting them relative to the Lowest Astronomical Tide. Photogrammetry sites were partitioned into deep and shallow sites in the survey design, but sites varied in depth enough for this to be included in regressions as a continuous variable (Table S2). A value for 'seabed waterflow intensity' was also determined for each site. The site polygons were also overlaid on a map of modelled seabed waterflow intensity [45] ('ubed mean' from the SWAN model https://espace.library.uq.edu.au/view/UQ:8246441) to assign the median seabed waterflow intensity per site. We elected to use 'Ubed mean', which is the mean horizontal velocity at the seafloor, as this gives an indication of how much force water movement at the seafloor exerts on corals, which may influence their growth and survival via physical impact and through the transfer of nutrients from the water to the corals [71].

## 5.3 Integral Projection Models

Integral Projection Models (IPMs) were developed following [44]. Vital rates (growth, survival, and fecundity) were estimated for each coral type using statistical regressions as a function of coral size (two-dimensional planar area), to reflect known size-dependence [72]. Building on principles explored by [12,73–75], we developed a spatially explicit framework where covariates describing local physical and environmental characteristics were selected based on their expected influence on coral growth and survival and their availability as spatial maps (Table S2).

In growth and survival regressions, site depth (m), modelled seabed waterflow intensity ($m.s^{-1}$) and GBR region were the main fixed environmental and spatial covariates (Table S2), alongside initial coral size (planar area, $cm^2$) and survey time (to allow standardisation to 365 days). To account for regional differences in size-dependent vital rates, an interaction between initial colony area and GBR region was incorporated. Nested random intercepts (plot within site within reef) accounted for the hierarchical sampling design (Appendix 1.2.2).

Growth was modelled as the log-transformed colony area at the end of the sampling period using a Student t-distribution with an identity link; the standard deviation was specified as a function of initial colony area to capture size-related heteroscedasticity. Survival (binary) was modelled using a Bernoulli distribution with a logit link. A combination of weakly and moderately informative priors was utilised (Appendix 1.2.2). Intercept priors were derived

575 from the median and median absolute deviation (MAD) of the initial colony area, while other
576 fixed effects were assigned weakly informative normal priors centred at 0. Standard
577 deviations of the random effects were assigned Student t-priors (Appendix 1.2.2).

578 Fecundity was estimated as size-dependent, colony-level reproductive output (as oocytes
579 (eggs), or larvae). For taxa with sufficient empirical data (tabular *Acropora*,
580 corymbose/digitate *Acropora* and *Goniastrea/Platygyra*) this was calculated as the product of
581 polyp density ($cm^{-2}$) and the number of oocytes per polyp. A hurdle model was used for
582 predicting the number of oocytes per polyp. The hurdle component, which determined the
583 probability of a polyp being fecund, was fit using a Bernoulli distribution with a logit link.
584 For fecund polyps, oocyte counts were modelled with a log link, incorporating colony nested
585 within species as random effects. To account for zero-inflation and overdispersion a hurdle-
586 Poisson was used for *Acropora* and hurdle-Negative Binomial distribution for
587 *Goniastrea/Platygyra*. Priors for these models were informed by preliminary linear and
588 generalised linear models to provide realistic intercepts and slopes. Polyp density was
589 assumed to be size-independent and was assigned a normal distribution for each coral type,
590 truncated to the minimum and maximum observed values, from data in (Madin et al. 2023,
591 Álvarez-Noriega et al. 2016). Uncertainty was propagated by integrating posterior draws of
592 oocyte counts with polyp densities [44].

593 For the remaining functional types, alternative estimation strategies were employed based on
594 literature-derived parameters (see Appendix 1.3.2).

595 All Bayesian regressions were implemented using Hamiltonian Monte Carlo in the brms
596 package (v.4.4.1 (Bürkner, 2017)) with Stan (Stan Development Team, 2023), using four
597 independent chains run for 4,000 iterations each. Following a 2,000-iteration warm-up, a total
598 posterior draw of 8,000 was retained per model. Convergence was verified by ensuring all
599 Rhat values were less than 1.01 and through visual inspection of trace plots [76]. For the growth
600 and survival models, predictive accuracy of models with different combinations of variables
601 depth, waterflow intensity, and GBR region were assessed using the Leave-One-Out
602 Information Criterion (LOOIC) via the *loo* package [77] in R. While various reduced covariate
603 combinations were explored (Table S5 and S6), the full model was ultimately retained to
604 ensure theoretically-relevant predictors were integrated, if equivalent predictive capacity was
605 retained (equivalent Bayes $R^2$ values). This approach facilitated a consistent comparison
606 across coral types. Although these regressions are based on a single year of vital rate data, the

established framework is designed to incorporate multi-year data as they become available to enhance model robustness.

To provide flexibility in the types of questions that could be investigated about reef functioning, multiple coral life stages are modelled explicitly, requiring parameterisation of several discrete transitions linking these major life stages: fecundity, fertilisation, larval dispersal, settlement, and post-settlement survival (Fig. S1). These parameters are detailed in Table S1, with the methodology for their estimation provided in Appendix 1.3.

Regressions and discrete stage transitions (Table S2, Appendix 1.3) were used to compute integral projection matrices. Matrices represent transitions from state $x$ (year $t$) to state $y$ (year $t+1$), constructed from separate matrices for survival, $s(x)$, growth $g(y,\mathrm{x})$, and reproduction and recruitment, $r(y,\mathrm{x})$ [78].

$$\mathbf{IPM_{ft,i,t}} = g(y,x)_{\mathrm{ft,i,t}}s(x)_{\mathrm{ft,i,t}} + r(y,\mathrm{x})_{\mathrm{ft,i,t}} \quad (1)$$

The integral projection matrices were constructed to be coral type (*ft*), site (*i*), and time (*t*) dependent. The growth function considers both positive and negative growth (partial mortality); fragmentation was not included as the target taxa were rarely noted to fragment in the empirical datasets. To avoid potential eviction, corals predicted to grow outside the defined size range (0.5 to 30-110 cm diameter) were allocated to the first or final bins, respectively [79].

Survival, $s(x)$, is the probability that an individual of size $x$ at time t will be alive at time t+1. Given large sample sizes are required to accurately quantify survival of long-lived taxa (i.e. *Goniastrea/Platygyra* and massive *Porites*) we introduced a size-independent survival cap of 97.5% to prevent implausibly high survival estimates [16,80].

For further details on IPM application to ecological populations see [12,14,81,82], and for corals specifically [74,75,78,83].

## 5.4 Population and community growth and mortality

The growth and vital rate transitions of coral populations were simulated using integral projection matrices calculated from the Bayesian regressions for growth, survival and fecundity, combined with the information on early life history discrete transitions. The population state of each coral type *ft* at site *i* and time *t* was defined by the state variable

637 $\overrightarrow{n_{ft,l}(x,\ t)}$ [81], which described the abundance of individuals across discrete life stages
638 (oocytes, larvae and settlers) and 100 size classes (the 'continuous stage', 0.25cm$^2$ planar area
639 to the maximum simulated coral colony area on the log-area scale, see Table S2).

640 $$\overrightarrow{n_{ft,l}(x,\ t)} = [n_{oocyte,t} \quad n_{larvae,t} \quad n_{settler,t} \quad n_{1,t} \quad n_{2,t} \quad n_{3,t} \ldots . \quad n_{100,t}] \quad (2)$$

641 Annual transitions in the population size structure and abundance were determined by
642 projection matrices, $\mathbf{IPM_{ft,i,t}}(x, y)$ , which were coral type, site and time dependent.
643 Multiplication of the projection matrix with the state vector yields the population state one
644 year later:

645 $$\overrightarrow{n_{ft,l}(y,\ t+1)} = \mathbf{IPM_{ft,i,t}}(x, y) \times \overrightarrow{n_{ft,l}(x,\ t)} \quad (3)$$

646 Community-level dynamics are represented by applying density dependent space limitation.
647 The available space varies temporally and results in a reduction of positive coral colony
648 growth towards stasis as space becomes limiting [12,84]. Thus, $\mathbf{IPM_{ft,i,t}}$, allowed for the
649 modulation of vital rate transitions based on available space at any given time, t. To facilitate
650 this, total coral cover $C_{i,t}$, was used as a time-dependent proxy for resource depletion. Coral
651 cover is calculated at each time step for each site by summing the product of colony
652 abundance and mean colony area across all size classes and functional types:

653 $$C_{i,t} = \sum_{ft=1}^{6} \sum_{n=1}^{100} n_{ft,i,t,n} \times a_{ft,n} \quad (3)$$

654 Where $a_{ft,n}$ was the colony area corresponding to the *n*th size class for coral type *ft,* and
655 $n_{ft,i,t,n}$ was the specific element of the abundance vector describing the number of colonies in
656 that class. By modulating the projection matrices $\mathbf{IPM_{ft,i,t}}$ based on this total cover, the
657 transition from intrinsic to density-dependent growth at the community level was captured.
658 Specifically, to ensure a logistic growth shape emerged as the total coral cover of the
659 community approached carrying capacity $\kappa_i$, the growth transitions within $\mathbf{IPM_{ft,i,t}}$ were
660 adjusted by a site-specific scalar, $d_{i,t}$, where

661 $$d_{i,t} = \frac{\kappa_i - C_{i,t}}{\kappa_i - \left(\kappa_i \times \frac{C_{c_{region}}}{90}\right)} \quad (4)$$

662 Where $C_{c_{region}}$ was the mean total coral cover across the original survey sites within each
663 GBR region (as per growth and survival regressions) from which the empirical vital rate data
664 were collected. This formulation recognised that the surveyed rates were likely subject to

some degree of space limitation at the time of survey; thus, the realised growth was adjusted to an intrinsic rate before being scaled by the current site conditions. The value of 90 represented the assumed carrying capacity (as a percentage) of those original survey sites, used to normalise the observed cover $C_{c_{region}}$ relative to its maximum potential.

The scalar $d_{i,t}$ was implemented by modifying the internal structure of the growth sub-matrix within $\mathbf{IPM_{ft}}$. Specifically, the probabilities of an individual growing into any larger size class were multiplied by $d_{i,t}$. To ensure that these adjustments to growth rates did not inadvertently alter survival probabilities, a constant column sum was maintained within the matrix. Any change in growth probability caused by $d_{i,t}$ was redistributed to the diagonal element of the matrix, representing the probability of remaining in the same size class. Consequently, as a site approached carrying capacity, $d_{i,t} \to 0$, the IPM transitions shifted so that individuals were more likely to persist in their current size class rather than increasing in area. This mechanism ensured that the cumulative effect across all populations resulted in community growth that followed a logistic trajectory, preventing the total coral cover from exceeding the site-specific maximum, $\kappa_i$.

In addition to the modulation of adult growth, space limitation was applied to the recruitment of new individuals to prevent juvenile densities from exceeding observed ecological limits [85]. This was achieved by imposing a coral type-specific cap on the density of juveniles (0.5-5cm diameter) that could occupy the available benthic space at any given site, $J_{ft}^{max}$. This cap was parameterised using the 99th percentile of juvenile counts observed in empirical surveys (Table S1, Appendix 1.3). The maximum number of juveniles permitted at a site at a given time, $n_{ft,i,t}^{max}$ was determined by multiplying this density cap by the available benthic space,

$$n_{ft,i,t}^{max} = J_{ft}^{max} \times Area_i \times \left(\frac{\kappa_i - C_{i,t}}{100}\right) \quad (5)$$

This cap was imposed via constraining the incoming coral settlers. Both new juveniles that would result from timestep *t*'s incoming settlers and the juveniles already present at the start of the timestep were summed. If this combined total exceeded the space-delimited cap, $n_{ft,i,t}^{max}$, the number of successful settlers was reduced proportionally such that the cap would not be exceeded. If the total coral cover met or exceeded the carrying capacity $\kappa_i < C_{i,t}$ the number of allowed new settlers was set to zero.

Three acute disturbances are included in the *C~scape* framework: temperature stress (as annual maximum Degree Heating Weeks), cyclones (as category 1-5), and *Acanthaster (*c.f *solaris)* crown-of-thorns (COTS) starfish (as density per COTS size classes). These act to kill a proportion of coral colonies within a site according to disturbance-mortality functions [44] (Appendix 4.2).

To incorporate natural adaptation, we track coral abundance not only across size classes but also across thermal tolerance classes, $\Delta DHW$, which represent deviations from the population's mean bleaching mortality response (Appendix 4.3). In this study we set 14 discrete thermal tolerance classes $\Delta DHW = \{-5, -4 \dots, 8\}$. Coral populations were initialised across these classes with a $sd = 1.91$ informed from empirical data in [64]. Corals within each thermal tolerance class retain the same $\Delta DHW$ throughout their life cycle.

We incorporated tolerance class, $\Delta DHW$, into the bleaching mortality function [86], which effectively shifted the bleaching mortality curve along the x-axis, where positive values ($\Delta DHW > 0$) equate to higher resistance (reduced mortality) and negative values ($\Delta DHW < 0$) higher susceptibility (increased mortality) (Fig. S31).

$$m_{init_{ft\_site}} = w_{site} \cdot s_{ft} \cdot ((e^{0.17+0.35\cdot(DHW_{site}-\Delta DHW)}) - 1)/100 \quad (5)$$

To allow for cross-generational selection the transmission of this phenotypic trait to the next generation was modelled by applying a generalisation of the Breeder's equation [87]. The Breeder's equation predicts the selection differential (the difference between the mean of the parental population and the mean of the breeding individuals) of a given trait over one generation after selection based on a parameter the trait's 'narrow-sense heritability' [88,89]. Narrow-sense heritability ($h^2$) has been investigated in many populations of organisms and found to tend towards $h^2$=0.3 for polygenic traits that are non-morphological and related to fitness (Moore et al 2019) and so we used this value in the present study (Appendix 4.3).

## 5.5 Metacommunities via connectivity modelling

We used biophysical modelling to simulate the dispersal, survival and settlement of larvae from the five broadcast spawning coral types to connect populations across the mosaic of sites in each of the four case studies. This workflow had four main steps: 1) hydrodynamic modelling, 2) particle tracking, 3) post-processing to impose coral larvae biology and behaviour onto the particles, and 4) generation of transition probability matrices describing

the probability of a larvae being produced at each site in the reef cluster travelling to every other site in the cluster, surviving its dispersal and successfully settling. Full details on this process are given in Appendix 2.2.3 and see [38].

For the Brooding Pocilloporidae coral type, we did not use this workflow, instead, we made several assumptions regarding the survival and settlement of brooding corals. We assumed that 3% of brooding corals would survive and successfully settle. Of these successful settlers, we assumed 90% would stay within the site of release, and the remaining 10% were partitioned to any sites within a 1 km radius of the release site [90,91].

Following approaches in previous work [25,44], we linked the fine-scale *C~scape* modelling to larger GBR-wide modelling (ReefMod-GBR [25,86]. While some reefs may be considered as isolated systems, we assumed that the reef clusters modelled in the present study receive coral larvae supplied from reefs outside the modelled domain given the high connectivity across reefs of the Great Barrier Reef [26,86,92]. Therefore, for the simulations presented here, the ReefMod-GBR model [25] was run in parallel, with the same environmental forcings (i.e. same thermal stress and cyclones), for 3,806 reefs across the Great Barrier Reef. From these simulations, we extracted the predicted number of larvae arriving to each reef modelled by *C~scape* , retaining only the larvae coming from reefs external to the modelled cluster. These 'external larvae' were distributed to *C~scape* reef sites proportionally based on the total site area, i.e., larger sites received more larvae. In the same way as for larvae arising from within the cluster, these external larvae settled on the reef with a probability dependent on their coral type (Table S1) and then were governed by the IPMs and the conditions at the site they were assigned to.

## 5.6 Model simulation details – representative reefs

To investigate how individual-level vital rates scale to community-level dynamics, we designed three simplified 'representative reefs,' each composed of four 1-hectare sites. We expected spatial differences in coral dynamics to emerge where growth and survival varied with environmental covariates, while uncertainty within the Bayesian regressions would propagate through to population and community projections. To test this across a range of physical/environmental conditions, we parameterised four distinct site types—shallow-low

757 waterflow, shallow-high waterflow, deep-low waterflow and deep-high waterflow (Figure
758 2a)—using depth and waterflow intensity values informed by our empirical survey sites and
759 the broader range of conditions across the GBR case studies.

760 For each of the six coral types, we first examined predictions of growth and survival specific
761 to these four site-level characteristics to understand the direction of these effects.

762 We then simulated coral-cover dynamics within the *C~scape* framework over a 50-year
763 period. To isolate the influence of uncertainty in estimated vital rates and demographic
764 variability across covariates (depth, waterflow and region), we fixed other model parameters
765 (these were explored with higher complexity in the GBR case studies). For instance, we
766 initialised communities at 5.4% cover divided equally among the six types (Table S3). We
767 assumed a direct stock-recruitment relationship where all larvae recruited to their source site,
768 using a settlement probability based on the median arrival probability from the four GBR
769 case study connectivity matrices. To evaluate both undisturbed population growth and
770 recovery capacity, all acute disturbances were disabled, except for a temperature stress
771 disturbances regime featuring an initial 20-year period without disturbance, followed by a
772 moderate-to-strong bleaching event every 10 years.

773

## 774 5.7 Great Barrier Reef case studies

775 Reef boundaries were defined using a geomorphic zonation map [93]. Following [36] we included
776 zones characterised by predominantly hard substrate (Reef Slope, Reef Crest, Outer Reef
777 Flat, and Sheltered Reef Slope) to represent suitable coral habitat. Sites were delineated by
778 partitioning these zones into smaller spatial units, which were then characterised by depth and
779 waterflow intensity (Fig. S5, [44]) by overlaying on 10x10 m pixel maps *(*Appendix 2.2.2*)*.
780 Benthic category maps [35] were used to estimate the proportion of each site suitable for coral
781 growth, 'coral habitat', by removing area that was categorised Sand or Rubble (Appendix
782 2.2.2 [44]). Across the four clusters, total modelled area ranged from 1,812 to 4,959 hectares
783 (Table S4), which translates to a maximum habitable coral cover of 1,432–2,895 hectares
784 once the characterisation of coral habitat is considered.

785 Historical (2008–2024) and future (2024–2100) environmental forcings (thermal stress,
786 cyclones, and COTS) follow [25,44,86]. Briefly, historical annual maximum DHW values were
787 obtained from climatology data from NOAA, historical exposure to cyclones was derived

788 from information from the Australian Bureau of Meteorology in combination with modelling
789 of wave heights (Puotinen et al. 2016), while the density of adult COTS arriving to each reef
790 was simulated for hindcast and future projections using the ReefMod-GBR model [25]
791 (Appendix 4.2).

792 For each case study, 30 scenarios across 20 stochastic realisations were run. The 30 scenarios
793 were characterised by projections of Sea Surface Temperatures (SST) from the sixth phase of
794 the Coupled Model Intercomparison Project (CMIP6) under three shared socioeconomic
795 pathways (SSPs) SSP1, SSP2, SSP3, and associated emissions trajectories SSP1-2.6, SSP2-
796 4.5, SSP3-7.0. Previous work [25,39] has downscaled SST projections from 10 CMIP6 global
797 climate models (GCMs): CNRM-ESM2-1, EC-Earth3-Veg, IPSL-CM6A-LR, MRI-ESM2-0,
798 UKESM1-0-LL, GFDL-ESM4, MIROC-ES2L, MPI-ESM1-2-HR, MIROC6, NorESM2-LM.
799 In hindcasts, DHW and cyclone inputs were fixed to the observed annual values across
800 scenarios and realisations, while COTS could vary due to the stochasticity in ReefMod-GBR.
801 We used 20 synthetic tracks of cyclones for forecasts, which were fixed across the 30
802 scenarios [25,94]. DHW varied according to the SSP and GCM across scenarios, while across
803 realisations the exact timing of DHW were shuffled within decades to create stochasticity and
804 reflect uncertainty in the exact timing of thermal stress [25]. The resulting 600 simulations per
805 cluster (10 GCMs x 3 SSPs x 20 realisations) utilised median growth and survival rates
806 derived from the Bayesian regressions.

807 While GCMs are generally best interpreted as an ensemble, computational constraints
808 necessitated selecting a single model (MRI-ESM2-0, single realisation) for the investigation
809 of vital rate uncertainty. We chose this GCM because it was available at fine resolution prior
810 to downscaling, and is considered to provide a fair representation of Australian past climate
811 [95], and it's Equilibrium Climate Sensitivity (ECS) was within the range of likely ECS (IPCC)
812 and fell within the middle range of the 10 GCMs we considered. For this single GCM we ran
813 a suite of 200 replicate scenarios, instead of using the median demography, we took a single
814 posterior draw in each simulation from the growth and survival Bayesian regressions.

815 Simulations were initialised based on the total coral cover recorded in the AIMS LTMP
816 manta tow observations from the starting year of the hindcast (2008) from reefs within the
817 simulated clusters (each had at least two reefs with LTMP data, Fig S11). The simulated reefs
818 that had data from LTMP were assigned the coral cover for that specific reef, which the
819 remaining reefs in the cluster were assigned the average off the reefs with data. While total

coral cover was taken from the manta tow observations (because this survey methodology covers a greater proportion of the simulated area of reef), this data does not provide coral community composition, and therefore we informed the relative composition of coral types with that observed in the fixed-position phototransects for this same year.

## 5.8 Model evaluation

A criterion for choosing the four GBR case study reef clusters was that they contained at least two reefs that were monitored as part of the AIMS Long-Term Monitoring Program (LTMP [47,96]. This allowed evaluation of model trajectories in the hindcast years (2008-2024) against empirical observations from this period. Two time-series datasets were available from the AIMS LTMP: coral cover from fixed-position photo transect data at three sites on the leeward north-east slope of the reefs, and total coral cover estimates from manta tow surveys. The fixed-position phototransects at each site comprise 5 x 50m transects along which photographs are taken and later analysed with a point-intercept method [47]. Manta tow is a monitoring technique where an observer (on snorkel) is towed behind a boat and makes visual assessments, recording the average total coral cover in ~ 10 m wide bands on consecutive tows which are ~ 200 m in length [47]. The surveys follow the reef perimeter, usually on the reef slope, and while they are less accurate than the fixed-position photo transects, they provide broader spatial information across the reef [47].

To assess the *C~scape* model performance at the GBR case studies, we compared simulated coral cover against the two empirical datasets. The *C~scape* model outputs were spatially filtered to select only the reef slope and sheltered slope sites of the 10 target reefs within the four clusters. Time-series of total cover was plotted for each of these modelled sites and visually examined against the three LTMP fixed-position sites in each reef, and against the mean manta tow estimates of total coral cover.

Empirical observations were then temporally aligned to the model's annual time steps (1 January-31 December) by assigning surveys conducted after July to the subsequent model year. For each reef, we calculated Pearson's correlation and Spearman's rank correlation to assess trend alignment, Root Mean Square Error to estimate absolute accuracy, and Percent Bias to identify systematic over- or under-estimation of the simulated coral cover relative to the observed empirical coral cover.

## 5.9 Partitioning variability in coral-cover trajectories

Two separate datasets were synthesised to quantify the relative contribution of different sources of variability to coral-cover trajectories. The first dataset combined all simulated data across years, SSPs, climate models (GCMs), and case study regions. The second dataset was designed to isolate the role of vital rate uncertainty, consisting of 200 separate posterior draws (as shown in Figure 4e) for a single climate model and realisation (SSP4.5, MRI-ESM2-0) across all case studies. On each of these datasets, we performed a two-step variance partitioning analysis: first, a pooled global analysis to determine the overall importance of predictive variables, and second, a temporal analysis to track how the influence of these variables changed over the century for each SSP.

For the climate-spatial analysis (approximately 92 million rows), we utilised a 10% proportional subsample (approximately 9 million rows). Similarly, for the vital rate-spatial analysis (approximately 30.7 million rows), a 10% subsample was taken (approximately 3 million rows). In both cases, subsampling followed a stratified approach to ensure equal representation across all simulation years and the relevant spatial and climate hierarchies. The 10% threshold was selected to maintain high statistical power and ensure the inclusion of sufficient data points for lower-level spatial groupings (e.g. reef sites) while remaining within the computational memory constraints of the high-performance computing environment. We fit nested mixed-effects models using the lme4 package in R with the following random intercept structures:

$$C_1 \sim (1|Year) + (1|SSP/GCM/Realisation) + (1|Region/Reef/Site)$$

$$C_2 \sim (1|Year) + (1|PosteriorDraw) + (1|Region/Reef/Site)$$

Variance components were extracted from this model and expressed as standard deviations to provide a global estimate of the magnitude of variability in coral cover associated with each factor.

To investigate how these sources of variability in coral cover evolved over time, we conducted a temporal analysis by fitting independent mixed-effects models for each simulation year. For the climate-spatial dataset, models were fit for each year within each SSP. For the vital rate-spatial dataset, models were fit for each year. In these annual models, the temporal random effect was removed, and the spatial and climate/demographic hierarchies were retained. Variance components were extracted for every year (and SSP). To

facilitate the visualisation of long-term trends and reduce annual stochastic noise, a three-year central rolling mean was applied to the resulting SD trajectories.

All mixed-effects models were implemented using the *lmer* function. To ensure robust convergence and stable variance estimates across these complex structures, we employed the *bobyqa* (Bounded Optimization by Quadratic Approximation) optimiser with a maximum of 100,000 function evaluations. This derivative-free optimiser was selected for its reliability in handling high-dimensional random effects and large-scale ecological datasets.

# 6 Acknowledgements

This work is part of The Reef Restoration and Adaptation Program, funded by the partnership between the Australian Governments Reef Trust and the Great Barrier Reef Foundation, with partners including: the Australian Institute of Marine Science, CSIRO, the Great Barrier Reef Foundation, Southern Cross University, the University of Queensland, Queensland University of Technology and James Cook University. Empirical data was collected by the Ecological Intelligence for Reef Restoration and Adaptation subprogram (EcoRRAP), with thanks to Eoghan Aston and Madison Becker and Kinam Salee, and the AIMS Long-Term Monitoring Program. All RRAP partners acknowledge Aboriginal and Torres Strait Islander Peoples as the first marine scientists and carers of Country. We acknowledge the Wulgurukaba, Bindal, Whadjuk Noongar, Turrbal and Jagera Peoples of the land on which the authors conducted the model development, analysis and writing for this study and the Traditional Owners of Sea Country that this study relates to: Gunggandji, Ngurumungu, Dingaal, Yirrganydji (Northern GBR), Wulgurukaba, Bindal (Central GBR); Bailai, Gurang, Gooreng Gooreng, Taribelang Bunda (Southern GBR). This model development was possible through building on the seminal ecological modelling of the *ReefMod* and *CocoNet* teams has benefitted greatly from being part of the RRAP Modelling and Decision Support subprogram — we are grateful to Scott Condie, Mayuran Sivapalan, Jerome Bowen, Michael Marinovich, Nikala Passaris, Ashley Whitt for their contributions, and specifically thank Takuya Iwanaga for insights on model evaluation and sensitivity that greatly improved the manuscript.

# 7 Author contribution statement

AKC, VHB, MGR, PO, JPG, JM, JCO developed the *C~scape* model concept. VHB, AKC, MGR, PO wrote the code. AKC, JCO, VHB, MGR, JPG, YMB, AA, KA, PM, BJR made substantial contributions to the conception and design of the approach to projecting coral reef

dynamics under climate change. RF, CD, KF, SG, ML, SN, MT, MAN, DBu were central to the conception, design and curation of ecological data via the EcoRRAP program. AKC, JO, MMB, KC, MP, MAN, CD, CCS decided coral types, developed the methods for coral early life history, applied long-term monitoring and/or environmental data. YMB orchestrated the downscaling of Global Climate Models to reef level. CJA and BJR conducted fine-scale hydrodynamic and particle tracking modelling to develop spatial maps of downscaled thermal stress and connectivity matrices; AKC, DBa, DBu, VHB, RSG, and MGR built the Integral Projection Models. All. AKC ran the *C~scape* model, YMB, PM & AA ran the *ReefMod-GBR* model in parallel. AKC wrote the first draft manuscript; AKC, JO, RSG, JPG refined the manuscript scope; AKC, MMB and ML generated visualisations. All authors contributed to the interpretation of results, writing and review and collaborated with AKC to integrate information and approaches into the *C~scape* framework.

# 8 Data availability statement

The model code and model outputs generated from this study will be made openly available in AIMS Data Repository upon acceptance to Journal.

# References


1. Mouquet, N. *et al.* REVIEW: Predictive ecology in a changing world. *J. Appl. Ecol.* **52**, 1293–1310 (2015).
2. Gauthier, G., Péron, G., Lebreton, J.-D., Grenier, P. & Van Oudenhove, L. Partitioning prediction uncertainty in climate-dependent population models. *Proc. R. Soc. B Biol. Sci.* **283**, 20162353 (2016).
3. Dietze, M. C. *et al.* Iterative near-term ecological forecasting: Needs, opportunities, and challenges. *Proc. Natl. Acad. Sci.* **115**, 1424 (2018).
4. Yates, D. N., Kittel, T. G. F. & Cannon, R. F. Comparing the Correlative Holdridge Model to Mechanistic Biogeographical Models for Assessing Vegetation Distribution Response to Climatic Change. *Clim. Change* **44**, 59–87 (2000).
5. Botsford, L. W. *et al.* Connectivity and resilience of coral reef metapopulations in marine protected areas: Matching empirical efforts to predictive needs. *Coral Reefs* **28**, 327–337 (2009).
6. Harfoot, M. B. J. *et al.* Emergent Global Patterns of Ecosystem Structure and Function from a Mechanistic General Ecosystem Model. *PLoS Biol.* **12**, e1001841 (2014).
7. van Woesik, R. *et al.* Coral-bleaching responses to climate change across biological scales. *Glob. Change Biol.* (2022).
8. Lu, Y. Time to model all life on Earth. *Nature* 295–297 (2013).
9. Lehmann, J. & Rillig, M. Distinguishing variability from uncertainty. *Nat. Clim. Change* **4**, 153–153 (2014).
10. Erickson, R. A. *et al.* A spatially discrete, integral projection model and its application to invasive carp. *Ecol. Model.* **387**, 163–171 (2018).
11. Boschetti, F. *et al.* Setting priorities for conservation at the interface between ocean circulation, connectivity, and population dynamics. *Ecol. Appl.* **30**, e02011 (2020).

12. Rees, M. & Ellner, S. P. Integral projection models for populations in temporally varying environments. *Ecol. Monogr.* **79**, 575–594 (2009).
13. Plard, F., Turek, D., Grüebler, M. U. & Schaub, M. IPM 2: toward better understanding and forecasting of population dynamics. *Ecol. Monogr.* **89**, e01364 (2019).
14. Elderd, B. D. & Miller, T. E. Quantifying demographic uncertainty: Bayesian methods for integral projection models. *Ecol. Monogr.* **86**, 125–144 (2016).
15. Simmonds, E. G. & Jones, O. R. Uncertainty propagation in matrix population models: Gaps, importance and guidelines. *Methods Ecol. Evol.* **15**, 427–438 (2024).
16. Edmunds, P. J. *et al.* Evaluating the causal basis of ecological success within the scleractinia: an integral projection model approach. *Mar. Biol.* **161**, 2719–2734 (2014).
17. Humanes, A. *et al.* Within-population variability in coral heat tolerance indicates climate adaptation potential. *Proc. R. Soc. B* **289**, 20220872 (2022).
18. Lange, I. D., Molina-Hernández, A., Medellín-Maldonado, F., Perry, C. T. & Álvarez-Filip, L. Structure-from-motion photogrammetry demonstrates variability in coral growth within colonies and across habitats. *PLOS ONE* **17**, e0277546 (2022).
19. Chollett, I., Enríquez, S. & Mumby, P. J. Redefining Thermal Regimes to Design Reserves for Coral Reefs in the Face of Climate Change. *PLoS ONE* **9**, e110634 (2014).
20. Sun, C. *et al.* Climate refugia in the Great Barrier Reef may endure into the future. *Sci. Adv.* **10**, eado6884 (2024).
21. Srednick, G., Davis, K. & Edmunds, P. Spatial Portfolios in Coral Metapopulations Are Shaped by Spatiotemporal Asynchrony in Environmental Conditions. *Ecol. Lett.* **29**, e70324 (2026).
22. Wolff, N. H., Mumby, P. J., Devlin, M. & Anthony, K. R. N. Vulnerability of the Great Barrier Reef to climate change and local pressures. *Glob. Change Biol.* **24**, 1978–1991 (2018).

980 23. McManus, L. C. *et al.* Extreme temperature events will drive coral decline in the Coral
981 Triangle. *Glob. Change Biol.* **26**, 2120–2133 (2020).
982 24. Lachs, L. *et al.* Natural selection could determine whether *Acropora* corals persist under
983 expected climate change. *Science* **386**, 1289–1294 (2024).
984 25. Bozec, Y.-M. *et al.* A rapidly closing window for coral persistence under global
985 warming. Preprint at https://doi.org/10.1101/2025.01.23.634487 (2025).
986 26. Condie, S. A. *et al.* Large-scale interventions may delay decline of the Great Barrier
987 Reef. *R. Soc. Open Sci.* **8**, 201296 (2021).
988 27. DeFilippo, L. B. *et al.* Assessing the potential for demographic restoration and assisted
989 evolution to build climate resilience in coral reefs. *Ecol. Appl.* **32**, e2650 (2022).
990 28. Adam, A. A., Bozec, Y., Hedley, J. D. & Mumby, P. J. Context-dependent benefits of
991 coral reef restoration. *Restor. Ecol.* e70252 (2025).
992 29. Bellwood, D. R. *et al.* Coral recovery may not herald the return of fishes on damaged
993 coral reefs. *Oecologia* **170**, 567–573 (2012).
994 30. Zawada, K. J. A., Madin, J. S., Baird, A. H., Bridge, T. C. L. & Dornelas, M.
995 Morphological traits can track coral reef responses to the Anthropocene. *Funct. Ecol.* **33**,
996 962–975 (2019).
997 31. Gordon, S. *et al. Field Photogrammetry in 4D. Reef Restoration and Adaption Program*
998 *(EcoRRAP). Standard Operational Procedure Number 1: Overview and in-Field*
999 *Workflow.* 62 pp https://doi.org/10.25845/SE7T-PS86 (2023).
1000 32. Lechene, M. A. A. *et al.* Evaluating error sources to improve precision in the co-
1001 registration of underwater 3D models. *Ecol. Inform.* **81**, 102632 (2024).
1002 33. Gordon, S. *et al. Field Photogrammetry in 4D: Model Processing Reef Restoration and*
1003 *Adaption Program (EcoRRAP) Standard Operational Procedure Number 16 (No. 2 of*
1004 *Series)*. (2025).

34. Toor, M. *et al. Field Photogrammetry in 4D: Digitisation and 2D Metric Extraction Reef Restoration and Adaption Program (EcoRRAP) Standard Operational Procedure Number 17 (No. 3 of Series)*. (2025).
35. Roelfsema, C. M. *et al.* Habitat maps to enhance monitoring and management of the Great Barrier Reef. *Coral Reefs* **39**, 1039–1054 (2020).
36. Kennedy, E. V. *et al.* Reef Cover, a coral reef classification for global habitat mapping from remote sensing. *Sci. Data* **8**, 196 (2021).
37. Grimaldi, C. M. *et al.* Hydrodynamic drivers of fine-scale connectivity within a coral reef atoll. *Limnol. Oceanogr.* **67**, 2204–2217 (2022).
38. Ani, C. J., Haller-Bull, V., Gilmour, J. P. & Robson, B. J. Connectivity modelling identifies sources and sinks of coral recruitment within reef clusters. *Sci. Rep.* **14**, 13564 (2024).
39. McWhorter, J. K. *et al.* The importance of 1.5° C warming for the Great Barrier Reef. *Glob. Change Biol.* **28**, 1332–1341 (2022).
40. Doropoulos, C. *et al.* Impact of environmental gradients on juvenile coral demography across the Great Barrier Reef and Torres Strait. *Coral Reefs* https://doi.org/10.1007/s00338-025-02742-6 (2025) doi:10.1007/s00338-025-02742-6.
41. AIMS, A. I. of M. S. EcoRRAP Coral Demographic Data. (2023).
42. Levins, R. The strategy of model building in population biology. *Am. Sci.* **54**, 421–431 (1966).
43. Leibold, M. A. *et al.* The metacommunity concept: a framework for multi-scale community ecology. *Ecol. Lett.* **7**, 601–613 (2004).
44. Cresswell, A. K. *et al.* Capturing fine-scale coral dynamics with a metacommunity modelling framework. *Sci. Rep.* **14**, 24733 (2024).

45. Callaghan, D. P., Leon, J. X. & Saunders, M. I. Wave modelling as a proxy for seagrass ecological modelling: Comparing fetch and process-based predictions for a bay and reef lagoon. *Estuar. Coast. Shelf Sci.* **153**, 108–120 (2015).
46. Oreskes, N., Shrader-Frechette, K. & Belitz, K. Verification, validation, and confirmation of numerical models in the earth sciences. *Science* **263**, 641–646 (1994).
47. Miller, I. R., Jonker, M. & Coleman, G. *Crown-of-Thorns Starfish and Coral Surveys Using the Manta Tow Technique*. (2018).
48. Hennessy, K., Lawrence, J. & Mackey, B. IPCC Sixth Assessment Report (AR6): Climate Change 2022-Impacts, Adaptation and Vulnerability: Regional Factsheet Australasia. (2022).
49. Capdevila, P., Stott, I., Beger, M. & Salguero-Gómez, R. Towards a Comparative Framework of Demographic Resilience. *Trends Ecol. Evol.* **35**, 776–786 (2020).
50. Gascoigne, S. J. L. *et al.* Structured Demographic Buffering: A Framework to Explore the Environmental Components and Demographic Mechanisms Underlying Demographic Buffering. (2023).
51. Aston, E. A. *et al.* Scale-dependent spatial patterns in benthic communities around a tropical island seascape. *Ecography* **42**, 578–590 (2019).
52. Thomson, D. P. *et al.* Zone specific trends in coral cover, genera and growth-forms in the World-Heritage listed Ningaloo Reef. *Mar. Environ. Res.* 105020 (2020).
53. Edmunds, P. *et al.* Long-term community dynamics are heterogeneous between fringing- and fore-reef habitats on an Indo-Pacific coral reef. *Ecosphere* **16**, e70398 (2025).
54. Pratchett, M. S., McWilliam, M. J. & Riegl, B. Contrasting shifts in coral assemblages with increasing disturbances. *Coral Reefs* **39**, 783–793 (2020).
55. Cresswell, A. K. *et al.* Coral reef state influences resilience to acute climate-mediated disturbances. *Glob. Ecol. Biogeogr.* **33**, 4–16 (2024).

56. Ortiz, J. C. *et al.* Important ecosystem function, low redundancy and high vulnerability: The trifecta argument for protecting the Great Barrier Reef's tabular Acropora. *Conserv. Lett.* **14**, e12817 (2021).
57. Mcleod, E. *et al.* The future of resilience-based management in coral reef ecosystems. *J. Environ. Manage.* **233**, 291–301 (2019).
58. Crone, E. E. Contrasting effects of spatial heterogeneity and environmental stochasticity on population dynamics of a perennial wildflower. *J. Ecol.* **104**, 281–291 (2016).
59. Hufbauer, R. A. *et al.* Three types of rescue can avert extinction in a changing environment. *Proc. Natl. Acad. Sci.* **112**, 10557–10562 (2015).
60. McWhorter, J. K., Halloran, P. R., Roff, G., Skirving, W. J. & Mumby, P. J. Climate refugia on the Great Barrier Reef fail when global warming exceeds 3° C. *Glob. Change Biol.* (2022).
61. McClanahan, T. R. *et al.* Diversification of refugia types needed to secure the future of coral reefs subject to climate change. *Conserv. Biol.* **38**, e14108 (2024).
62. Mellin, C. *et al.* Cumulative risk of future bleaching for the world's coral reefs. *Sci. Adv.* **10**, eadn9660 (2024).
63. Lachs, L. *et al.* High coral heat tolerance at local-scale thermal refugia. *PLoS Clim.* **3**, e0000453 (2024).
64. Humanes, A. *et al.* Selective breeding enhances coral heat tolerance to marine heatwaves. *Nat. Commun.* **15**, 8703 (2024).
65. Quigley, K. Breeding and selecting corals resilient to global warming. *Annu. Rev. Anim. Biosci.* **12**, 209–332 (2024).
66. Darling, E. S., Alvarez-Filip, L., Oliver, T. A., McClanahan, T. R. & Côté, I. M. Evaluating life-history strategies of reef corals from species traits. *Ecol. Lett.* **15**, 1378–1386 (2012).

67. Pratchett, M. S. *et al.* Spatial, temporal and taxonomic variation in coral growth—implications for the structure and function of coral reef ecosystems. *Oceanogr. Mar. Biol. Annu. Rev.* **53**, 215–295 (2015).
68. Álvarez-Noriega, M. *et al.* Fecundity and the demographic strategies of coral morphologies. *Ecology* **97**, 3485–3493 (2016).
69. Madin, J. S. *et al.* Six years of demography data for 11 reef coral species. *Ecology* **104**, e4017 (2023).
70. Jonker, M., Johns, K. & Osborne, K. *Surveys of Benthic Reef Communities Using Underwater Digital Photography and Counts of Juvenile Corals*. (2008).
71. Madin, J. S., Baird, A. H., Dornelas, M. & Connolly, S. R. Mechanical vulnerability explains size-dependent mortality of reef corals. *Ecol. Lett.* **17**, 1008–1015 (2014).
72. Hughes, T. P. Population dynamics based on individual size rather than age: a general model with a reef coral example. *Am. Nat.* **123**, 778–795 (1984).
73. Boyce, M., Haridas, C., Lee, C., & Thenceasstochasticdemographyw. Demography in an increasingly variable world. *Trends Ecol. Evol.* **21**, 141–148 (2006).
74. Kayal, M. *et al.* Predicting coral community recovery using multi-species population dynamics models. *Ecol. Lett.* **21**, 1790–1799 (2018).
75. Cant, J., Salguero-Gómez, R. & Beger, M. Transient demographic approaches can drastically expand the toolbox of coral reef science. *Coral Reefs* **41**, 885–896 (2022).
76. Gelman, A. & Rubin, D. B. Inference from Iterative Simulation Using Multiple Sequences. *Stat. Sci.* **7**, 457–472 (1992).
77. Vehtari, A., Gelman, A., Gabry, J. & Yao, Y. Package 'loo'. *Effic. Leave-One- Cross-Valid. WAIC Bayesian Models* (2021).
78. Shlesinger, T. & Van Woesik, R. Different population trajectories of two reef-building corals with similar life-history traits. *J. Anim. Ecol.* **90**, 1379–1389 (2021).

79. Williams, J. L., Miller, T. E. X. & Ellner, S. P. Avoiding unintentional eviction from integral projection models. *Ecology* **93**, 2008–2014 (2012).
80. Precoda, K. *et al.* How does a widespread reef coral maintain a population in an isolated environment? *Mar. Ecol. Prog. Ser.* **594**, 85–94 (2018).
81. Ellner, S. P. & Rees, M. Integral projection models for species with complex demography. *Am. Nat.* **167**, 410–428 (2006).
82. Coulson, T. Integral projections models, their construction and use in posing hypotheses in ecology. *Oikos* **121**, 1337–1350 (2012).
83. Mulla, A. J. *et al.* Natural coral recovery despite negative population growth. *Ecology* **105**, e4368 (2024).
84. Miller, D. H., Jensen, A. L. & Hammill, J. H. Density dependent matrix model for gray wolf population projection. *Ecol. Model.* **151**, 271–278 (2002).
85. Vermeij, M. J. A. & Sandin, S. A. DENSITY-DEPENDENT SETTLEMENT AND MORTALITY STRUCTURE THE EARLIEST LIFE PHASES OF A CORAL POPULATION. *Ecology* **89**, 1994–2004 (2008).
86. Bozec, Y.-M. *et al.* Cumulative impacts across Australia's Great Barrier Reef: a mechanistic evaluation. *Ecol. Monogr.* **92**, e01494 (2022).
87. Lynch, M. & Walsh, B. *Genetics and Analysis of Quantitative Traits*. vol. 1 (Sinauer Sunderland, MA, 1998).
88. Postma, E. Four decades of estimating heritabilities in wild vertebrate populations: improved methods, more data, better estimates. *Quant. Genet. Wild* **16**, 33 (2014).
89. de Villemereuil, P., Morrissey, M. B., Nakagawa, S. & Schielzeth, H. Fixed-effect variance and the estimation of repeatabilities and heritabilities: issues and solutions. *J. Evol. Biol.* **31**, 621–632 (2018).

90. Doropoulos, C., Ward, S., Roff, G., González-Rivero, M. & Mumby, P. J. Linking demographic processes of juvenile corals to benthic recovery trajectories in two common reef habitats. *PLoS ONE* **10**, e0128535 (2015).
91. Sartori, G. *et al.* Stock-recruitment relationships in pocilloporid corals are likely disrupted by thermal stress. *Bull. Mar. Sci.* **101**, 231–246 (2025).
92. Hock, K. *et al.* Connectivity and systemic resilience of the Great Barrier Reef. *PLoS Biol.* **15**, e2003355 (2017).
93. Roelfsema, C. M. *et al.* How Much Shallow Coral Habitat Is There on the Great Barrier Reef? *Remote Sens.* **13**, 4343 (2021).
94. Wolff, N. H. *et al.* Temporal clustering of tropical cyclones on the Great Barrier Reef and its ecological importance. *Coral Reefs* **35**, 613–623 (2016).
95. Virgilio, G. D. *et al.* Selecting CMIP6 GCMs for CORDEX Dynamical Downscaling: Model Performance, Independence, and Climate Change Signals. *Earths Future* **10**, e2021EF002625 (2022).
96. Emslie, M. J. *et al.* Decades of monitoring have informed the stewardship and ecological understanding of Australia's Great Barrier Reef. *Biol. Conserv.* **252**, 108854 (2020).

# Supporting Information for:
# Multi-scale collapse of coral cover under climate change

Anna K. Cresswell[1,2], Vanessa Haller-Bull[3], Manuel Gonzalez-Rivero[3], James P. Gilmour[1,2], Yves-Marie Bozec[4], Arne Adam[4], Mariana Alvarez-Noriega[3], Ken Anthony[3,5], Chinenye J. Ani[3,6], Molly-Mae Baker[7,2,1], Diego R. Barneche[1,2], Deborah Burn[3], Carolina Castro-Sanguino[1], Kerryn Crossman[3], Christopher Doropoulos[8], Katharina Fabricius[3], Renata Ferrari[3], Sophie Gordon[3], Marine Lechene[3], Justin Moore[3], Peter Mumby[4], Sam Noonan[3], Pascal Omondiagbe[3], Marji Puotinen[1], Barbara J. Robson[3,6], Roberto Salguero-Gomez[9], Maren Toor[3], Juan Carlos Ortiz[3]

[1] Australian Institute of Marine Science, Perth, WA, Australia, 6009
[2] Oceans Institute, University of Western Australia, Perth, WA, Australia, 6009
[3] Australian Institute of Marine Science, Townsville, QLD, Australia, 4810
[4] School of The Environment, The University of Queensland, Brisbane, QLD, Australia, 4072
[5] Nature Assets Consulting, Brisbane, QLD, Australia, 4000
[6] AIMS@JCU, College of Science and Engineering, James Cook University, Townsville, QLD, Australia, 4811
[7] School of Biological Sciences, University of Western Australia, Perth, WA, Australia, 6009
[8] CSIRO Environment, St. Lucia, QLD, Australia, 4067
[9] Department of Biology, University of Oxford, Wellington Square, Oxford, UK, OX1 2JD

## APPENDIX 1. Vital rate analyses and parameters

### 1.1. Coral types and parameters

Selecting six coral types required balancing multiple considerations. For computational and complexity reasons we targeted a maximum of six coral types. We wanted these to represent common coral types that occur on the Great Barrier Reef, and be distinct in their growth form, vital rates, mode of reproduction and/or susceptibility to disturbance. This required grouping some taxa that are known to have different traits. For example, we combined corymbose and digitate *Acropora* corals despite evidence that these two groups have different growth and mortality rates (with corymbose being faster growers and with lower survival than digitate growth forms (Pratchett et al. 2015)).

Notably, certain important coral groups were not included, for example foliose corals, branching *Porites* spp., or branching *Acropora* spp. thickets, due to difficulties in distinguishing individuals for growth and survival monitoring and incorporation into Integral Projection Models.

The corals were parameterised with a maximum size that was informed by the size distribution of the colonies sampled for growth and survival and considering the reported maximum size of these corals (coraltraits.org/). We avoided predicting outside of the sampled sizes where possible, but in the case of massive *Porites* the maximum size was increased such that the simulated corals better represented this group of corals which are known to be long-lived with capacity to grow exceptionally large.

The six coral groups and relevant parameters are provided in Table S 1.

*Table S 1.* ***Summary and description of six coral types modelled in the C~scape metacommunity model.*** *Details of taxa selected for parameterisation, specification of parameters relating to discrete transitions in the Integral Projection Models and other parameters such as disturbance susceptibility.*

| **Coral group** | **Tabular *Acropora*** | **Corymbose/ Digitate *Acropora*** | **Spawning *Pocillopora*** | ***Goniastrea / Platygyra*** | **Massive *Porites*** | **Brooding Pocilloporidae** | **Source** |
|---|---|---|---|---|---|---|---|
| Description | Colonies in the *Acropora* genus characterised by flat, table-like structures with horizontal growth and fused branches. | Dense, bushy, growth forms in the *Acropora* genus. | Dense, bushy, growth forms of the *Pocillopora* genera that reproduce predominately via broadcast spawning – i.e. releasing eggs and larvae into the water column. E.g. *Pocillopora verrucosa*. | Domed mound-like semi-spherical or spherical shaped colonies of the genera *Platygyra* and *Goniastrea*. | Domed mound-like semi-spherical or spherical shaped colonies of the *Porites* genus, that can grow to large sizes (>>1m diameter). | Dense, bushy, growth forms in genus *Pocillopora* that reproduce predominately via brooding, meaning they produce fertilized larvae and their offspring tend to settle relatively close to the parent colony. | (Pratchett et al. 2015)<br><br>(Althaus et al. 2015) |
| Taxa growth and survival (juvenile dataset) | *Acropora* spp.<br><br>n growth = 218<br>n survival = 438 | *Acropora* spp.<br><br>n growth = 281<br>n survival = 438 | *Pocillopora* spp.<br><br>n growth = 30<br>n survival = 43 | *Goniastrea* spp.<br>*Platygyra* spp.<br><br>n growth = 27<br>n survival = 33 | *Porites* spp.<br><br>n growth = 150<br>n survival = 214 | *Pocillopora* spp.<br>*Seriatopora* spp.<br>*Stylophora* spp.<br>n growth = 76<br>n survival = 130 | (Doropoulos et al. 2025b) |
| Taxa growth and survival (photogramme try dataset) | *Acropora anthocercis, A. clathrata, A. cytherea, A. sarmentosa, A. solitaryensis, A. hyacinthus,* Tabular *Acropora* spp.<br><br>n growth = 643<br>n survival = 880 | *Acropora cerealis, A. digitifera, A. gemmifera, A. humilis, A. latistella, A. millepora, A. nasuta, A. secale, A. tenuis, A. valida,* 'corymbose' *Acropora* spp.[c], 'digitate' *Acropora* spp.[c]<br><br>n growth = 2350<br>n survival = 3039 | *Pocillopora verrucosa* Pocillopora damicornis* Seriatopora hystrix, Stylophora pistillata.*<br><br>n growth = 1129<br>n survival = 1312 | *Goniastrea* spp. and *Platygyra* spp. with main species being *P. daedalea, P. sinensis, G. edwardsi, G. retiformis.*<br><br>n growth = 814<br>n survival = 876 | *Porites lobata, P. australiensis, P. lutea, P. myrmidonensis, P. solida, P. murrayensis* and *P. mayeri*<br><br>n growth = 1595<br>n survival = 1779 | *Pocillopora damicornis* Pocillopora verrucosa* Seriatopora hystrix, Stylophora pistillata.*<br><br>n growth = 1835<br>n survival = 2232 | (Gordon et al. 2023) |
| Maximum modelled size (cm) | 110 | 50 | 30 | 50 | 80 | 30 | (Madin et al. 2016) |
| Genera used to inform fecundity | *Acropora cytherea, A. hyacinthus,* | *Acropora nasuta, A. spathulata, A. cf. digitifera, A. humilis* | *Pocillopora verrucosa* | *Goniastrea pectinata, G. retiformis* | *Goniastrea pectinata, G. retiformis* | *Stylophora pistillata, Pocillopora damicornis* | (Álvarez-Noriega et al. 2016a) Section 1.3.2 |
| Fertilisation to larvae (proportion) | 0.3 | 0.3 | 0.2 | 0.2 | 0.1 | 1 | (Tsounis and Edmunds 2016) (Dela Cruz and Harrison 2020) |

**P. damicornis and P. verrucosa* were included to boost sample size for building growth and survival regressions in both Brooding Pocilloporidae and Spawning *Pocillopora* groups although they are typically considered brooder and spawners, respectively. However, other than for growth and survival regressions, these groups were considered separately (i.e. for parameterising fecundity and susceptibility to disturbances).

*Table S 1 continued.* ***Summary and description of six coral types modelled in the C~scape metacommunity model.*** *Details of taxa selected for parameterisation, specification of parameters relating to discrete transitions in the Integral Projection Models and other parameters such as disturbance susceptibility.*

| **Coral group** | **Tabular *Acropora*** | **Corymbose/ Digitate *Acropora*** | **Spawning *Pocillopora*** | ***Goniastrea / Platygyra*** | **Massive *Porites*** | **Brooding Pocilloporidae** | **Source** |
|---|---|---|---|---|---|---|---|
| External egg to settler (proportion) | 0.0084 | 0.0084 | 0.0056 | 0.0056 | 0.0028 | 0 | (Tsounis and Edmunds 2016) (Dela Cruz and Harrison 2020) |
| Larval mortality (proportion per 24 hours) | 0.4 | | | | | NA | Section 2.2.3 Fig S 6 (Heyward et al. 2002, Gilmour et al. 2009, Connolly and Baird 2010) |
| Settlement (proportion per 24 hours) | 0.62 in the case where a simulated larvae is above reef substrate (i.e. above a *C~scape* site polygon) | | | | | NA | (Randall et al. 2024) Fig S 6 |
| Survival to 1-year old coral (proportion) | 0.02 (2%) of settlers survive to transition from the discrete 'settler' state to the continuous state of the Integral Projection Models. | | | | | | (Randall et al. 2023) (Suzuki et al. 2024) (Doropoulos et al. 2022) |
| Mean and standard deviation of size at 1-year old (sampled from normal distribution) (cm diameter) | 2.45 (1.43) | 2.45 (1.43) | 1.80 (1.19) | 2.72 (2.00) | 2.34 (1.58) | 2.50 (1.53) | Informed by data in Doropoulos et al 2025 |
| Juvenile cap per $m^2$ available space | 23 | 23 | 12 | 10 | 7 | 12 | Section 1.3.5 |
| Bleaching susceptibility | 1.6 | 1.3 | 0.4 | 0.3 | 0.3 | 2.1 | (Ortiz et al. 2014, Hughes et al. 2018) |
| COTS susceptibility | 35.5 | 7.6 | 7.6 | 8.3 | 1.0 | 7.6 | (Bozec et al. 2025) |
| Cyclone susceptibility | Yes | Yes | Yes | No | No | Yes | (Fabricius et al. 2008) |

## 1.2. Methods growth and survival regressions

### 1.2.1. Predictor variables

*Table S 2.* ***Variables considered in regressions of coral growth and survival.***

| Variable | Details | Specifications regarding fixed or random variable and transformations |
|---|---|---|
| Size at time t0 | Coral colony two-dimensional planar area $cm^2$ at the beginning on the monitoring period. Photogrammetry data was obtained as planar area in $cm^2$ through analysis of orthomosaics (Toor et al. 2025) while juvenile quadrat data was obtained as maximum colony diameter which was converted to area by assuming the colonies were circular.<br><br>It is established that growth and survival are size dependent (Hughes 1984, Pratchett et al. 2015). | Fixed.<br>Continuous.<br>Natural log-transformation. |
| Sampling period | Days between initial and final measurement on coral colonies. This was included to account for variation in the time between colony measurements. Annual predictions are then made from the regressions by setting this variable to 365 days.<br><br>Range: 240-488<br>Median: 365<br>Mean: 351 | Fixed.<br>Continuous.<br>Scaled. |
| Seabed waterflow intensity | Output from a wave model (the SWAN model https://espace.library.uq.edu.au/view/UQ:8246441, (Callaghan et al. 2015)) was used to gives an estimate of the force water movement at the seabed exerts on corals. We selected the metric 'root mean squared horizontal velocity amplitude', or 'ubed_mean', which is a metric describing the water velocity at the seabed in m/s.<br><br>EcoRRAP Range: 0.05-0.38<br>EcoRRAP Median: 0.22<br>EcoRRAP Mean: 0.22<br>*C~scape* Case Studies 10th percentile: 0.11<br>*C~scape* Case Studies 10th percentile: 0.45<br>*C~scape* Case Studies Median: 0.23<br>*C~scape* Case Studies Mean: 0.26 | Fixed.<br>Continuous.<br>Scaled. |
| Depth (m) | EcoRRAP Range: 2.9-12<br>EcoRRAP Median: 4.4<br>EcoRRAP Mean: 5.2<br>*C~scape* Case Studies 10th percentile: 0.8<br>*C~scape* Case Studies 90th percentile: 15.4<br>*C~scape* Case Studies Median: 6.2<br>*C~scape* Case Studies Mean: 6.8 | Fixed.<br>Continuous.<br>Scaled. |
| Region | Data included in the models come from three regions on the GBR:<br>Offshore Central Great Barrier Reef<br>Offshore Northern Great Barrier Reef<br>Offshore Southern Great Barrier Reef<br>(Fig S 4) | Fixed.<br>Categorical. |
| 1 \| Reef / Site / Plot | There were at least two reefs surveyed per Region and 2-5 sites per reef. Each site had four plots. | Random.<br>Categorical. |

### 1.2.2. Growth, survival and fecundity Bayesian models

Bayesian linear and generalised linear mixed-effects models were fit for growth and survival as a function of the initial log-transformed coral colony area ($cm^2$), $\ln A_t$. We considered site depth (m), $D$, modelled seabed waterflow intensity ($m.s^{-1}$), $W$, and GBR region, $R$, as covariates (Table S2). We also included the number of days, $N$, between surveys to account for the variable time between resampling surveys (while surveys aimed to be approximately annual, this is not exact due to the logistics of field surveys). We incorporated an interaction between initial colony area and the GBR region, to allow for potential spatial differences in the relationship between initial colony size and growth and survival along the GBR's latitudinal gradient (Table S2). To account for the hierarchical sampling design, we included nested random intercepts for plot within site, and site within reef.

Coral growth was modelled as the natural log-transformed colony area at the end survey point ($\ln A_{t+1}$) assuming a Student *t*-distribution with an identity link; this distribution was a robust alternative to a Gaussian distribution, as it is less sensitive to outliers in the data.

$$\ln A_{t+1} \sim \text{Student}(\mu, \sigma, \nu)$$

with the mean structure as

$$\mu = \beta_0 + \beta_{1-8} X + \zeta Z$$

where $\beta$ is a vector of fixed effects ($\beta_0$ is the model intercept and $\beta_{1-8}$ are the slopes), $X$ is a matrix of predictors (survey time period, waterflow intensity, depth, GBR region), $\zeta$ a vector of random effects, $Z$ is matrix of random effects (plot nested in site nested in reef).

The standard deviation, $\sigma$, was modelled as a function of the initial log-transformed colony area ($\ln A_t$) to allow for variability in growth to change with coral size. The model was specified as:

$$\sigma = \gamma_0 + \gamma_1 \ln A_t$$

and $\gamma_0$ is the standard deviation when area is 1 $cm^2$ ($\ln A_t = 0$) and $\gamma_1$ is the slope that controls how the residual standard deviation changes with $\ln A_t$; $\nu$ the degrees of freedom for the Student t-distribution.

We used a combination of weakly and moderately informative priors for $\beta, \zeta, \gamma, \nu$. Priors for the intercept were set based on the median and median absolute deviation (MAD) of the initial log-transformed colony area data for each functional type, while other fixed effects were given a weakly informative normal prior centred at 0, with a standard deviation of 1. $\nu$ was given a gamma prior, and the standard deviations of the random effects were given a Student t-prior via group centering.

$$\beta_0 \sim N(5.9, 2.2); \beta_{1-8} \sim N(0, 1);\ \nu \sim \Gamma(2, 0.1);$$
$$\zeta \sim \text{Student}(3, 0, 1.5);\ \gamma_0 \sim \text{Student}(3,0,2.5); \gamma_1 \sim \text{U}(-\infty, \infty)$$

Coral survival was modelled using a Bayesian generalised linear mixed-effects model (GLMM). We assumed that the binary response variable, $S_{t+1}$ where 1 represents survival and 0 represents mortality), followed a Bernoulli distribution with a logit link function.

The model structure was specified as:

$$S_{t+1} \sim \text{Bernoulli}(\rho)$$

$$\text{logit}(\rho) = \beta_0 + \beta_{1-8} X + \zeta Z$$

Where $\rho$ is the probability of coral survival. The vectors and matrices for fixed effects ($\beta$) and random effects ($\zeta$) retain the same meaning as defined in the growth model. The priors for the survival model were specified as:

$$\beta_0 \sim N(0, 2.5); \beta_{1-8} \sim N(0, 2);\ \zeta \sim \text{Student}(3, 0, 2.5)$$

An interaction was considered between initial size and the region, to allow the potential for regional-specific trends with size.

Both growth and survival models were fitted using Hamiltonian Monte Carlo (HMC) with no-U-turn sampler (NUTS) in R (version 4.4.1) using the brms package (Bürkner, 2017) and implemented with Stan (Stan Development Team, 2023). We set four independent chains, each with 4000 iterations. The first 2000 iterations were discarded as warm-up, leading to a total of 8000 posterior draws. Convergence was assessed by ensuring all $\hat{R}$ (Gelman and Rubin 1992) values were less than 1.01. Sampling was controlled using an adaptation delta of 0.99 and a maximum tree depth of 20 to ensure adequate convergence.

We explored different covariate combinations between depth, waterflow intensity, and GBR region and compared models using the Leave-One-Out Information Criterion (LOOIC) via the *loo* package (Vehtari et al. 2021) in R. We considered models to have comparable predictive accuracy if the difference in Expected Log Predictive Density (ELPD) was less than twice the standard error (SE) of the difference. Predictors provided varying levels of predictive support across coral types, and several models demonstrated similar predictive performance and equivalent Bayesian R2 values (Table S3). Ultimately, we retained the full model—incorporating initial colony size, survey period, depth, GBR region, and waterflow intensity—to ensure all theoretically relevant drivers were accounted for within the *C~scape* framework. This approach facilitated a consistent comparison of variable importance across the entire community and will allow for the future incorporation of more data, noting that the regressions reflect a single year of vital rate data.

Coral-level fecundity, $F_{t+1}$, defined as the total number of oocytes produced by a colony, was modelled in a comparable way to growth and survival, as a function of coral size, $\ln A_t$ ($cm^2$). This was calculated as the product of colony size, $\ln A_t$, polyp density ($\delta$), and oocytes abundance per polyp ($\psi$) (Mulla et al. 2024, Cresswell et al. 2024):

$$F_{t+1} \sim \delta \times \psi \times lnA_t$$

Due to limited data availability for all taxa, this multi-component approach was only employed for tabular *Acropora*, Corymbose/Digitate *Acropora* and *Goniastrea/Platygyra*.

Polyp density, $\delta$, was assumed to be independent of colony size. Using data described in in (Álvarez-Noriega et al. 2016b) and provided in (Madin et al. 2023) which measured the polyp density we assigned a truncated normal distribution for polyp density ($\delta$, per 2D projected colony surface area ($cm^{-2}$)):

$$\delta \sim \overline{N}(\mu, \sigma, \theta, \omega)$$

We empirically calculated the mean ($\mu$) standard deviation ($\sigma$) lower ($\theta$) and upper ($\omega$) bounds from the available data for each of these coral types. This allowed us to capture uncertainty in a way that could be linked to the Bayesian posterior draws from the other models. We chose to truncate the normal distribution to prevent sampling from the long tails of the standard normal distribution outside of the available observed data, thereby ensuring all values remained within a biologically realistic range.

Data for these same coral types were available (Madin et al. 2023) for oocytes per polyp $\psi$, and this was modelled as a function of coral size, $lnA_t$, to account for the transition of corals from non-reproductive to fecund states. We used a Bayesian hurdle model to separately account for the presence or absence of oocytes and the subsequent count for fecund polyps.

The hurdle component, determining the probability (pi) of a polyp being fecund, followed a Bernoulli distribution with a logit link:

$$b(\psi) \sim \text{Bernoulli}(\pi)$$

$$\text{logit}(\pi) = \gamma_0 + \gamma_1 \ln A + \zeta_{HU} Z$$

where $\gamma_0$ is the hurdle intercept, $\gamma_1$ is the effect of colony size on the of being fecund, and $Z$ represents the random effects.

For fecund polyps, the count component ($\lambda$) followed a log link:

$$\psi \sim \text{Poisson}(\lambda) | \psi \sim \text{NB}(\lambda, \phi)$$

$$\log(\lambda) = \beta_0 + \zeta Z$$

In this framework, $\beta_0$ represents the expected oocyte count for a fecund polyp at the reference size, and $Z$ represents the random effects for colonies nested within species. Tabular and Corymbose/Digitate *Acropora* were modelled assuming a Poisson distribution, whereas *Goniastrea/Platygyra* utilised a Negative Binomial distribution to account for overdispersion, with a gamma(3, 0.5) prior assigned to the shape parameter.

Priors were derived from preliminary fits of simple linear and generalised linear models to the data to derive informative means for the intercepts and slopes. The specific fixed-effect priors for each coral type were as follows:

Tabular *Acropora*: $\beta_0 \sim N(1.65, 0.1);\ \gamma_0 \sim N(-1.83, 1.0);\ \gamma_1 \sim N(0.35, 0.5)$

Corymbose/Digitate *Acropora*: $\beta_0 \sim N(1.8, 0.05);\ \gamma_0 \sim N(-7.65, 1.0);\ \gamma_1 \sim N(1.81, 0.5)$

*Goniastrea/Platygyra*: $\beta_0 \sim N(3.98, 0.2);\ \gamma_0 \sim N(-2.25, 1.0);\ \gamma_1 \sim N(0.82, 0.5)$

For all functional types, random effects were specified as:
$\zeta \sim \exp(5)\ ;\ \zeta_{HU} \sim \text{Student}(3, 0, 2.5)$

Finally, 8,000 posterior draws from these models were multiplied by 8,000 samples from the empirical polyp density distributions to allow propagation of fecundity uncertainty into the Integral Projection Model (IPM).

## 1.3. Parameterising early life history

### 1.3.1. Coral life cycle processes and parameters

Various parameters in Table S 1 relate to transitions in the coral life cycle. *C~scape* is designed to model the major life stages and the processes linking them; these are categorised as fecundity, fertilisation, larval dispersal (connectivity), settlement, survival and growth in the first year, and survival and growth in the continuous stage (Fig S 1).

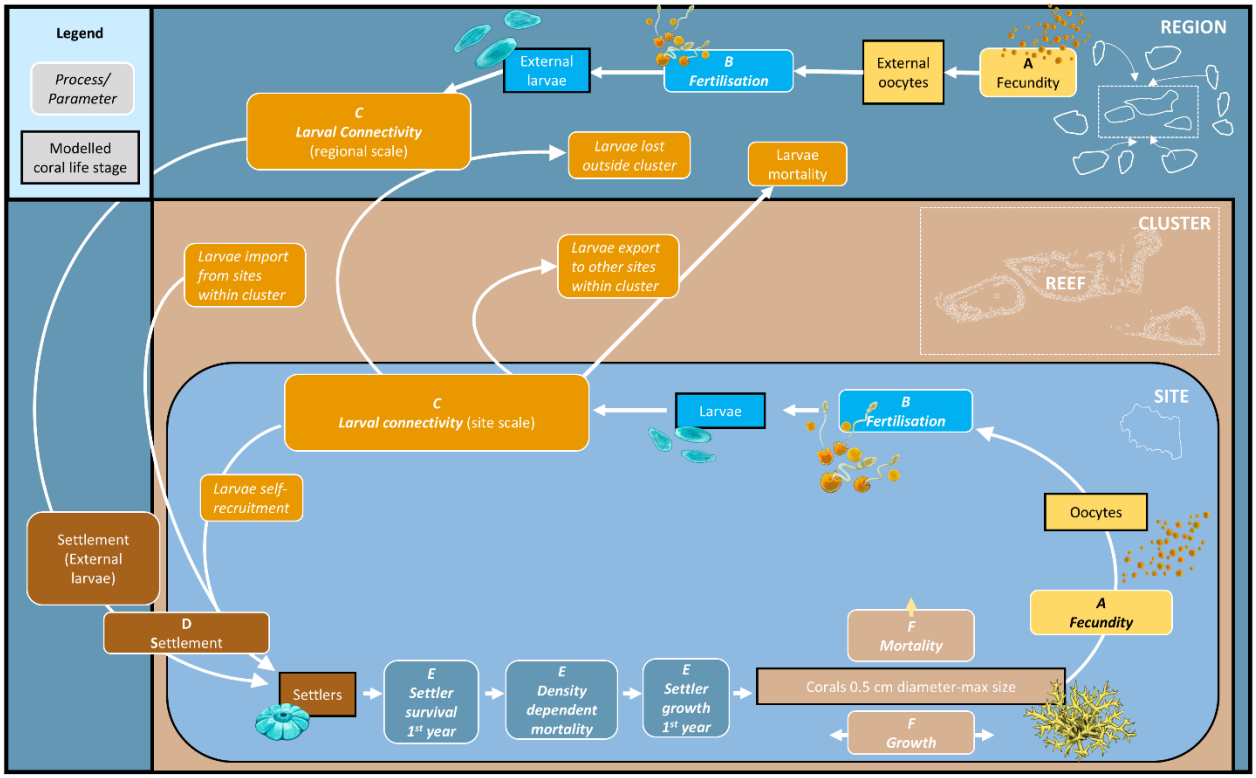


*Fig S 1.* ***A schematic representation of the coral life cycle as simulated in the C~scape framework.*** *Major life stages (black-outlined rectangles) and the biophysical processes/parameters linking them (white-outlined rounded boxes). Three major spatial scales are represented by the large nested rectangular boundaries: the site scale, at which each coral population is simulated, the cluster scale (at which a cluster of reefs composed of several hundred sites is captured), and the region scale, which accounted for the influence of larvae from outside of the cluster simulated using C~scape. Transitions between life stages are categorised into (A) size-dependent fecundity, (B) fertilisation of oocytes to larvae, (C) larval dispersal and connectivity at site and regional scales, (D) settlement, (E) survival and growth during the first year of life (subject to density-dependent mortality), and (F) survival and growth within the continuous stage of the IPM. Early life stage icons by Dean Tysdale.*

### 1.3.2. Fecundity

Details of fecundity functions for the coral groups with detailed empirical data are in the main text.

Given the limited and highly variable empirical data for massive *Porites*, we applied the fecundity scaling relationships derived from *Goniastrea/Platygyra.* We adjusted the *Goniastrea/Platygyra* function for massive *Porites* based on information in the literature which suggested initial size of reproduction was 9 cm diameter (Rapuano et al. 2023). For the Spawning Pocillopora we followed the calculated in (Tsounis and Edmunds 2016), to estimate reproductive output of 6,327±1,882 eggs $cm^{-2}$ (range: 4,158–7,524). These values were used to generate a truncated normal distribution to simulate egg production across the size range, with maturity set at 12 cm diameter (Tsounis and Edmunds 2016, Rapuano et al. 2023). For brooding Pocilloporidae, annual planulae production was estimated by integrating monthly release data assuming a six-month reproductive window. Assuming a mean mature colony size of 20 cm diameter (314 $cm^2$), we derived a reproductive output of 68 larvae cm-2 (21,498±3,522 per colony). Reproductive onset for this group was parametrised at 5 cm diameter.

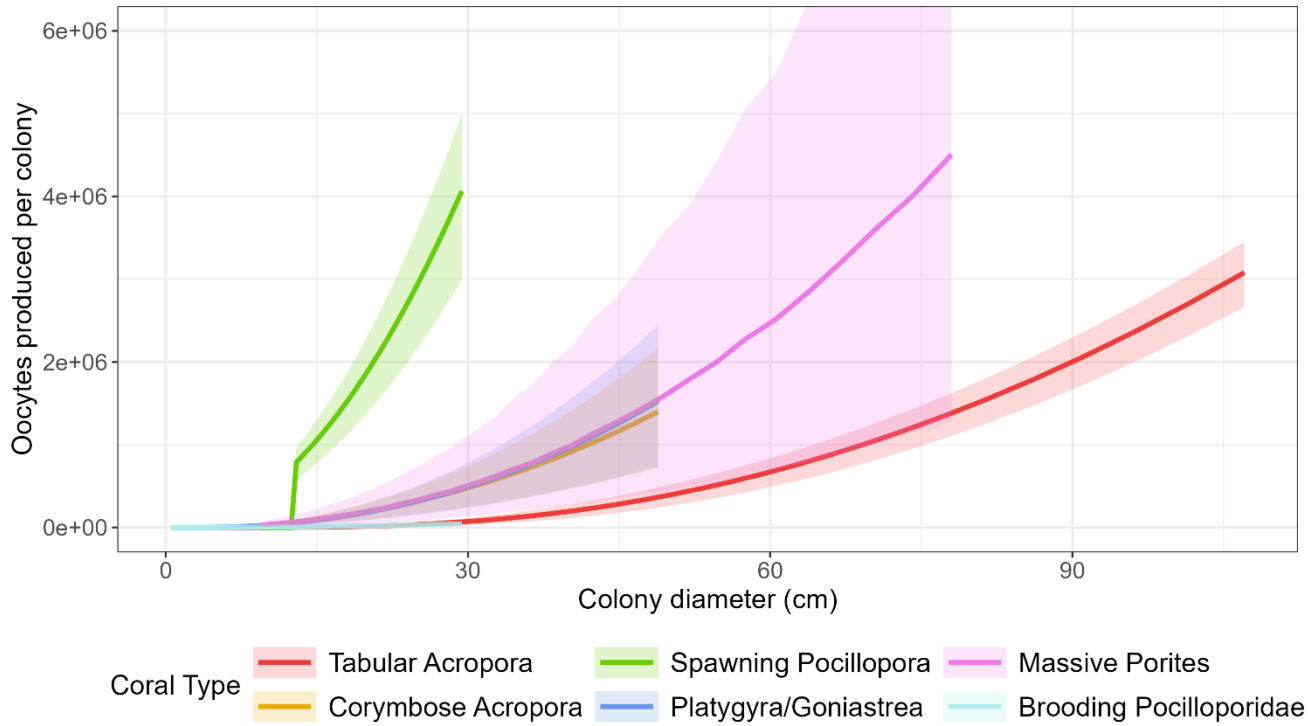


*Fig S 2.* ***Reproductive output as a function of colony size across coral types.*** *Colony-level fecundity (total oocytes (or larvae in the case of the brooding coral) produced) as a function of colony diameter for the six coral types (modelled as log-colony area ($cm^2$), shown in diameter for ease of interpretation). For tabular Acropora, corymbose Acropora, and massive Goniastrea/Platygyra, fecundity was estimated by integrating Bayesian hurdle models of oocyte density (oocytes per polyp as a function of colony area) with truncated normal distributions of polyp density ($cm^{-2}$). For spawning Pocillopora, brooding Pocilloporidae and massive Porites, reproductive output was derived from parameters in the literature. Solid lines represent mean posterior predictions or the mean, and shaded areas indicate the 95% credible intervals.*

### 1.3.3. Fertilisation

Information of fertilisation success in broadcast-spawning corals suggested high variability with limited field measurements. Estimates ranged from 5% to 95% depending on taxa, sperm concentration, colony proximity, and hydrodynamic conditions (Tsounis and Edmunds 2016, Dela Cruz and Harrison 2020, Mumby et al. 2024). For instance, *Acropora millepora* and *A. tenuis* showed fertilisation rates of ~8% at low sperm concentrations, rising to >97% at higher densities (Dela Cruz and Harrison 2020). Similar variability was observed in merulinid species such as *Favites colemani* (28.4% to 95.2%) and the *Orbicella* species complex (Levitan et al. 2014). We applied mid-range fertilisation probabilities of 0.3 for *Acropora* species, 0.2 for spawning *Pocillopora* and *Goniastrea/Platygyra*, and 0.1 for massive *Porites*.

To account for the arrival of settlers from external reef sources—for which we obtained oocyte count data—we defined an additional parameter to describe the probability of an external egg surviving to settlement. Within the Cscape framework, this was captured in the connectivity modelling via a daily mortality (Fig S 1); however, for external larvae, we assumed a minimum travel time of seven days to reach the reef cluster. Over this period, the same daily mortality rate of 0.4 was applied ($0.6^7$). The resulting total probability for external settlement ranged from 0.0028 to 0.0084 across the five spawning functional types, while brooding Pocilloporidae were assigned a value of 0, assuming recruitment was primarily driven by internal or immediate local supply.

### 1.3.4. Survival and growth to 1-year old

Benthic marine organisms typically exhibit Type III survivorship curves (Gosselin and Qian 1997, Hunt and Scheibling 1997, Doropoulos et al. 2022), characterised by very high mortality immediately following settlement which decreases as individuals increase in size. Empirical studies on the GBR and globally report first-year survivorship of <1% (Sato 1985, Babcock and Mundy 1996, Raymundo and Maypa 2004, Suzuki et al. 2024). However, recent studies on the GBR utilising various settlement substrates have recorded higher mean survival rates; for instance, *Acropora tenuis* exhibited proportional survival between 2-7% after approximately one year (Randall et al. 2021, 2023) and up to 2% (Doropoulos et al. 2019). Given the high spatial variation in post-settlement mortality (Doropoulos et al. 2016, 2022), we parameterised the transition from the discrete 'settler' state to the continuous stage of the integral projection models using 2% (0.02) survival. This value reflects the consensus regarding the intense post-settlement bottleneck observed in the region while aligning with recent empirical measurements, but we acknowledge high uncertainty in this parameter.

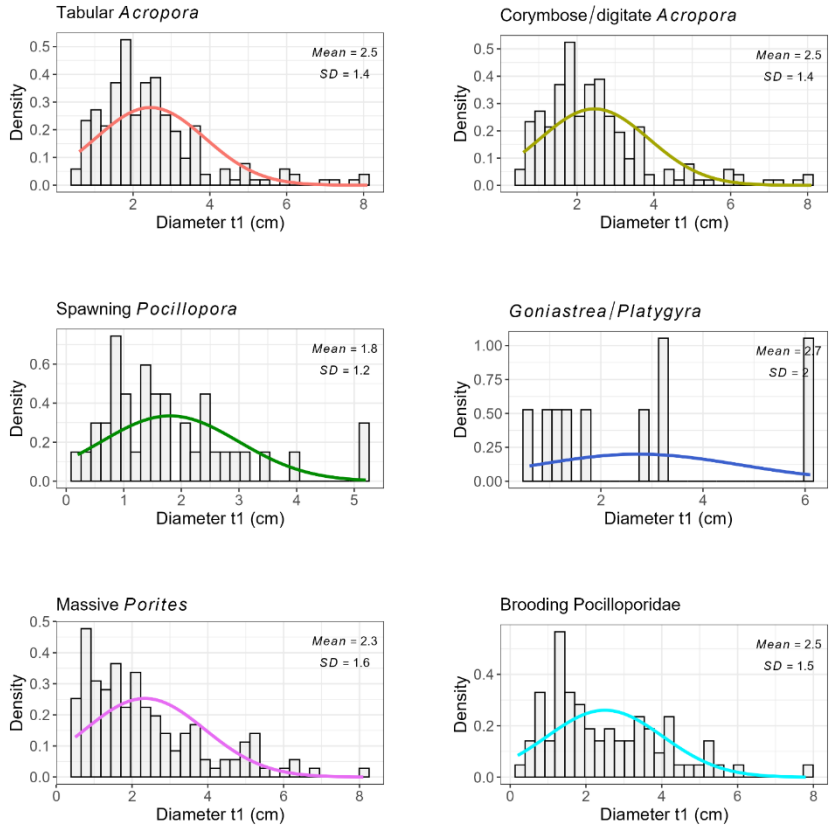


*Fig S 3.* ***Size frequency distributions of newly observed coral recruits assumed to be approximately 1-year old across six coral types.*** *Data represent individuals recorded within juvenile quadrats (<30 mm diameter) in 2022 that were not present in 2021. Grey bars indicate the observed density of colony diameters (cm). Coloured lines represent a fitted normal distribution for each coral type, with corresponding mean and standard deviation (SD) values provided in the top-right corner of each panel. Functional types include tabular Acropora, corymbose/digitate Acropora, spawning Pocillopora, Goniastrea/Platygyra, massive Porites and brooding Pocilloporidae. This distribution was used to parameterise the size at which corals enter the continuous stage of the integral projection models.*

### 1.3.5. Calculation of density dependent mortality (juvenile cap)

To establish the juvenile density threshold (see main text), we calculated the 99th percentile of juvenile counts (<5 cm diameter) observed across offshore reef clusters in the EcoRRAP field surveys, resulting in a total maximum density of 88 juveniles $m^{-2}$ of available substrate. To partition this aggregate limit among the six modelled coral types, we first determined the mean density of each group using field-derived transect data. For the massive *Porites* group, we applied a correction factor by dividing the observed Porites juvenile density by three; this adjustment accounts for the high prevalence of encrusting and branching Porites morphologies in field datasets that do not align with the massive growth forms simulated in the model. These adjusted densities were subsequently converted into proportional ratios to reflect the relative

taxonomic composition of the juvenile community. By multiplying these proportions by the 88 juveniles $m^{-2}$ aggregate threshold, we derived type-specific caps that preserve the observed community structure within the model's ecological limits (Table S 1). This approach ensured that the functional types collectively represent the broader coral assemblage while remaining grounded in empirical density distributions.

# APPENDIX 2. Model simulations and inputs

## 2.1. Representative reefs Study

*Table S 3. Specifications and parameters for representative reefs simulations. Abbreviations are: GBR = Great Barrier Reef; DHW = Degree Heating Weeks.*

| Specification | Details | Parameter value |
|---|---|---|
| Spatial characteristics: Location, reef and site size, proportion coral habitat | Three representative reefs were simulated in each of the North, Central and South regions. Each reef was 40 ha in total area, composed of four sites, each which were 10 ha each.<br>Each site was parameterised with 85% of the area as 'coral habitat' (the median across the GBR case study sites), meaning the maximum coral cover that may be obtained at a site was 85%. | Sites per reef: 4<br>Reef area: 40 ha<br>Site area: 10 ha<br>Proportion coral habitat per site: 85% |
| Site characteristics: Environmental | To represent the range of depth and seabed waterflow intensity conditions that occur within reefs (and reflecting those that were sampled in the vital rate dataset) each of the four sites in all reefs were characterised with different combinations of depth and seabed waterflow intensity representing a high and low value for both conditions. | Shallow-Low waterflow: 3m, 0.1m/s<br>Shallow-High waterflow: 3m, 0.3m/s<br>Deep-Low waterflow: 12m, 0.1m/s<br>Deep-High waterflow: 12m, 0.3m/s |
| Connectivity assumptions | For simplicity we assumed no connectivity between the four sites. To determine a representative parameter for settlement success in each site we analysed connectivity matrices for GBR case studies (see section 3.2) for spawning corals. These matrices describe the probability of a larvae produced at each site successfully settling at every other site.<br>We had 12 connectivity matrices available, three for each cluster. We calculated the column sums of the matrix (settlement probability at each receiving site), then took the median of these values per matrix.<br>To get a single parameter to took the mean (0.0003) of these.<br>The brooding Pocilloporidae group was parameterised to have 10 times higher settlement success in the site of production as a reflection of their life history strategy. | Self-recruitment spawning coral: 0.0003<br><br>Self-recruitment brooding coral: 0.003 |
| Demographic parameters | Growth and survival were predicted as a function of the spatial characteristics of the reef and sites -- region (North, Central or South), depth and seabed waterflow intensity – via the covariate factors in the growth and survival regressions. | Unique to the region (North, Central or South) of the representative reefs, and the seabed waterflow intensity and depth of the sites. |
| Adaptation specifications | Heritability has been investigated in many studies across different species and locations, and generally it tends to 0.3 for large sample sizes. Thermal tolerance classes were assigned based on computational requirements as well as representation of current and likely future distributions. The range matches the one investigated in Bozec et al. (2025) for the upper limit DHW=8, while the lower limit has been adjusted to reduce the amount of thermal classes. The minimum of DHW=-5 was chosen as this represents 95% of the current range (Humanes et al, 2022) and overall thermal tolerance is not likely to reduce in the future. The starting distribution of heat tolerances was assigned based on a 30-day temperature stress test experiment (Humanes et al, 2022). | Heritability: 0.3<br>Thermal tolerance classes:<br>Minimum: 5DHW<br>Maximum: 8DHW<br>(14 tolerance classes total)<br>Initial heat tolerance:<br>mean= 0; S.D.= 1.91 |
| Disturbance regime | Simulations were run for each of the three representative reefs for 50 years. Following an undisturbed period of 20 years, a heatwave disturbance was parameterised every 10 years so that the dynamics of impact and recovery could be explored. | Simulations run for 50 years.<br>Disturbance timing: year 20, 30, 40 and 50.<br>Disturbance magnitude: 8DHW |
| Initialisation | All scenarios were initialised with equal coral cover, split equally across the six coral types. | Initial total coral cover: 5% |

## 2.2. GBR case studies

### 2.2.1. Spatial context

In the representative reefs study, we simulated a theoretical reef for each region; for the GBR case studies, we selected clusters of reefs grouped together spatially. We focussed on offshore reefs, as distinct from inshore reefs which tend to be more turbid and subject to other stressors such as water quality which were not considered here. The selection of case studies was guided by the location where EcoRRAP vital rate data on growth and survival was collected, and whether long-term monitoring was conducted in at least two reefs

in the chosen cluster by the Australian Institute of Marine Science Long-Term Monitoring Program (LTMP) Table S 11.

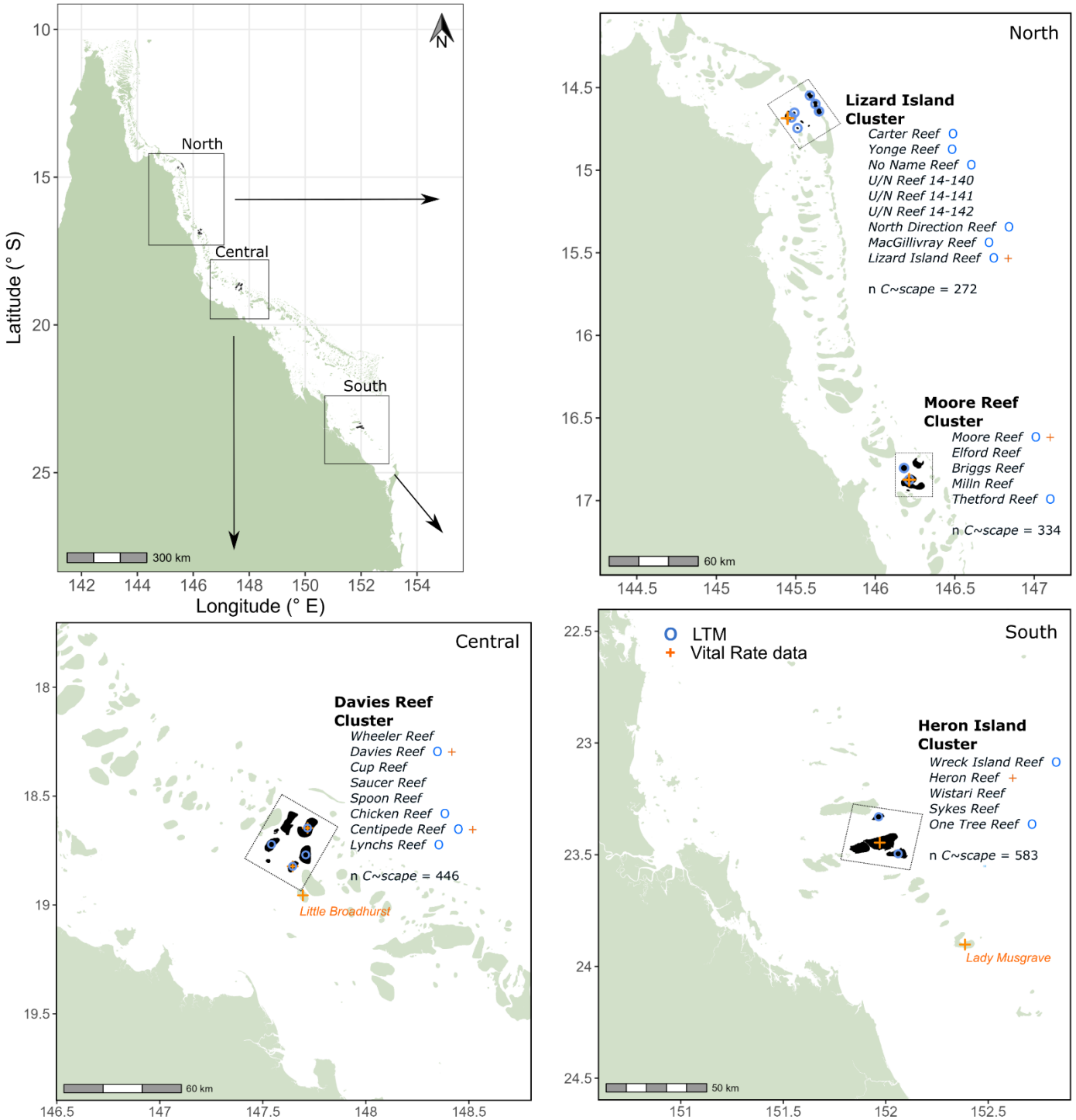


*Fig S 4.* ***Spatial context of the Great Barrier Reef case studies and data acquisition.*** *North, central, and southern regions are shown in panels alongside a map of Queensland, Australia. Within these regions, four reef clusters were selected as case studies: two in the north, and one in each of the central and southern regions. Reefs modelled in the C~scape framework are coloured black, with rectangular polygons indicating cluster boundaries. Underneath each cluster name, individual simulated reef names are listed; symbols next to these names indicate if they are an Australian Institute of Marine Science Long-Term Monitoring Program (LTMP) reef (blue circle) or a location where vital rate data (EcoRRAP) was collected (orange plus). The total number of sites simulated in the C~scape framework is denoted by n. Reefs where vital rate data (EcoRRAP) were obtained but were not inside the case study cluster are named in orange text.*

### 2.2.2. Reef partitioning to sites

Reef boundaries were determined using a publicly available geomorphic zonation map (GBRMPA, 2021) that depicted features such as reef crests, slopes, flats, and lagoons (Roelfsema et al., 2021). This mapping extended to ~20 m depth and was generated via machine learning (random forest classifier) using Sentinel-2 imagery (10 m pixels) and physical attributes (depth, slope, wave environment), followed by expert-driven contextual editing (Lyons et al., 2020).

It is well established that different geomorphic zones are formed by distinctive environmental conditions (Done, 1982). Consequently, coral community composition and dynamics are generally more similar within geomorphic zones than between them. Following the recommendations of Kennedy et al. (2021), we only considered the zones that are expected to have predominantly hard substrate — Reef Slope, Reef Crest, Outer Reef Flat and Sheltered Reef Slope — as these are areas we expect appropriate habitat and conditions for corals to grow (description in table S1, Roelfsema et al., 2021).

To simulate spatially varying processes (e.g., connectivity, depth), each geomorphic zone was partitioned into smaller units. We first pixelated zones into hexagonal cells (~20 m diameter) using the H3 geospatial indexing system (resolution 12) via the package h3 (Cooley and Shao 2023). These hexagons were merged using a step-wise spanning tree approach. Delaunay triangulation was employed to identify proximal hexagons, bridging gaps between distant reef areas. Vertices were weighted based on Euclidean distance and depth differences. A minimum spanning tree (MST) identified the path that connected all hexagons while minimising depth variation (mst() function in the sfnetworks package (Van der Meer et al. 2024) in R software). Finally, cluster analysis divided hexagons into groups along the MST path using the skater package (Turner et al. 2022). The goal was to obtain sites of similar area to the RECOM grid size (used for connectivity and temperature downscaling within reefs) of approximately 62,500 m.

Sites were further characterised by overlaying polygons on a 10×10 m bathymetric map (https://www.eomap.com/) to assign median depth. Waterflow intensity was assigned from SWAN model outputs (Callaghan et al. 2015) ('ubed mean' https://espace.library.uq.edu.au/view/UQ:8246441). Benthic category maps (Roelfsema et al. 2020) were used to calculate the actual proportion of 3D surface area that is available for coral colonisation. In this mapping product, each 10×10 m pixel is classified as one of four benthic categories: Sand, Rubble, Rock, Coral/Algae. Site polygons were overlaid on the benthic map and the number of pixels of each of the four categories were used to determine the proportion of suitable habitat for corals by assuming Sand and Rubble were not appropriate substrates. Although each 10×10 m pixel is assigned a specific type of benthic cover48, this does not imply that each pixel consists entirely of the assigned benthic type. Instead, this assignment indicates the predominant cover within a given pixel (having largest proportional cover), yet other benthic types could be present. Therefore, in this study we assumed that 90% of any pixel classified as Coral/Algae or Rock was potential coral habitat, whereas pixels classified as Sand or Rubble were assumed to only be 10% potential coral habitat.

Each site has a two-dimensional (2D) area according to the boundaries of its polygon. However, many parts of a reef are sloping, and therefore may have larger area than captured by the planar area. Therefore, a three-dimensional (3D) area was calculated for each site using a "surface-to-horizontal-area ratio" derived from the slope value estimated for each pixel. Slope was estimated by using a local gradient method (3×3 m window) from the bathymetric map. The slope-adjusted surface area, i.e., 3D surface area, was calculated using the trigonometric formula for all pixels within a site.

$$A_{3D} = A_{2D} / \cos(\text{slope})$$

where slope is expressed in radians.

The final 3D area per site was then calculated as the 2D area times the calculation of 2D to 3D ratio based on the average slope of pixels.

For each of the four clusters, a variable number of sites was delineated (Fig S 4, Fig. S12) with total modelled reef areas within the four clusters ranging from 1812−4959 hectares. Once the characterisation of coral habitat is considered this translates to a maximum possible coral cover that could theoretically be achieved on these reefs ranging from 1432-2895 hectares.

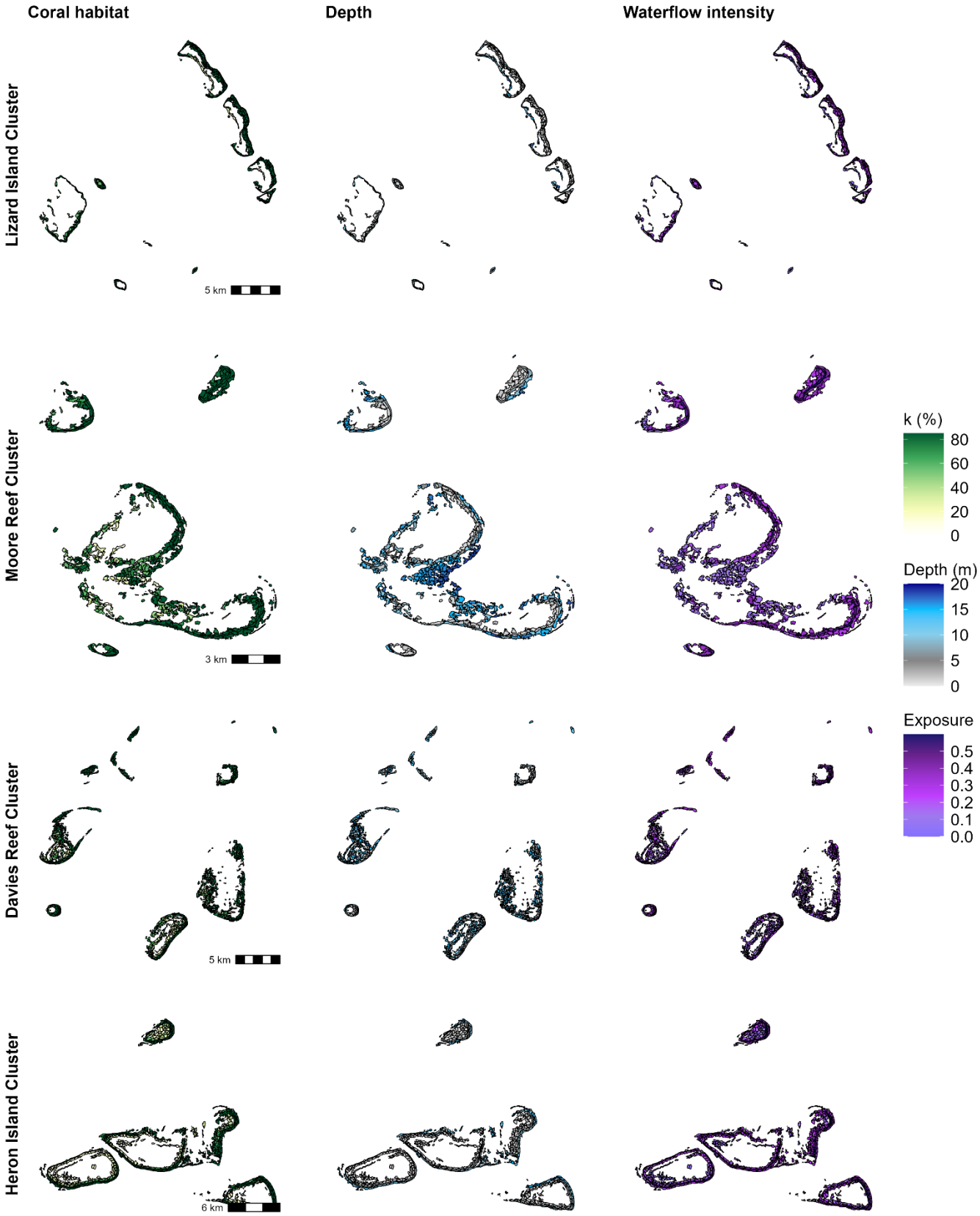


*Fig S 5.* ***Characterisation of sites in the Great Barrier Reef case study clusters.*** *Reef clusters were selected across the north, central, and southern regions of the Great Barrier Reef (Fig S 4). Case study regions are in descending latitudinal order in rows: Lizard Island Cluster and Moore Reef Cluster (North), Davies Reef Cluster (Central), and Heron Island Cluster (South). Each cluster is partitioned into reef sites, with columns illustrating the spatial distribution of key environmental variables: coral habitat (%), median depth (m); and waterflow intensity (m/s).*

### 2.2.3. Connectivity

**Step 1**

We required a hydrodynamic model that could capture fine-scale hydrodynamics that influence larvae dispersal or retention to a reef.

We used hydrodynamic model (SHOC, driven by RECOM—Relocatable Coastal Model (https://research.csiro.au/ereefs/models/models-about/recom/, (Herzfeld 2009; Steven *et al.* 2019), using a rectilinear grid with a spatial resolution of 200–250 m, nested this within a subset of the 1 km grid hydrodynamic model (GBR-1 version 2.0), of the Great Barrier Reef Marine Park (Steven et al. 2019). This setup provided hourly 2D and 3D velocity fields at the fine spatial scale, while accounting for the larger scale processes captured by the 1 km model. Detailed methods are available in (Ani et al. 2024). Hydrodynamic modelling was conducted for the period from October to January for 2015, 2016 and 2017.

**Step 2**

Larval dispersal was simulated using OceanParcels (Delandmeter and Van Sebille 2019), a Lagrangian ocean analysis tool that can be used to create customisable particle tracking simulations using velocity outputs from hydrodynamic models.

For the connectivity application the most likely spawning times and days were identified, and particle tracking was simulated during this time. Therefore, we used the hydrodynamic outputs for the 10-day period following three estimated annual mass-spawning night in 2015 and 2016 and split-spawning in 2017 (Table 1). Split spawning occurs when the annual reproductive event of a coral population is divided over two consecutive months, instead of a single synchronised spawning event. Coral mass spawning usually occurs around the spring-summer transition and peaks 4–6 days after the full moon, but varies depending on the reef location, the timing of the full moon and other environmental conditions. Spawning days were identified as: 2015 - November 30, December 1 and 2; 2016 - November 18, 19 and 20; 2017 - November 8, 9 and 10, December 8, 9 and 10. Passive particles were released from random locations within the site polygons of each reef cluster (see fig 9. (Ani et al. 2024)) every 27 sec from 8:00 pm to 11:00 pm, at 2.25 m below the surface during each spawning day. In each of the spatial polygons, 401 particles were released every spawning day. This equates to, for example for Moore Reef Cluster, a total 133,934 of virtual larvae released within the cluster domain every spawning day.

The particle tracking model was run for a duration of 10 days with a 3-minute time step but driven by hourly water velocities from the hydrodynamic model. The released particles were tracked over time, and their location was updated every 15 min until the end of the simulation. Although water velocities were calculated on a grid resolution of approximately 250 m, the Lagrangian particle tracking was not limited to a grid and hence locations to be tracked at a sub grid-scale resolution.

**Step 3 – Post processing**

Larvae were assumed to be neutrally buoyant and competent to settle between 4 and 10 days after spawning. Processes such as larval mortality are highly variable and poorly characterised. Here we followed assumptions in (Grimaldi et al. 2022, Ani et al. 2024). Based on data from larval rearing experiments and *in-situ* decreases in abundances of larvae following spawning (Heyward et al. 2002; Gilmour et al. 2009, Connolly and Baird 2010) we applied a constant daily mortality rate of 0.40 $d^{-1}$ implemented across 15-minute timesteps. This equates to a mortality rate of approximately 0.0053 per timestep (i.e. 0.5% of larvae are assumed to die during each 15-minute time-step) (Fig S 6).

We developed the post-processing approach in (Ani et al. 2024) which assumed that larvae settled immediately upon encountering the first suitable site polygon during the competency window. The approach used here incorporates greater ecological realism by accounting for both the stochastic nature of settlement and probabilistic mortality throughout the competency period. Under this approach, larvae do not automatically settle upon contact; instead, the probability that larvae successfully settle when positioned over a reef site during the competency window was set at 0.01 per 15-minute timestep. This settlement threshold was selected to reflect that not all larvae encounter suitable micro-habitats or successfully transition from the water column upon first contact with a reef area, and was loosely informed to give a

cumulative settlement probability that aligned with those presented in fig. 3 (Randall et al. 2024) for *Acropora* species.

**Step 4 – Transition probability matrix**

The post-processed settlement data were used to compute a connectivity (or transfer probability) matrix among sites for each night and year of spawning. Connection strength between source and sink sites was defined as the proportion of larvae released at a source site that successfully settled at a sink site. The sum of each row in the matrix is ≤ 1, reflecting the total proportion of larvae released from a site that settle on one or more other reef sites. In contrast, the sum of each column can exceed 1, as it represents the cumulative arrival of larvae from multiple source sites: For example, a sum of 1.5 would indicate that the total number of larvae arriving at the site in question was 150% of the number of larvae released from any one site, and this might be a collection point for larvae from many sites.

For the simulations in this study, we averaged connectivity matrices across the spawning nights. We used data from three different years and cycled through these years in the *C~scape* simulations, except for the Lizard Island cluster. Due to extremely low connectivity in two of the three years for this cluster, we used only the 2016 matrix for Lizard Island.

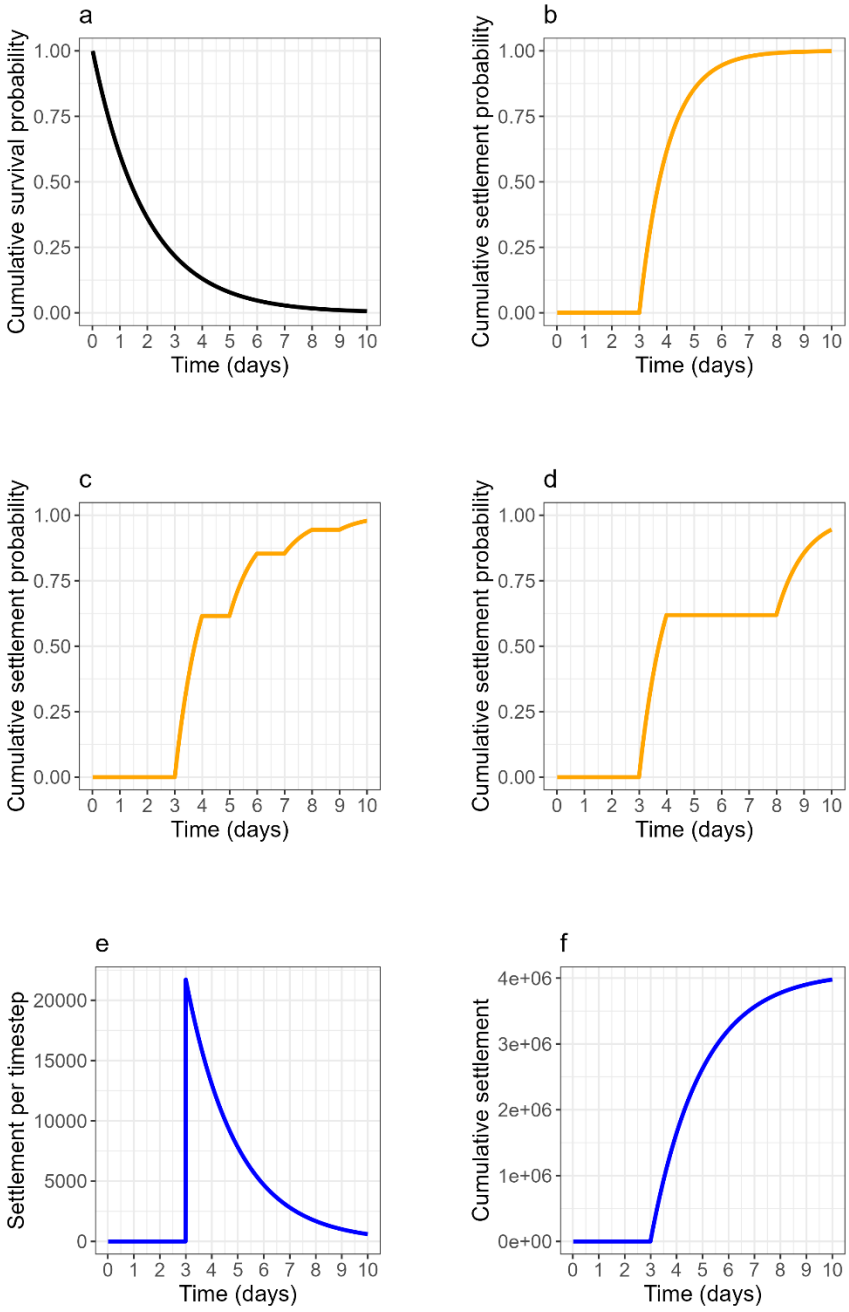


*Fig S 6. Larval survival and settlement dynamics modelled at 15-minute resolution over a 10-day period under several scenarios. (a) Cumulative probability of a larva remaining alive, assuming a constant daily mortality rate of 40% from the time larvae are released. (b) Cumulative probability of settlement for larvae that are unable to settle during the first 3 days (pre-competency period) but can settle thereafter with a per-timestep settlement probability of 0.01 when they are above the simulated reef area. (c) Cumulative settlement probability for a scenario identical to (b), except larvae are presumed to be in the open ocean every second day after day 3, during which settlement cannot occur. (d) Cumulative settlement probability for a scenario where larvae spend days 5–8 off the reef (settlement prohibited) but are assumed to be above the reef on all other days. (e) and (f) show results for a scenario in which the initial larval cohort consists of 10 million individuals: (e) shows the expected number of larvae settling per 15-minute timestep (alive × settlement probability), and (f) shows the cumulative number of larvae settled across the 10-day period, integrating mortality and settlement processes across all timesteps. In all panels, settlement is possible only when larvae are assumed to be above reef habitat, mortality is applied continuously through time, and the x-axis represents days since release.*

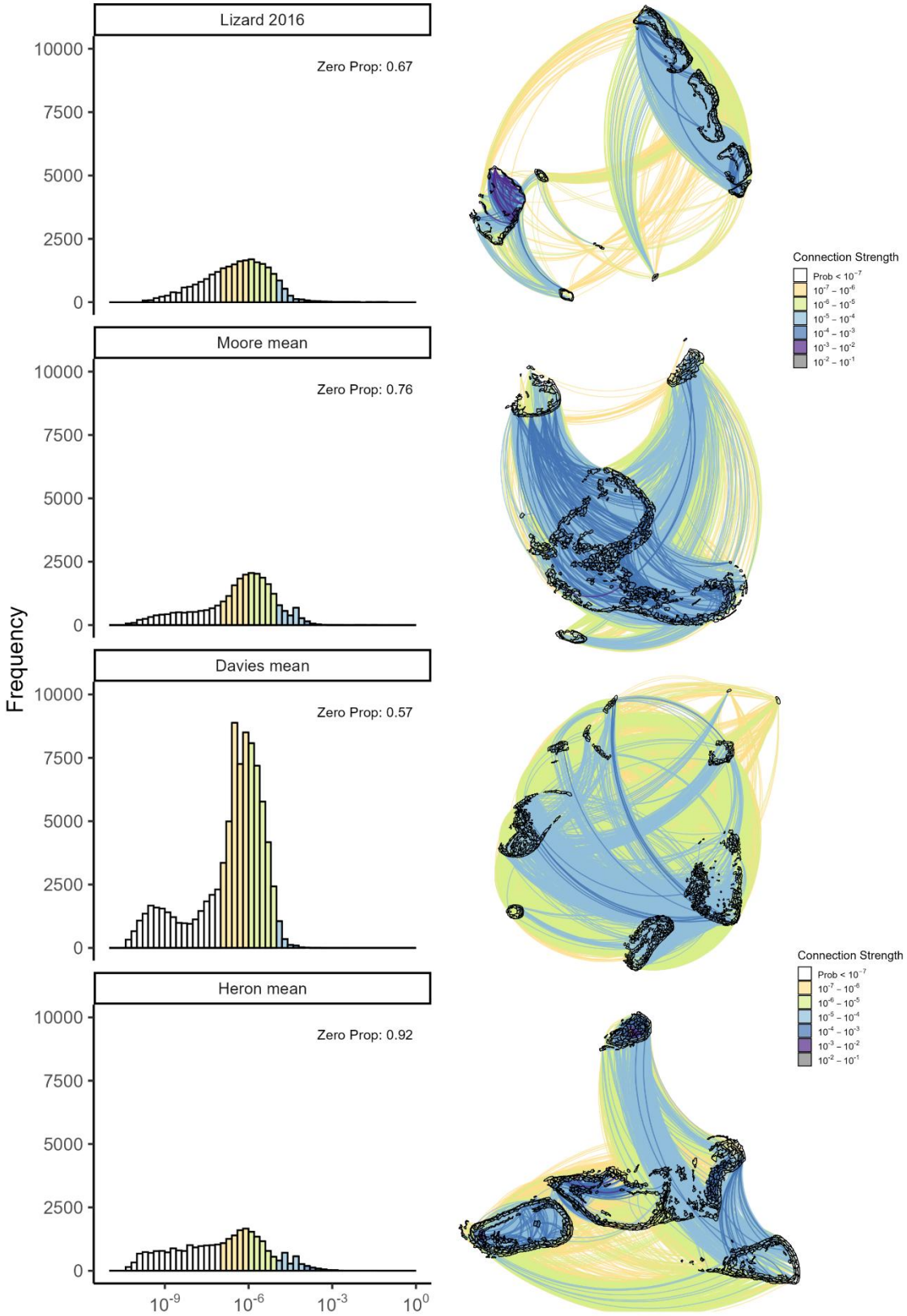


*Fig S 7. Connectivity as the probability that larvae spawned at one site are transported, survive, and successfully settle at another. Values shown are the mean across the three modelled years, except for the Lizard Island Cluster, where only 2016 is shown due to extremely low connectivity in the other years. Left panels show histograms of non-zero transition probabilities (including self-recruitment) on a $\log_{10}$ scale (the proportion of zero transitions which are not show here is given in the top right of the plot). Right panels visualise the relative strength of connections between sites. On the $\log_{10}$ scale, probabilities can be interpreted as follows: if 10 million ($1\times10^{7}$) larvae are produced at a site, and the connectivity probability to another site is $1\times10^{-6}$, then 10 larvae will successfully arrive and settle at the receiving site.*

### 2.2.4. Simulation details

*Table S 4. Specifications and parameters for GBR case studies.*

| Specification | Details | Parameter value |
|---|---|---|
| Spatial characteristics: Location, reef and site size, proportion coral habitat | Two reef clusters were simulated in the north, and one in each of the central and southern GBR regions | **Lizard Island Cluster (North)**<br>Reefs within cluster: 9<br>Sites within cluster: 272<br>Total 3D reef area (ha):<br>1812 Total 3D coral habitat area (ha): 1432<br>**Moore Reef Cluster (North)**<br>Reefs within cluster: 5<br>Sites within cluster: 334<br>Total 3D reef area (ha): 2396<br>Total 3D coral habitat area (ha): 1796<br>**Davies Reef Cluster (Central)**<br>Reefs within cluster: 8<br>Sites within cluster: 446<br>Total 3D reef area (ha): 3551<br>Total 3D coral habitat area (ha): 2583<br>**Heron Island Cluster (South)**<br>Reefs within cluster: 5<br>Sites within cluster: 583<br>Total 3D reef area (ha): 4959<br>Total 3D coral habitat area (ha): 2895 |
| Demographic parameters | Growth and survival were predicted as a function of the spatial characteristics of the reef and sites -- region (North, Central or South), depth and seabed waterflow intensity – via the covariate factors in the growth and survival regressions. | Unique to the region (North, Central or South) of the representative reefs, and the seabed waterflow intensity and depth of each sites. |
| Regional variation in coral cover at time of demographic survey | A site-specific scale, $d_{i,t}$, is applied in the application of density dependence (equation (4) main text) and requires a parameter on the coral cover at the time demographic data was collected to account for the influence this may have on observed growth rates. | Assumed carrying capacity at EcoRRAP sites: 90% total coral cover.<br>Coral cover 2021 North: 21.2<br>Coral cover 2021 Central: 24.4<br>Coral cover 2021 South: 40.1 |
| Adaptation specifications | Heritability has been investigated in many studies across different species and locations, and generally it tends to 0.3 for large sample sizes. Thermal tolerance classes were assigned based on computational requirements as well as representation of current and likely future distributions. The range matches the one investigated in Bozec et al 2025 for the upper limit DHW=8, while the lower limit has been adjusted to reduce the amount of thermal classes. The minimum of DHW=-5 was chosen as this represents 95% of the current range (Humanes et al, 2022) and overall thermal tolerance is not likely to reduce in the future. The starting distribution of heat tolerances was assigned based on a 30-day temperature stress test (Humanes et al, 2022). | Heritability: 0.3<br>Thermal tolerance classes: Minimum—5DHW<br>Maximum = 8DHW<br>(14 tolerance classes total)<br>Initial heat tolerance:<br>mean= 0; S.D.= 1.91 |
| Disturbance regime | Multi-model GCM ensembles, in which each model provides quasi-independent estimates of future climate, are commonly used to represent structural uncertainty (Qian et al. 2016). For each case study, 30 scenarios across 20 stochastic realisations were run under three shared socioeconomic pathways and 10 Global Climate Models (GCMs). | SSPs: SSP1-2.6, SSP2-4.5, SSP3-7.0<br><br>GCMs: CNRM-ESM2-1, EC-Earth3-Veg, IPSL-CM6A-LR, MRI-ESM2-0, UKESM1-0-LL, GFDL-ESM4, MIROC-ES2L, MPI-ESM1-2-HR, MIROC6, NorESM2-LM |
| Initialisation | Simulations were initialised based on the total coral cover recorded in the AIMS LTMP manta tow observations from the starting year of the hindcast (2008) from reefs within the simulated clusters that had LTMP data. Coral type composition was informed from the fixed-position transects | |

### 2.2.5. Acute disturbance scenarios – Thermal stress

These SST projections were available at coarse spatial resolution (80-500km), but downscaled to 10 km resolution using semi-dynamical shelf-sea modelling (McWhorter et al. 2022). Annual maximum Degree Heating Weeks (DHW) were computed from the SST projections.

A major uncertainty in climate projections is how sensitive global warming is to greenhouse gas emissions. Equilibrium Climate Sensitivity (ECS), which measures the temperature rise from a sustained doubling of $CO_2$, helps compare climate models. This selection of climate models span a range of climate sensitivities (Bozec et al. 2025).

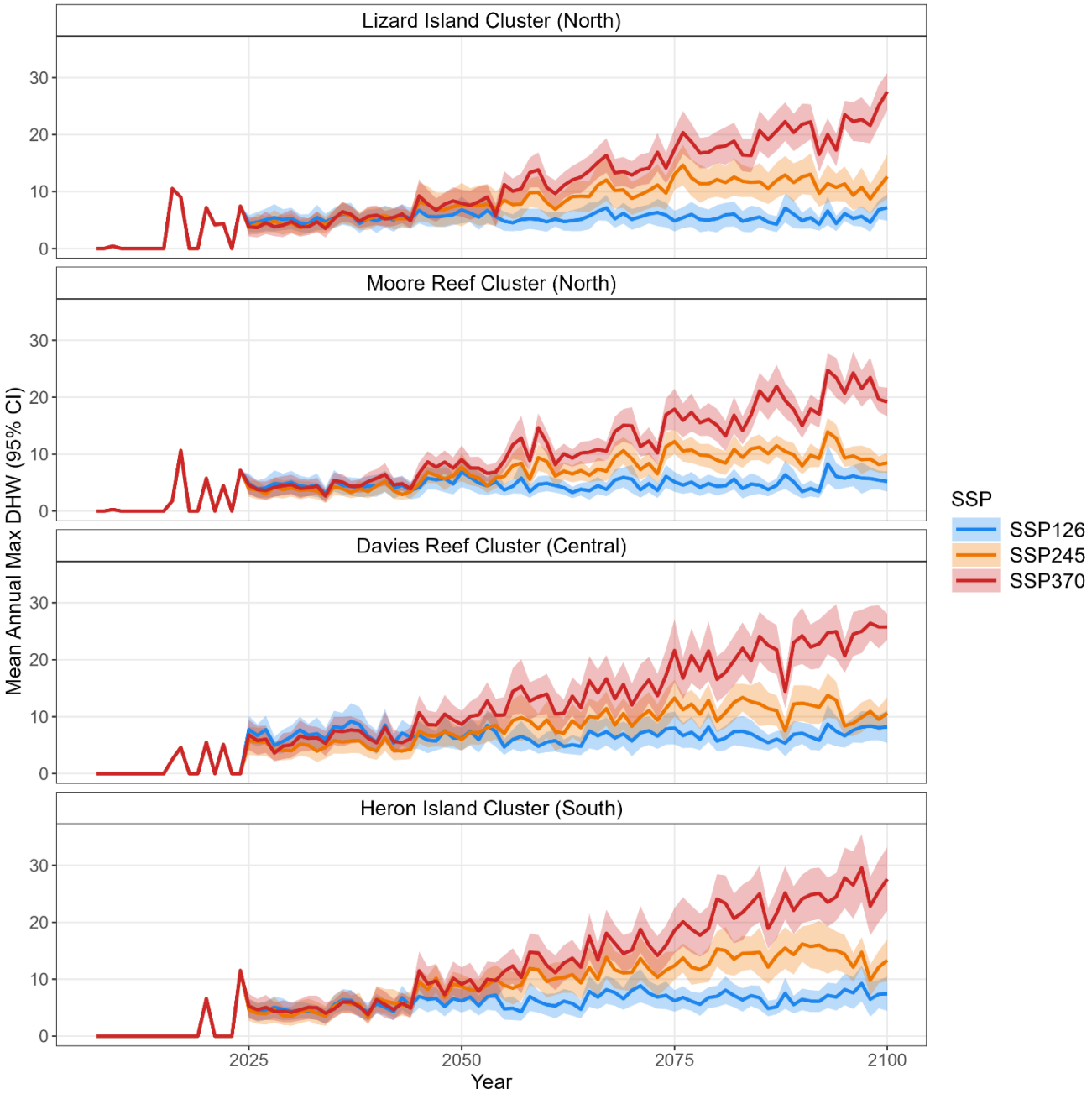


*Fig S 8.* ***Average Degree Heating Weeks (DHW) projections for each Great Barrier Reef case study (panels) and each Shared Socioeconomic Pathway (coloured lines and ribbons).*** *Solid lines indicate the ensemble mean for each Shared Socioeconomic Pathway (SSP), representing the average across all contributing climate models and site-specific realisations. Shaded ribbons represent the 95% confidence interval, illustrating the degree of uncertainty and spread between different climate model projections.*

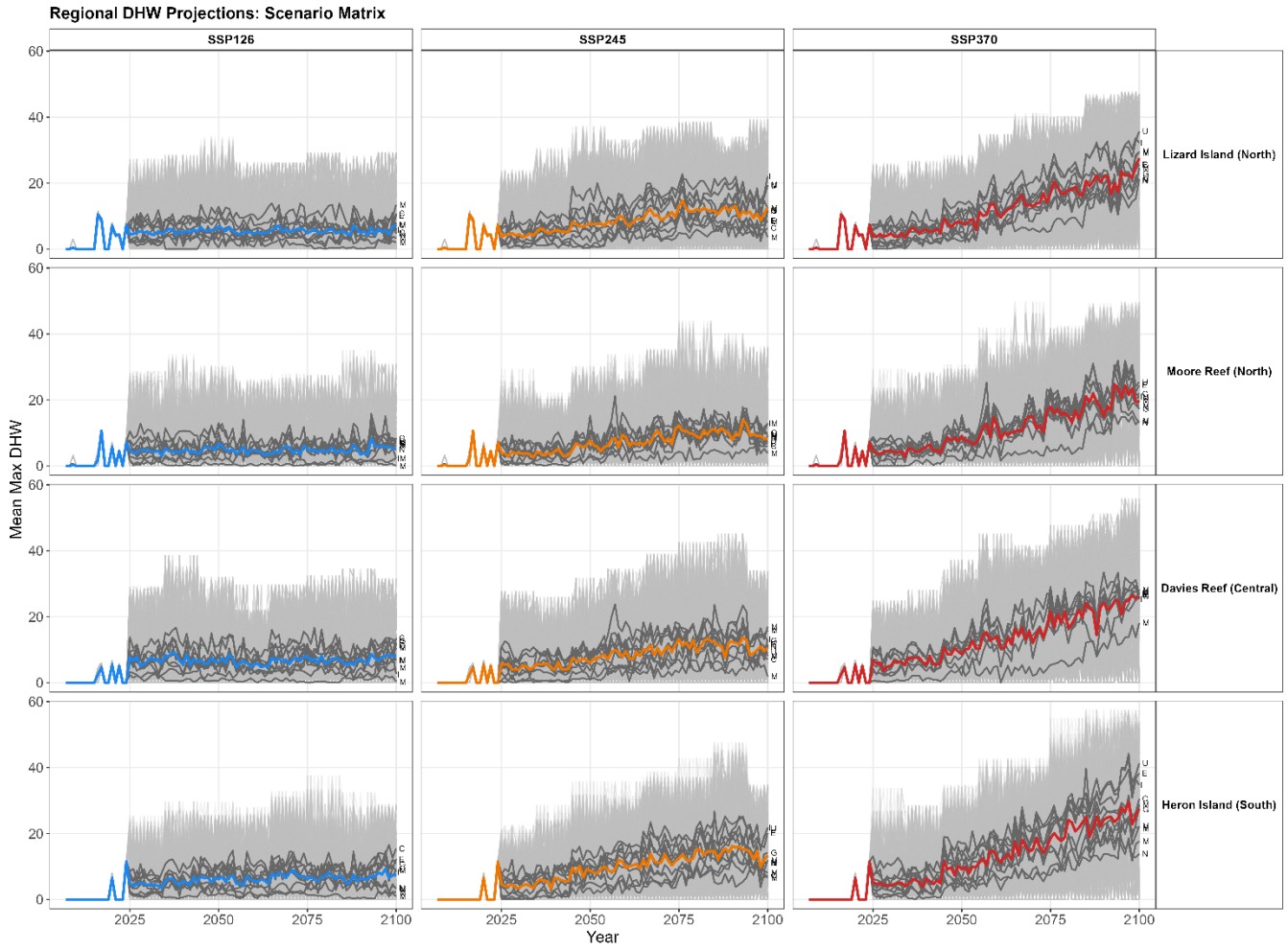


*Fig S 9.* ***Degree Heating Weeks (DHW) projections for each Great Barrier Reef (GBR) case study (panels) and each Shared Socioeconomic Pathway (coloured lines and ribbons).*** *Panels are organised with Shared Socioeconomic Pathways (SSPs) as columns and the 4 GBR case studies as rows. Within each panel, light grey lines represent individual realisations (n=20) of each Global Climate Models (n=10). Dark grey lines denote the mean trajectories of each climate model (n= 10), with letter indicating the starting letter of the specific climate model. The bold, coloured lines represent the multi-model ensemble mean for each scenario.*

We further downscaled future thermal stress from the reef level to the individual site level (~250 m), using high-resolution hindcasts from the eReefs RECOM model (Steven et al. 2019). This was done for the period from 1 November in the preceding year through to 30 April in the years 2016, 2017 and 2020 (i.e., years with the historically higher acute thermal stress) for each of the four GBR case studies. Sea surface DHW was modelled, as depth was handled separately in the coral mortality functions (Fig S 29).

We overlaid the *C~scape* reef sites onto the RECOM grid (~250x250m) and assigned each site with the closest RECOM grid value.

For each site, *i* within a reef, we calculated the residual deviation, $R_{i,y}$, for each year, *y,* from the reef-wide mean DHW ($DHW_{reef,y}$).

$$R_{i,y} = DHW_{i,y} - DHW_{reef,y}$$

Preliminary data analysis suggested that the spatial variability scaled with increasing heat stress; we therefore fitted a global logarithmic relationship between the site residuals and reef-level DHW across all clusters:

$$|R| = a_0 + a_1 \log\left(DHW_{reef}\right)$$

Where $a_0$ and $a_1$ are the estimated parameters ($a_0 = 0.301, a_1 = 0.109$).

To preserve site-specific spatial characteristics, we derived a modifier ($b_i$) representing the relative deviation of a site's observed residual from the globally predicted mean residual:

$$b_{i,y} = \frac{R_{i,y}}{a_0 + a_1 \log(DHW_{reef,y})}$$

For each site, we calculated the mean modifier, $b_i$, across the three RECOM years. Site-level DHW was then calculated annually as:

$$DHW_{i,t} = DHW_{reef,t} + b_i(a_0 + a_1 \log(DHW_{reef,t}))$$

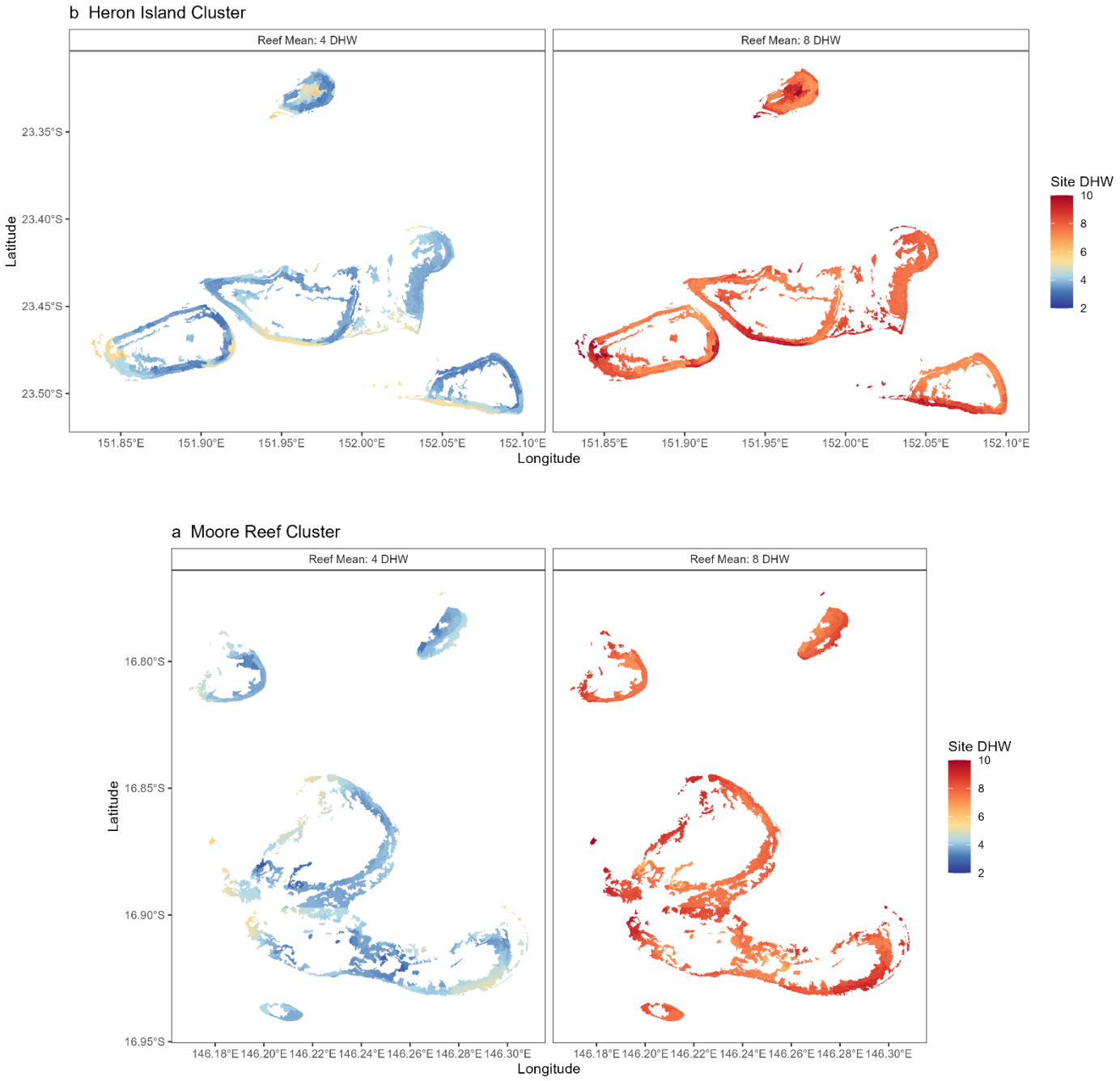


*Fig S 10.* ***Spatial downscaling of reef-level thermal stress.*** *The reef-level average annual maximum Degree Heating Weeks (DHW) value is translated into site-specific values (colour gradient) based on analysis on RECOM modelling during historical bleaching events. The spread of DHW across sites that would result for (a) the Moore Reef and (b) the Heron Island Cluster is shown for a 4 DHW event (left) and an 8 DHW event (right).*

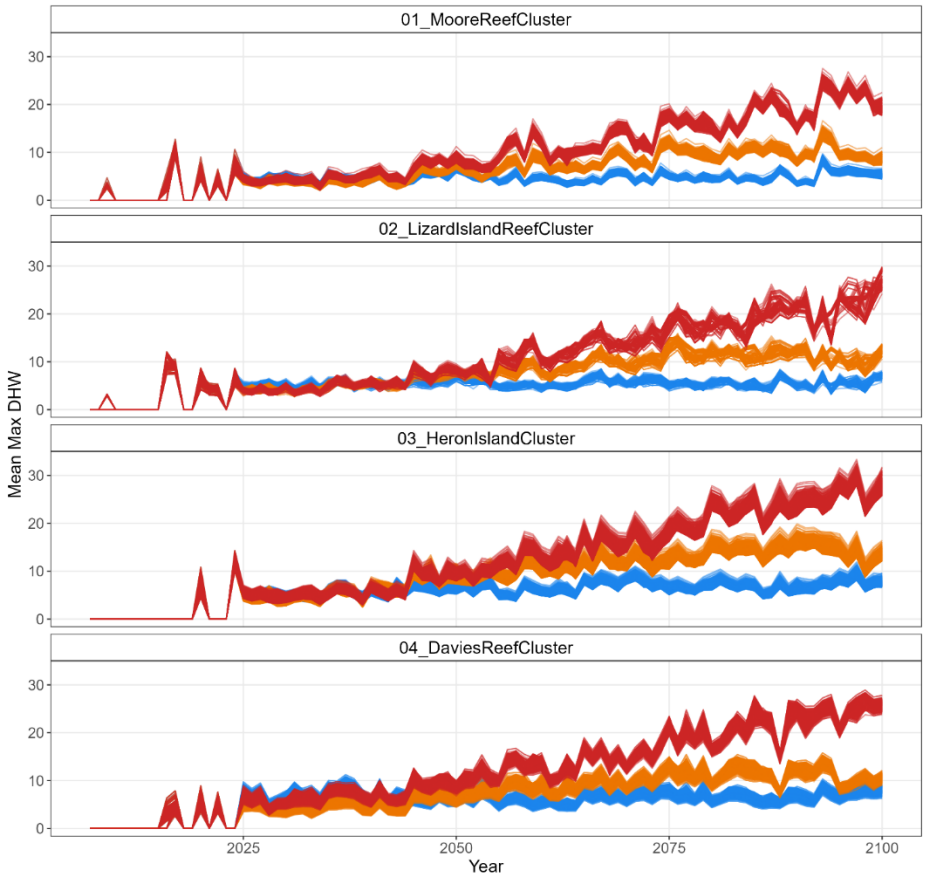


*Fig S 11. Degree Heating Weeks (DHW) projections averaged to the site level across Global Climate Models and realisations for each cluster and each Shared Socioeconomic Pathway.*

The cyclone exposure at each reef in each year was determined with the approach used in (Bozec et al. 2022, Cresswell et al. 2024) and all sites within a reef received the same cyclone category value. Past exposure to cyclones for all GBR reefs was derived from sea-state predictions of wave height (Puotinen et al. 2016). The potential for a coral-damaging sea state (wave height >4 m) was determined using a map of wind speed every hour within 4 km pixels across the GBR for cyclones between 2008 and 2024. Any reef containing a combination of wind speed and duration capable of generating >4 m waves, assuming sufficient fetch, was scored as positive for potential coral-damaging sea state in the respective year. In these cases where damaging waves were predicted, an estimate of cyclone category was deduced from the distance to the cyclone track extracted from the BoM historical database (http://www.bom.gov.au/cyclone/tropical-cyclone-knowledge-centre/understanding/tc-info/)

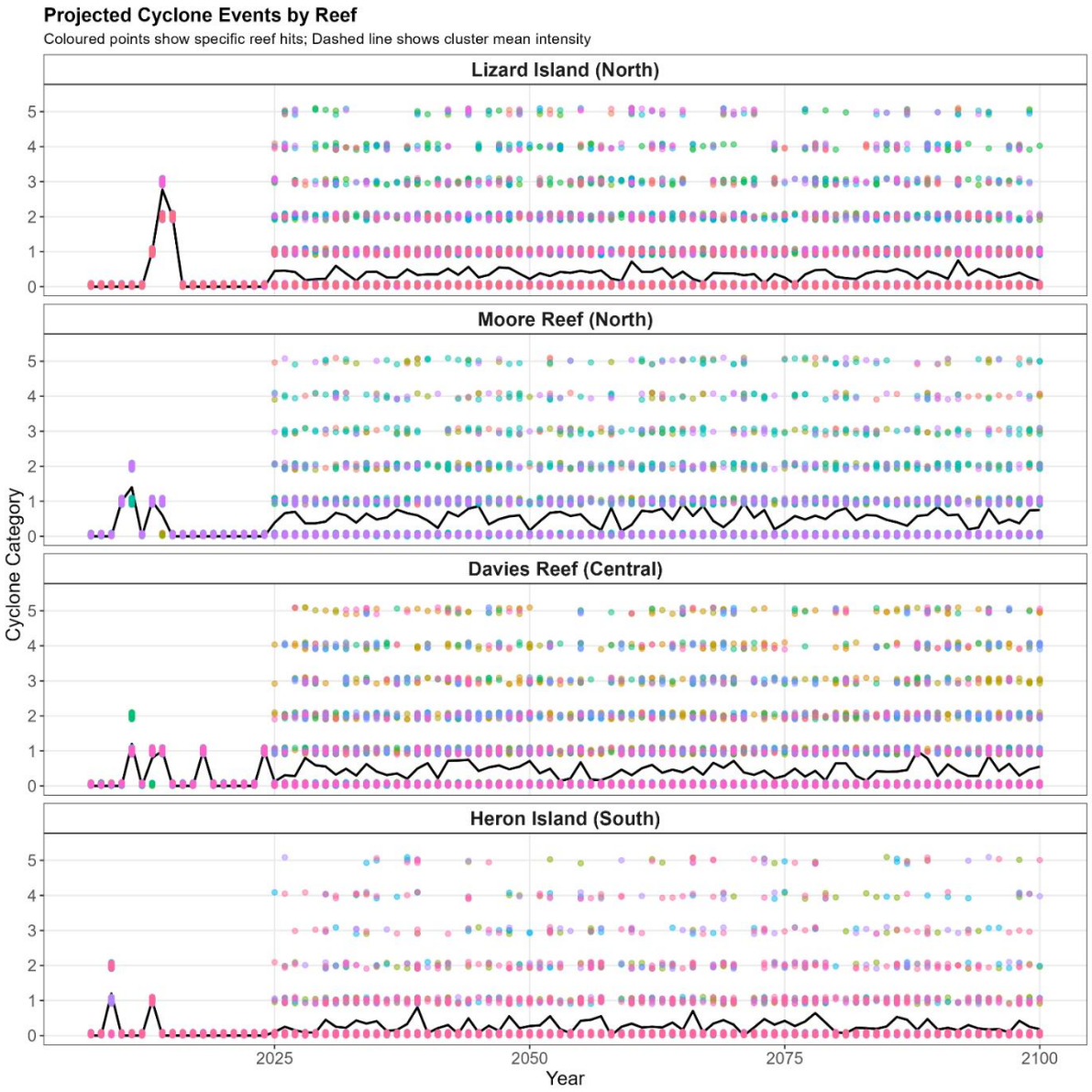


*Fig S 12.* ***Cyclone events by reef across Great Barrier Reef (GBR) case studies.*** *Annual projections of cyclone intensity (Categories 0–5) across the simulated time period. Panels represent the four GBR case studies (rows), arranged latitudinally. Within each panel, individual points represent discrete cyclone realisations (n = 20), jittered to illustrate the frequency and magnitude of events. Points are coloured according to individual reefs within each case study. The black line represents a cluster-wide mean intensity per year. Within this modelling framework, cyclone trajectories are treated as a stochastic disturbance regime that remains stationary across all Shared Socioeconomic Pathways (SSPs) and Global Climate Models (GCMs).*

The projected density of adult COTS individuals per hectare (10,000 m2) was obtained for each reef and year from output from the ReefMod-GBR (v7.2) simulations (Fig S 13).

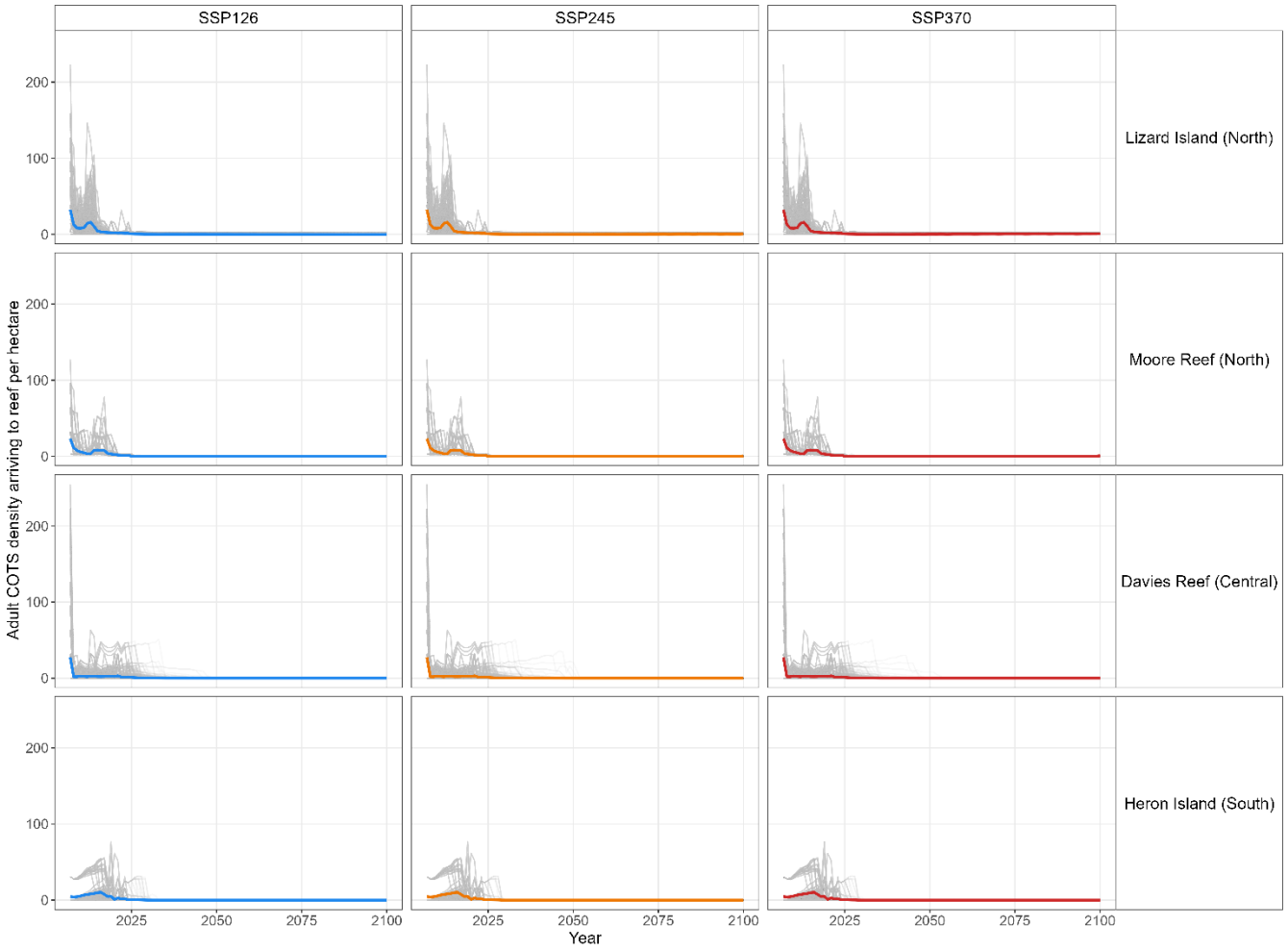


*Fig S 13.* ***Adult Crown-of-Thorns-Starfish (COTS) density by Shared Socioeconomic Pathway (SSP) and Great Barrier Reef (GBR) case study.*** *Projections of adult COTS density arriving to reefs per hectare as simulated by ReefMod-GBR. Within each panel, light grey lines represent individual realisations (n = 20 replicates x 10 Global Climate Models) across all reefs within the cluster. The bold, coloured lines represent the multi-model ensemble mean for each scenario.*

# APPENDIX 3. Supplementary results and discussion

## 3.1. Growth and survival regression analysis

We identified six distinct coral types on the Great Barrier Reef (GBR) for which demographic data were sufficient to build IPMs describing growth and survival as a function of coral size and environmental and spatial gradients: 'tabular *Acropora'*, 'corymbose/digitate *Acropora'*, 'spawning *Pocillopora'*, 'brooding Pocilloporidae', '*Goniastrea/Platygyra*' and 'massive *Porites'* (here, 'massive' denotes a rounded morphology, also encompassing 'sub-massive' forms (Pratchett et al. 2015), Table S1). Vital rate data were obtained by tracking individual colonies over an approximate 1-year interval in 2021-2022 (a period of low thermal and cyclonic disturbance at the monitoring sites). In total, annual measurements of planar area from 9621 coral colonies were suitable for analysis, with sampling occurring in three GBR regions (north, central, south) on mid-shelf and offshore reefs (Fig S 4). We statistically modelled growth and survival of each coral group as a function of coral size (log planar area in $cm^2$), GBR region, site depth and waterflow intensity (Table S2).

Strong differences in coral growth and survival rates were evident across the six coral types, with initial coral size being the strongest influence on these vital rates (main text Figure 2b, Fig S 14). This was particularly the case for growth (Fig S 14a), which was expected as initial size as planar area acts as a structural variable that intrinsically predicts a final size more similar to its initial size. Annual growth was highest in tabular *Acropora*, followed by corymbose/digitate *Acropora,* and then the two Pocilloporidae groups. The slowest growth rates were observed in *Goniastrea/Platygyra* and massive *Porites* (Fig S 14a). While growth generally increased with colony area, this plateaued for some of the largest colonies, which tended toward stasis or negative growth (partial mortality) (Fig S 14a, S3). Survival varied across coral types, with highest survival for the *Platygyra*/*Goniastrea* and massive *Porites* coral types (Fig S 14b). These differences in growth and survival across were generally consistent with other studies of coral demography on the GBR (Pratchett et al. 2015, Ferrari et al. 2017, Doropoulos et al. 2025a).

Analysis of standardised effect sizes showed the magnitude and direction of influence of environmental and spatial variables relative to initial colony size (Fig S 15a). The magnitude of the effects of depth, waterflow intensity and GBR region on growth were comparatively minor relative to initial coral size. However, the standardised effect magnitude of geographic region on survival rivalled that of size for several groups, including massive *Porites* and brooding Pocilloporidae, for which survival was higher in northern and central regions than the southern region, supported by the 80% Highest Posterior Density Interval (HPDI)—the range containing the most likely parameter values—which did not overlap zero (Fig S 15b, S4). There was also an indication of this for tabular *Acropora* for which the survival predictions were lower in the southern region. Growth performance also varied across the GBR regions, with tabular *Acropora* growing faster in northern regions compared to central and southern reef clusters (Fig S 15). Similar directional trends were noted for corymbose/digitate *Acropora* and both Pocilloporidae groups, though these patterns were characterised by higher posterior uncertainty (Fig S 15).

Increased depth was correlated with reduced growth for tabular *Acropora*, *Goniastrea/Platygyra*, and massive *Porites* (80% HPDI excludes zero, Fig S 15). Brooding Pocilloporidae had lower survival at greater depth, while other coral groups (the *Acropora* and spawning *Pocillopora*) also exhibited negative directionality but there was more uncertainty about this negative effect (Fig S 15). Only massive *Porites* showed weak evidence (80% HDCI crossed zero) of higher survival at depth.

Waterflow intensity was also linked to vital rate variation; higher waterflow was associated with lower growth in both spawning and brooding Pocilloporidae and correlated with reduced survival for *Goniastrea/Platygyra*.

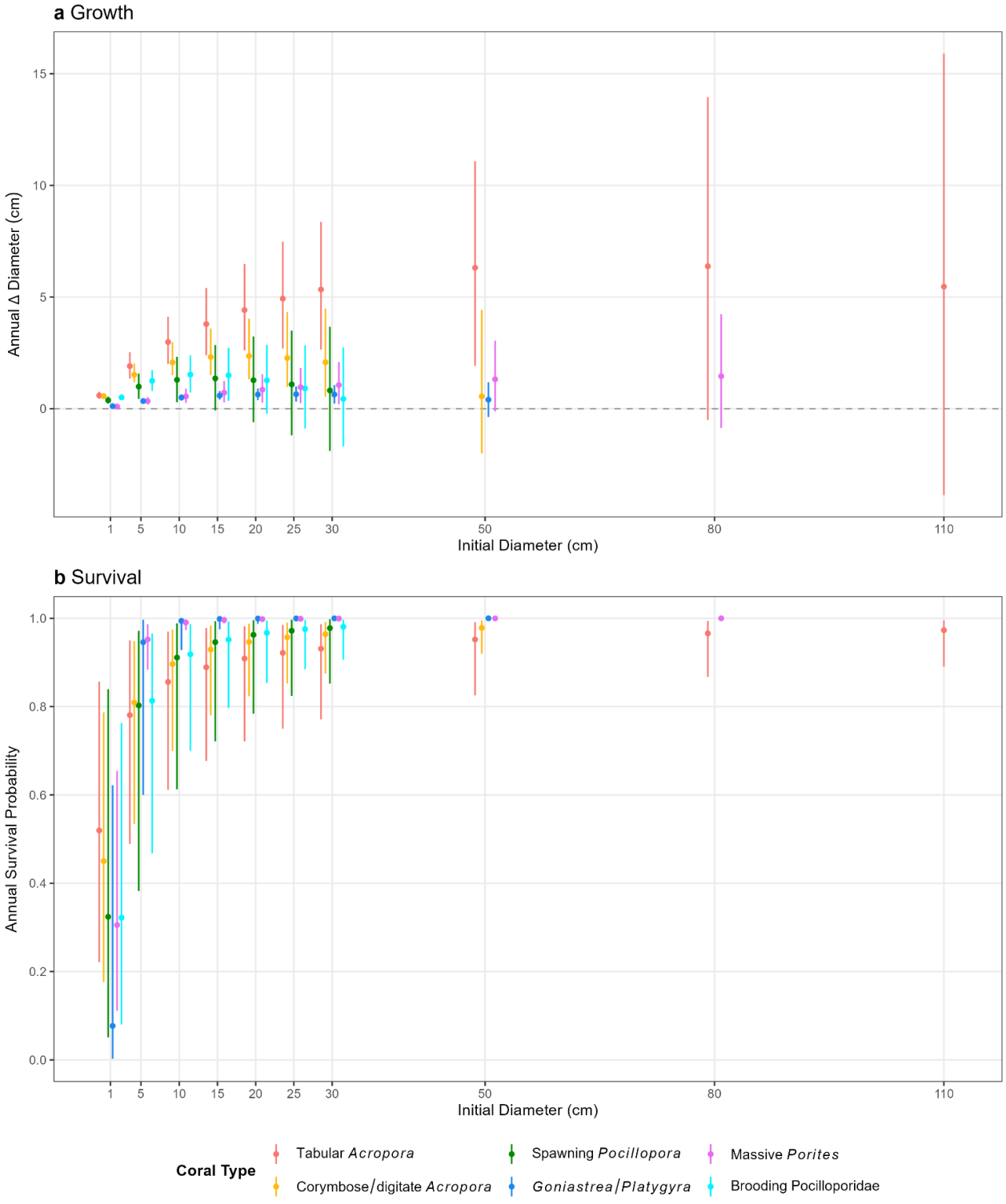


572

573 *Fig S 14.* ***Predicted annual growth and survival across sizes for six coral types****. (a) Growth is represented as the annual change*
574 *in colony diameter, where the dashed horizontal line indicates zero net growth. (b) Survival is represented as the annual*
575 *probability of survival (0–1). Points represent the posterior medians, and error bars represent the 95% Highest Posterior Density*
576 *Intervals (HPDI). Predictions are for the central GBR, at approximately mid-range values of depth (7 m) and waterflow (0.2 m/s).*
577 *Size classes for each functional type are truncated based on the maximum observed diameter simulated in the C~scape*
578 *framework. Coral types are distinguished by colour as indicated in the legend.*

579

*Table S 5. Comparison of candidate Bayesian hierarchical models for coral growth rates across six coral types. Models are ranked by Leave-One-Out Information Criterion (LOOIC), where lower values indicate better expected out-of-sample predictive performance. The 'base' model includes colony size, survey time period, and hierarchical random effects (Reef, Site, Plot) (see Predictor variables Table S 2). ΔELPD represents the difference in Expected Log Predictive Density between a model and the top-ranked model, with SE(ΔELPD) providing the standard error. Bayes $R^2$ summarises the proportion of variance explained by each model. Bold text indicates the model that was used in the C~scape simulations.*

**GROWTH MODELS**

| Coral type | Model form | LOOIC | ΔELPD | SE(ΔELPD) | Bayes $R^2$ |
|---|---|---|---|---|---|
| Tabular *Acropora* | base + region*size + depth | 1022.7 | 0.00 | 0.00 | 0.95 |
| **Tabular *Acropora*** | **base + region*size + exposure + depth** | **1024.4** | **-0.86** | **0.42** | **0.95** |
| Tabular *Acropora* | base + region*size + exposure | 1025.0 | -1.19 | 1.61 | 0.95 |
| Tabular *Acropora* | base | 1026.5 | -1.91 | 3.51 | 0.94 |
| Tabular *Acropora* | base + region*size | 1026.8 | -2.06 | 2.05 | 0.95 |
| **Corymbose/ Digitate *Acropora*** | **base + region*size + exposure + depth** | **1205.1** | **0.00** | **0.00** | **0.92** |
| Corymbose/ Digitate *Acropora* | base + region*size + depth | 1205.7 | -0.32 | 0.26 | 0.92 |
| Corymbose/ Digitate *Acropora* | base + region*size + exposure | 1206.2 | -0.58 | 0.49 | 0.92 |
| Corymbose/ Digitate *Acropora* | base + region*size | 1206.4 | -0.69 | 0.77 | 0.92 |
| Corymbose/ Digitate *Acropora* | base | 1231.9 | -13.44 | 6.43 | 0.91 |
| Spawning *Pocillopora* | base + region*size + exposure | -313.6 | 0.00 | 0.00 | 0.90 |
| **Spawning *Pocillopora*** | **base + region*size + exposure + depth** | **-311.7** | **-0.94** | **0.29** | **0.90** |
| Spawning *Pocillopora* | base + region*size + depth | -306.2 | -3.70 | 1.73 | 0.90 |
| Spawning *Pocillopora* | base + region*size | -305.3 | -4.14 | 1.92 | 0.90 |
| Spawning *Pocillopora* | base | -299.2 | -7.18 | 4.56 | 0.90 |
| *Platygyra/Goniastrea* | base + region*size + depth | -1071.3 | 0.00 | 0.00 | 0.98 |
| ***Platygyra/Goniastrea*** | **base + region*size + exposure + depth** | **-1069.9** | **-0.70** | **0.57** | **0.98** |
| *Platygyra/Goniastrea* | base + region*size + exposure | -1049.1 | -11.11 | 4.58 | 0.98 |
| *Platygyra/Goniastrea* | base + region*size | -1047.2 | -12.07 | 4.76 | 0.98 |
| *Platygyra/Goniastrea* | base | -1042.6 | -14.35 | 5.84 | 0.98 |
| Massive *Porites* | base + region*size | -1541.7 | 0.00 | 0.00 | 0.97 |
| Massive *Porites* | base + region*size + exposure | -1540.0 | -0.81 | 1.22 | 0.97 |
| Massive *Porites* | base + region*size + depth | -1539.1 | -1.28 | 2.38 | 0.97 |
| **Massive *Porites*** | **base + region*size + exposure + depth** | **-1538.7** | **-1.46** | **2.31** | **0.97** |
| Massive *Porites* | base | -1518.6 | -11.50 | 6.66 | 0.97 |
| Brooding Pocilloporidae | base + region*size + exposure | 235.2 | 0.00 | 0.00 | 0.87 |
| **Brooding Pocilloporidae** | **base + region*size + exposure + depth** | **237.2** | **-1.03** | **0.21** | **0.87** |
| Brooding Pocilloporidae | base + region*size | 243.6 | -4.20 | 1.95 | 0.87 |
| Brooding Pocilloporidae | base + region*size + depth | 244.1 | -4.45 | 1.75 | 0.87 |
| Brooding Pocilloporidae | base | 248.2 | -6.51 | 4.31 | 0.87 |

*Table S 6. Comparison of candidate Bayesian hierarchical models for coral survival rates across six coral types. Models are ranked by Leave-One-Out Information Criterion (LOOIC), where lower values indicate better expected out-of-sample predictive performance. The 'base' model includes colony size, survey time period, and hierarchical random effects (Reef, Site, Plot) (see Predictor variables Table S 2). ΔELPD represents the difference in Expected Log Predictive Density between a model and the top-ranked model, with SE(ΔELPD) providing the standard error. Bayes $R^2$ summarises the proportion of variance explained by each model. Bold text indicates the model that was used in the C~scape simulations.*

**SURVIVAL MODELS**

| Coral type | Model form | LOOIC | ΔELPD | SE(ΔELPD) | Bayes $R^2$ |
|---|---|---|---|---|---|
| Tabular Acropora | base + region*size | 1331.2 | 0.00 | 0.00 | 0.17 |
| Tabular Acropora | base + region*size + depth | 1331.8 | -0.31 | 0.88 | 0.17 |
| **Tabular Acropora** | **base + region*size + exposure + depth** | **1333.1** | **-0.99** | **1.06** | **0.17** |
| Tabular Acropora | base + region*size + exposure | 1333.8 | -1.30 | 0.74 | 0.17 |
| Tabular Acropora | base | 1344.3 | -6.58 | 4.46 | 0.16 |
| **Corymbose/ Digitate Acropora** | **base + region*size + exposure + depth** | **2876.6** | **0.00** | **0.00** | **0.12** |
| Corymbose/ Digitate Acropora | base + region*size + exposure | 2876.8 | -0.13 | 0.99 | 0.12 |
| Corymbose/ Digitate Acropora | base + region*size + depth | 2878.0 | -0.70 | 0.81 | 0.12 |
| Corymbose/ Digitate Acropora | base + region*size | 2878.7 | -1.05 | 1.61 | 0.12 |
| Corymbose/ Digitate Acropora | base | 2899.9 | -11.69 | 5.51 | 0.11 |
| Spawning Pocillopora | base | 722.8 | 0.00 | 0.00 | 0.13 |
| Spawning Pocillopora | base + region*size + depth | 725.2 | -1.18 | 1.88 | 0.14 |
| Spawning Pocillopora | base + region*size | 725.3 | -1.27 | 1.38 | 0.14 |
| **Spawning Pocillopora** | **base + region*size + exposure + depth** | **725.7** | **-1.43** | **1.92** | **0.14** |
| Spawning Pocillopora | base + region*size + exposure | 726.5 | -1.84 | 1.46 | 0.14 |
| *Platygyra/Goniastrea* | base + region*size + exposure | 212.4 | 0.00 | 0.00 | 0.24 |
| *Platygyra/Goniastrea* | base + region*size | 212.9 | -0.25 | 0.99 | 0.22 |
| ***Platygyra/Goniastrea*** | **base + region*size + exposure + depth** | **213.7** | **-0.65** | **0.72** | **0.24** |
| *Platygyra/Goniastrea* | base + region*size + depth | 215.0 | -1.32 | 1.07 | 0.23 |
| *Platygyra/Goniastrea* | base | 223.1 | -5.38 | 2.50 | 0.17 |
| Massive Porites | base + region*size | 603.4 | 0.00 | 0.00 | 0.29 |
| Massive Porites | base + region*size + depth | 604.5 | -0.54 | 0.75 | 0.29 |
| Massive Porites | base + region*size + exposure | 605.0 | -0.83 | 0.33 | 0.29 |
| **Massive Porites** | **base + region*size + exposure + depth** | **605.9** | **-1.24** | **0.82** | **0.29** |
| Massive Porites | base | 611.3 | -3.97 | 3.28 | 0.27 |
| Brooding Pocilloporidae | base + region*size + depth | 1546.3 | 0.00 | 0.00 | 0.18 |
| **Brooding Pocilloporidae** | **base + region*size + exposure + depth** | **1546.5** | **-0.11** | **0.24** | **0.18** |
| Brooding Pocilloporidae | base + region*size + exposure | 1551.4 | -2.55 | 2.07 | 0.18 |
| Brooding Pocilloporidae | base + region*size | 1552.2 | -2.92 | 2.43 | 0.18 |
| Brooding Pocilloporidae | base | 1563.2 | -8.45 | 4.65 | 0.17 |

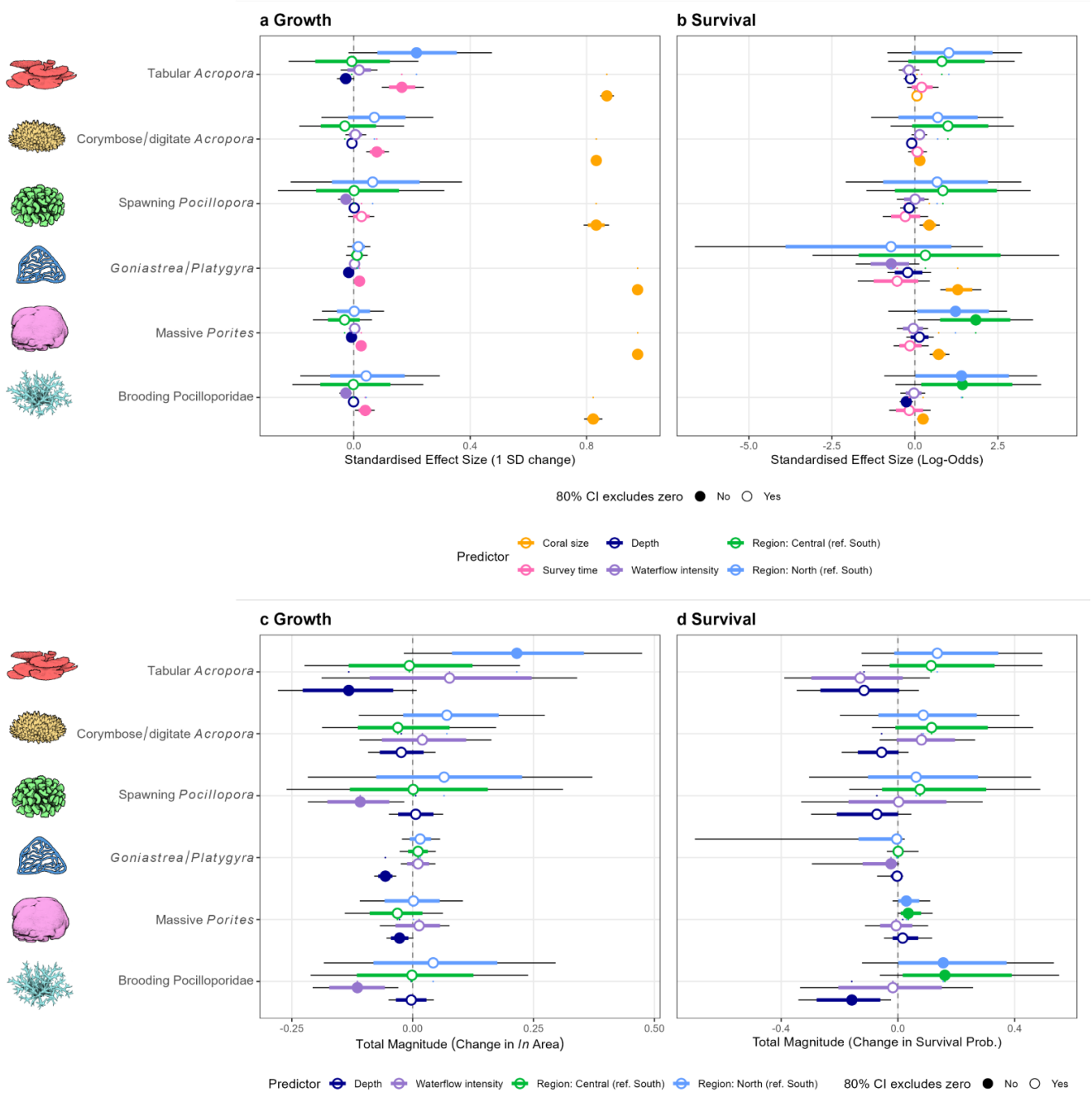


*Fig S 15.* ***Comparative influence of predictor variables on coral growth and survival****. Standardised effect sizes (beta) representing the relative influence of predictors on (a) coral growth (ln colony area) and (b) survival probability. Continuous variables (coral size, survey time, depth, and waterflow intensity) were mean-centred and standardised by one standard deviation to allow direct comparison. Regional effects (central and north) are shown as the difference from the southern region reference at the mean colony size (4.6 ln cm$^2$). c,d, Total magnitude of effect for environmental and regional covariates on (c) growth and (d) survival. Magnitude is calculated as the absolute change in the response variable across the observed environmental range (Depth: 2.8–12 m; Waterflow: 0.05–0.38 m s-1) while holding all other variables constant. Points represent posterior medians; thick and thin horizontal bars represent 80% and 95% highest posterior density intervals (HPDI), respectively. Points are filled where the 80% HPDI excludes zero and hollow otherwise. Calculations are based on Bayesian multilevel regressions across six coral functional types.*

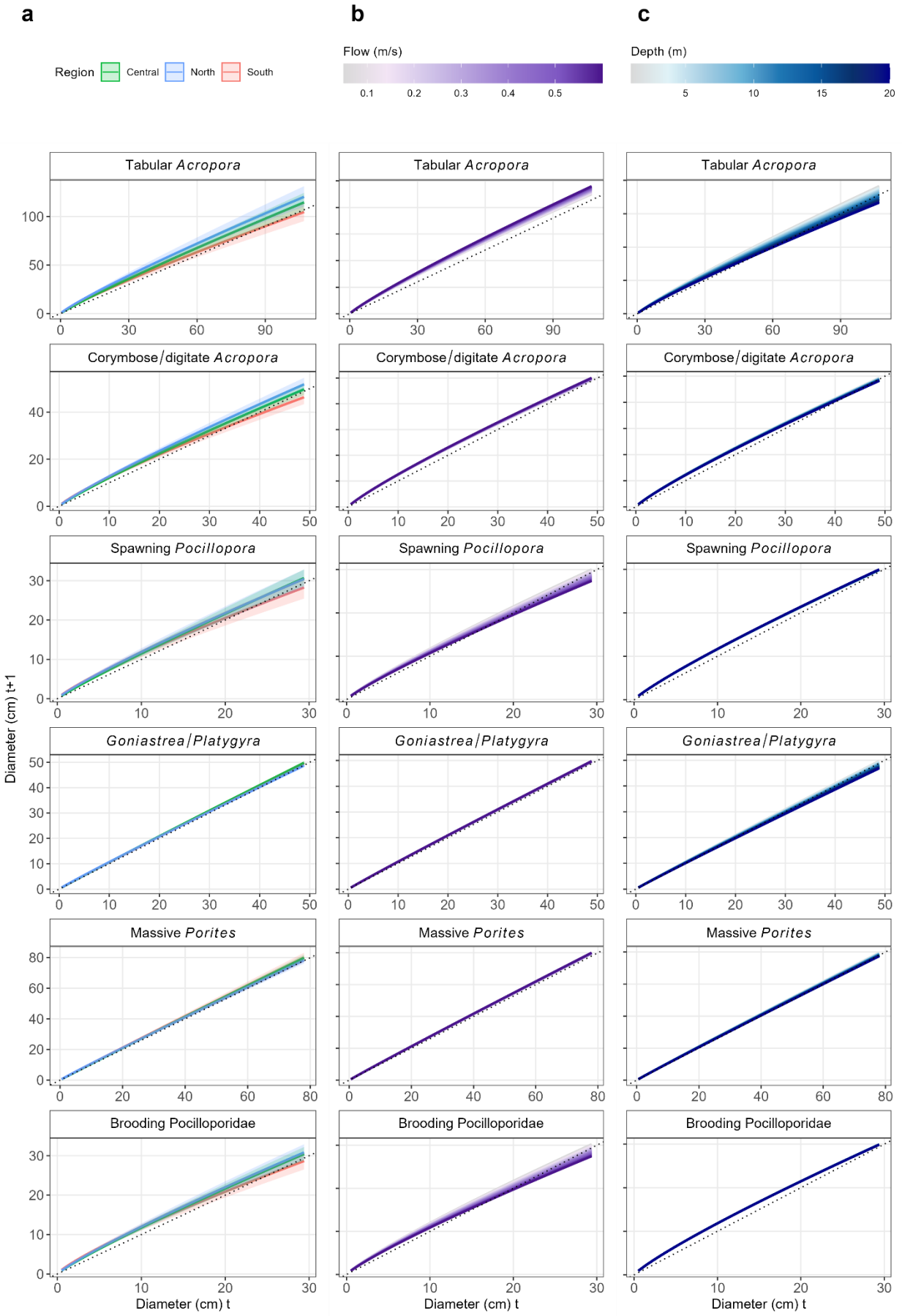


*Fig S 16.* ***Annual growth across gradients of predictor variables for six coral functional types.*** *Each row represents a distinct coral functional type: Tabular Acropora, Corymbose/digitate Acropora, Spawning Pocillopora, Goniastrea/Platygyra, Massive Porites, and Brooding Pocilloporidae. (a) Predicted colony diameter at time t+1 across three geographic regions of the Great Barrier Reef (south, central, and north) with waterflow intensity fixed at 0.2 m/s and depth at 7 m; shaded areas represent 90% credible intervals. (b) Influence of waterflow intensity on growth, averaged across regions at 7 m depth; colour gradient indicates increasing flow intensity (0.05–0.6 m/s). (c) Influence of depth on growth, averaged across regions at 0.2 m/s waterflow; colour gradient indicates increasing depth (1–120 m). The dotted diagonal line represents the 1:1 isometry (zero growth).*

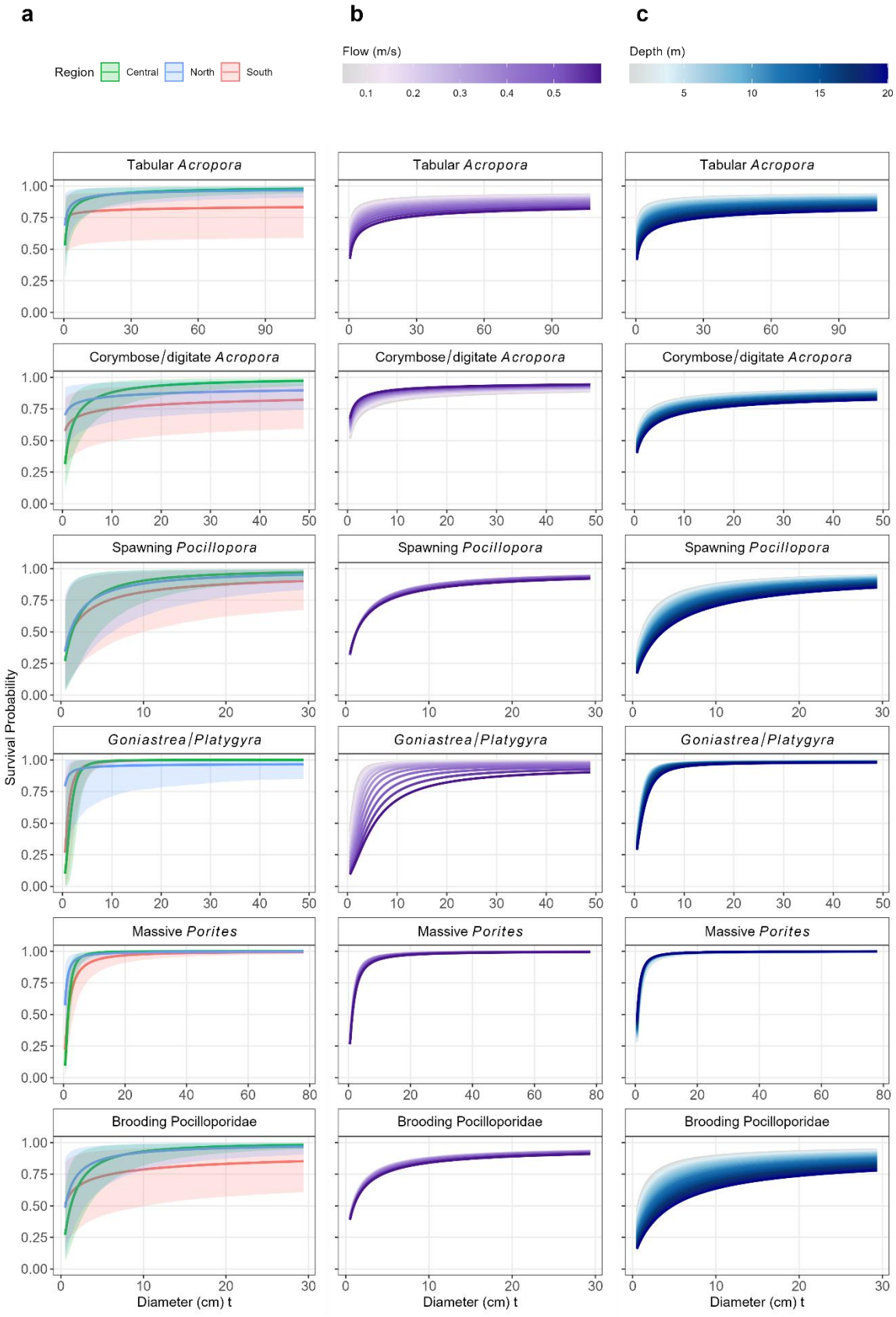


*Fig S 17.* ***Annual survival across gradients of predictor variables for six coral functional types.*** *Panels are organised by coral type (rows) and environmental drivers (columns). (a) Annual survival probability across three geographic regions of the Great Barrier Reef (south, central and north) with depth fixed at 7 m and waterflow intensity at 0.2 m/s; shaded ribbons denote 90% credible intervals. (b) Predicted survival as a function of waterflow intensity, marginalised across regions at 7 m depth; darker purple tones indicate higher flow intensities. (c) Predicted survival as a function of depth, marginalised across regions at 0.2 m/s waterflow; darker blue tones indicate deeper reef environments. All survival estimates are bounded between 0 and 1.*

## 3.2. Representative reefs simulations

Some covariates (section 3.1) showed contrasting associations with growth and survival rates, suggesting demographic trade-offs. For example, tabular *Acropora* colonies showed higher predicted growth but lower survival at higher waterflow intensity sites. In contrast depth was unidirectional, associated with both lower growth and lower survival at deeper sites for this coral type (Fig S 15, Fig S 16, Fig S 17). These coupled and contrasting relationships highlight the complexity of demographic variability, where a single spatial context may be correlated with enhanced performance in one demographic dimension while being associated with increased risk in another.

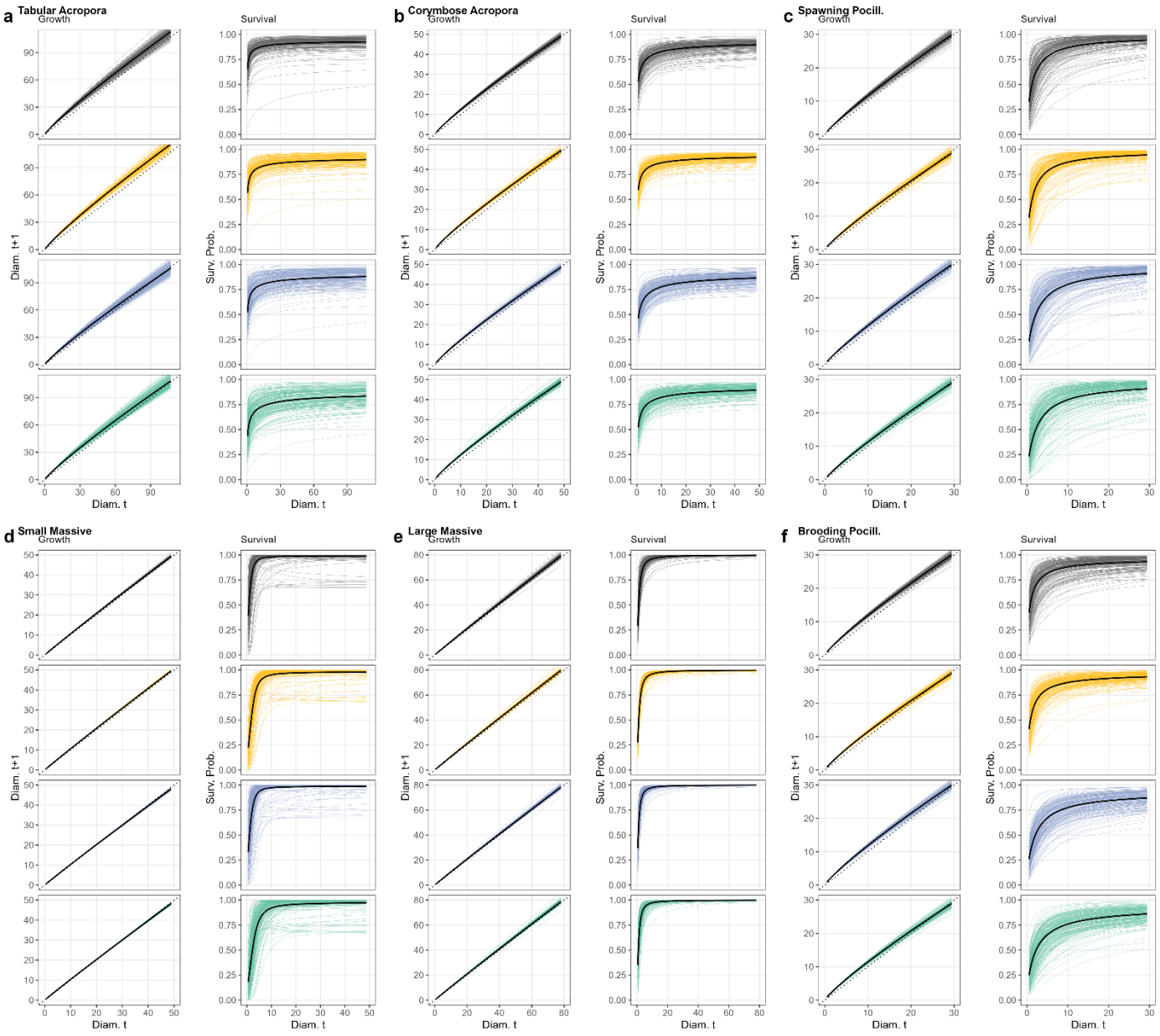


*Fig S 18.* ***Vital rate predictions for six coral types across environmental gradients, depth and wave exposure.*** *Each panel (a–f) displays predicted growth (left) and survival probability (right) for a specific coral type. Growth plots show predicted colony diameter at time t+1 relative to diameter at time t (cm). The dotted diagonal line represents the 1:1 "no growth" isometric line. Survival plots show predicted annual survival probability (0.0–1.0) relative to colony diameter at time t. Predictions are faceted by the four sites in the representative reefs, which have combinations of depth (3m or 12m) and wave exposure (0.1 or 0.3 m/s). Individual coloured lines represent 200 random draws from the Bayesian posterior distribution to illustrate regression uncertainty, while the solid black line represents the posterior mean across 8000 posterior draws. All predictions are marginalised across regional clusters (offshore south, central, and north). Complementary to Figure 2d, main text.*

The influence of the covariates in the growth and survival regressions was further investigated in the representative reefs studies, simulated using the *C~scape* framework in each of the north, central and southern regions. Regional-scale spatial patterns across the GBR were explained in part by differences in vital rates: northern reefs consistently recovered faster than central or southern reefs in both the representative-reef simulations and the GBR case studies. This pattern of coral cover across regions is in contrast with empirical observations suggesting instead that the southern GBR has faster recovery potential and higher realised coral cover (Castro-Sanguino et al. 2021, Álvarez-Noriega et al. 2024). This discrepancy likely arises from several interacting ecological and methodological factors. Reliance on a single year of vital rate data (2021–2022) assumes growth and survival are similar across years, likely overlooking region-specific interannual variability (Appendix 5). Furthermore, the fast recovery observed in the southern GBR in long-term monitoring studies is thought to be driven by fast-growing tabular *Acropora*, and while we found tabular *Acropora* had the fastest growth rates, the other coral groups had higher background survival in the southern region (Fig S 16).

Depth exerted the strongest influence on the recovery rates of coral cover, while waterflow intensity produced more muted effects. Shallow sites recovered fastest, deep sites lagged, and low waterflow habitats recovered faster than high waterflow habitats (Fig S 19d). While we accounted for indirect competition via density dependent modifications to growth rates, such processes are highly complex and empirical data on how vital rates are impacts in direct competition are limited and difficult to parameterise at this scale (Appendix 5). Future research should build in multiple years of vital rate data and further analyse the role of coral composition.

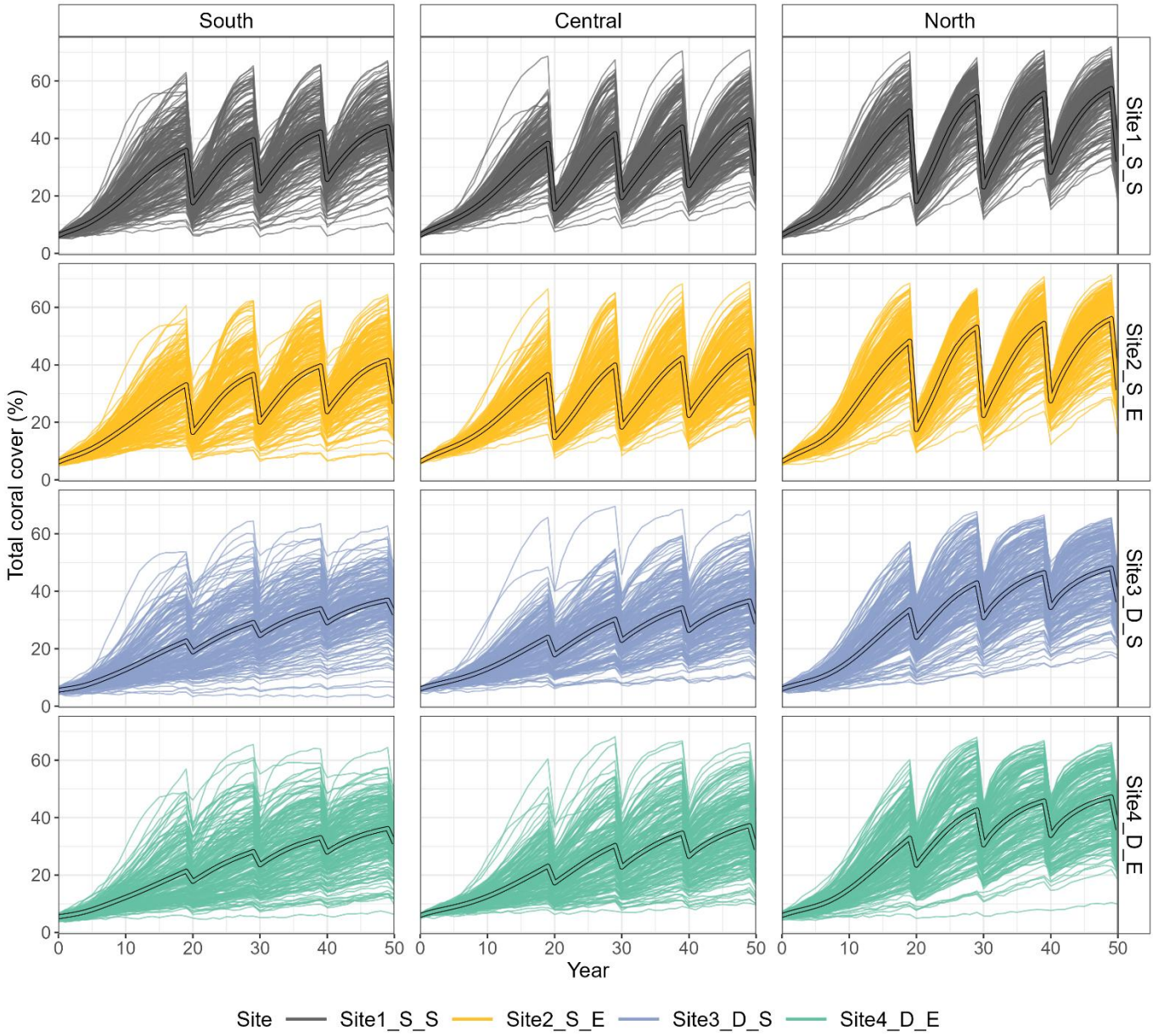


*Fig S 19. Total coral-cover projections for each site in the representative reefs (rows), simulated in each of the three regions of the Great Barrier Reef (columns): south, central, north). Narrow lines represent 200 simulations each driven by a single posterior draw to illustrate vital rate uncertainty. Complementary to Figure 2g, main text.*

## 3.3. GBR case studies: Evaluation of model hindcast

Hindcasts for four GBR case studies indicated the *C~scape* framework adequately reproduced historic coral-cover dynamics. This was achieved without any major calibration using population-level data (aside from minor calibration of the bleaching mortality function used, see Appendix 1 (Bozec et al. 2022)), indicating that the key ecological processes governing coral recovery and disturbance impacts were captured mechanistically.

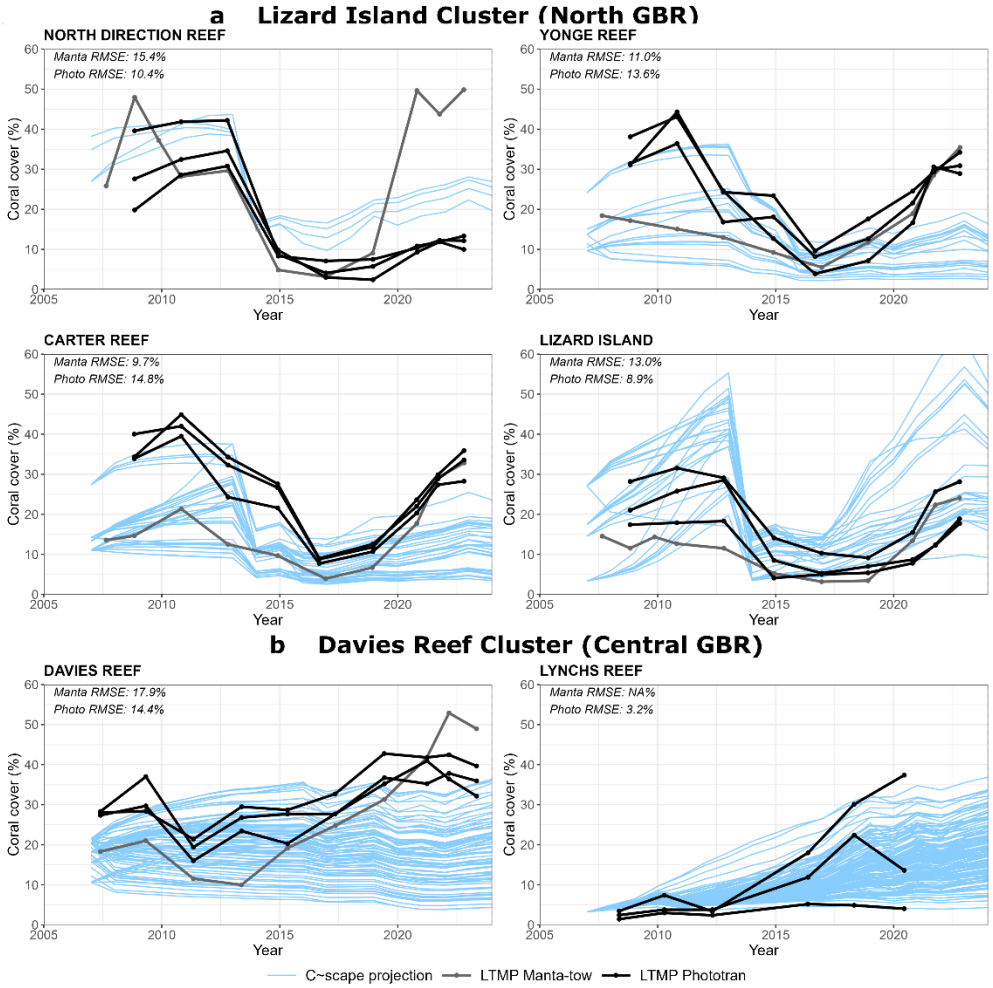


*Fig S 20.* ***Complementary to main text Figure 4: Evaluation of C~scape hindcast trajectories of total coral cover (%) against empirical monitoring data.*** *Trajectories from C~scape are shown for individual sites (blue lines) for reefs within the four case study clusters that had Long-Term Monitoring Program (LTMP) data, subset for those sites in the 'slope' or 'sheltered slope' geomorphic zones. Data from the Australian Institute of Marine Science (AIMS) LTMP are shown from fixed-position phototransects (black lines) and manta tow surveys (grey lines). The fixed-position photo transect data are from three sites on the leeward north-east slope of the reefs. In contrast, manta tow surveys provide estimates from around the reef perimeters, targeting the reef slope. While manta tow surveys are less accurate than fixed-position phototransects, they offer broader spatial information across the reef. The Root Mean Square Error (RMSE) is shown for the comparison of model trajectories to manta tow and phototransects in the top left of each panel.*

*Table S 7. Summary of statistical performance metrics for simulated total coral cover. Metrics are provided for each reef within the four case study clusters for which long-term monitoring data were available, and for the pooled dataset. For each reef, evaluation was performed against both manta-tow and phototransect data where available. Columns include: Pearson's correlation coefficient, Spearman's rank correlation to assess linear and monotonic trend alignment; RMSE (Root Mean Square Error) for absolute deviation in percentage units; Percent Bias to indicate systematic over- or under-estimation. 'NA' values indicate instances where empirical data were unavailable for that specific methodology.*

| GBR Region | Cluster | Reef | Methodology | Pearson's correlation | Spearman's rank correlation | RMSE | Percent Bias |
|---|---|---|---|---|---|---|---|
| North | Lizard | MACGILLIVRAY REEF | Manta-tow | 0.68 | 0.73 | 9.5 | 15.3 |
| North | Lizard | MACGILLIVRAY REEF | Phototransect | 0.92 | 0.88 | 7.4 | 33.1 |
| North | Lizard | NO NAME REEF | Manta-tow | 0.32 | 0.32 | 7.8 | -25.9 |
| North | Lizard | NO NAME REEF | Phototransect | 0.84 | 0.90 | 15.3 | -52.8 |
| North | Lizard | NORTH DIRECTION REEF | Manta-tow | 0.44 | 0.38 | 15.4 | -4.5 |
| North | Lizard | NORTH DIRECTION REEF | Phototransect | 0.97 | 0.95 | 10.4 | 58.0 |
| North | Lizard | YONGE REEF | Manta-tow | -0.07 | 0.04 | 11.0 | -21.9 |
| North | Lizard | YONGE REEF | Phototransect | 0.63 | 0.67 | 13.6 | -45.9 |
| North | Lizard | CARTER REEF | Manta-tow | 0.15 | 0.43 | 9.7 | -15.3 |
| North | Lizard | CARTER REEF | Phototransect | 0.79 | 0.90 | 14.8 | -49.3 |
| North | Lizard | LIZARD ISLAND | Manta-tow | 0.63 | 0.54 | 13.0 | 91.2 |
| North | Lizard | LIZARD ISLAND | Phototransect | 0.86 | 0.88 | 8.9 | 48.1 |
| North | Moore | MOORE REEF | Manta-tow | 0.11 | 0.10 | 11.3 | 78.1 |
| North | Moore | MOORE REEF | Phototransect | 0.06 | 0.00 | 8.4 | -8.9 |
| North | Moore | THETFORD REEF | Manta-tow | 0.55 | 0.45 | 8.3 | 31.7 |
| North | Moore | THETFORD REEF | Phototransect | 0.10 | 0.19 | 8.7 | 2.1 |
| Central | Davies | CHICKEN REEF | Manta-tow | 0.80 | 0.76 | 9.2 | 42.7 |
| Central | Davies | CHICKEN REEF | Phototransect | 0.85 | 0.82 | 7.8 | -7.2 |
| Central | Davies | LYNCHS REEF | Manta-tow | NA | NA | NA | NA |
| Central | Davies | LYNCHS REEF | Phototransect | 0.98 | 0.89 | 3.2 | -7.2 |
| Central | Davies | CENTIPEDE REEF | Manta-tow | 0.96 | 0.60 | 3.3 | 27.8 |
| Central | Davies | CENTIPEDE REEF | Phototransect | 0.81 | 0.77 | 2.8 | -6.6 |
| Central | Davies | DAVIES REEF | Manta-tow | -0.78 | -0.73 | 17.9 | -33.0 |
| Central | Davies | DAVIES REEF | Phototransect | -0.62 | -0.73 | 14.4 | -40.0 |
| South | Heron | ONE TREE REEF | Manta-tow | 0.78 | 0.60 | 19.8 | -36.9 |
| South | Heron | ONE TREE REEF | Phototransect | 0.79 | 0.60 | 24.0 | -32.2 |
| South | Heron | WRECK ISLAND REEF | Manta-tow | 0.67 | 0.48 | 26.6 | -42.9 |
| South | Heron | WRECK ISLAND REEF | Phototransect | 0.88 | 0.71 | 28.6 | -42.7 |
| North | Lizard | **Pooled** | Manta-tow | 0.47 | 0.45 | 11.33 | 2.8 |
| North | Lizard | **Pooled** | Phototransect | 0.28 | 0.27 | 12.12 | -11.3 |
| North | Moore | **Pooled** | Manta-tow | 0.47 | 0.36 | 9.45 | 44.0 |
| North | Moore | **Pooled** | Phototransect | 0.09 | 0.12 | 8.60 | -1.1 |
| Central | Davies | **Pooled** | Manta-tow | 0.43 | 0.50 | 12.20 | 4.2 |
| Central | Davies | **Pooled** | Phototransect | 0.78 | 0.77 | 9.13 | -19.6 |
| South | Heron | **Pooled** | Manta-tow | 0.70 | 0.54 | 23.65 | -40.1 |
| South | Heron | **Pooled** | Phototransect | 0.82 | 0.66 | 26.27 | -37.4 |
| | | **Pooled** | **Manta-tow** | **0.47** | **0.50** | **13.4** | **-2.3** |
| | | **Pooled** | **Phototransect** | **0.50** | **0.49** | **13.6** | **-17.3** |

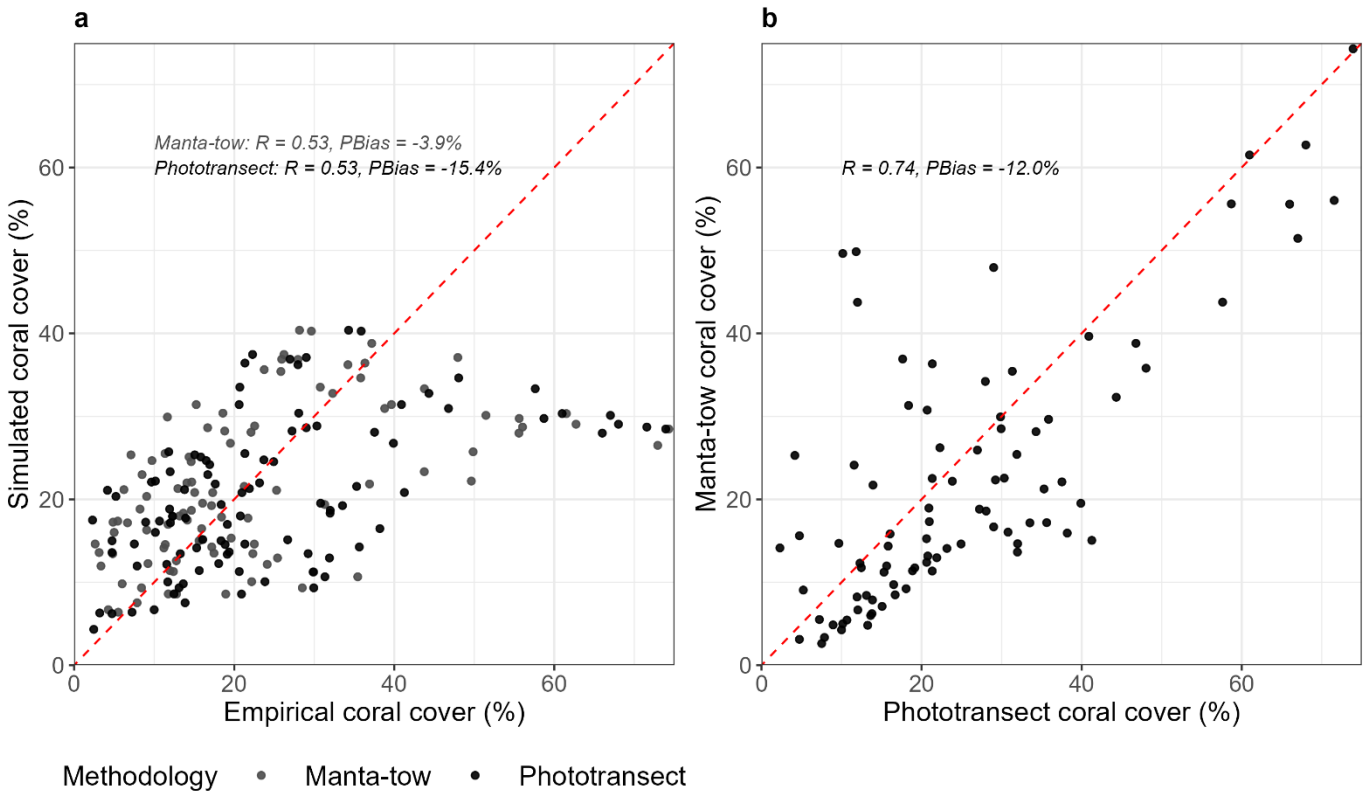


687

688 *Fig S 21. Scatterplots of the pooled evaluation of simulated total coral cover against independent empirical observations. (a)*
689 *Comparison of simulated coral cover against manta-tow (dark grey) and phototransect (black) observations pooled across all*
690 *reefs and years. The red dashed line represents the 1:1 identity line; points below this line indicate the model is underestimating*
691 *the observed coral cover. (b) Consistency between the two independent empirical benchmarks (manta-tow versus phototransect*
692 *coral cover). In both panels, points represent reef-year averages. Statistical metrics provided are Pearson's correlation (R) and*
693 *Percent Bias (PBias).*

694

## 3.4. GBR case studies: Projections of coral-cover trajectories

Regional differences emerged from the GBR case studies, aligning with what emerged in the representative reefs case study. Under SSP2-4.5 the northern case studies exhibited generally faster recovery, achieved higher coral cover and retained variability in coral-cover projections longer into the century than those in the central and southern GBR.

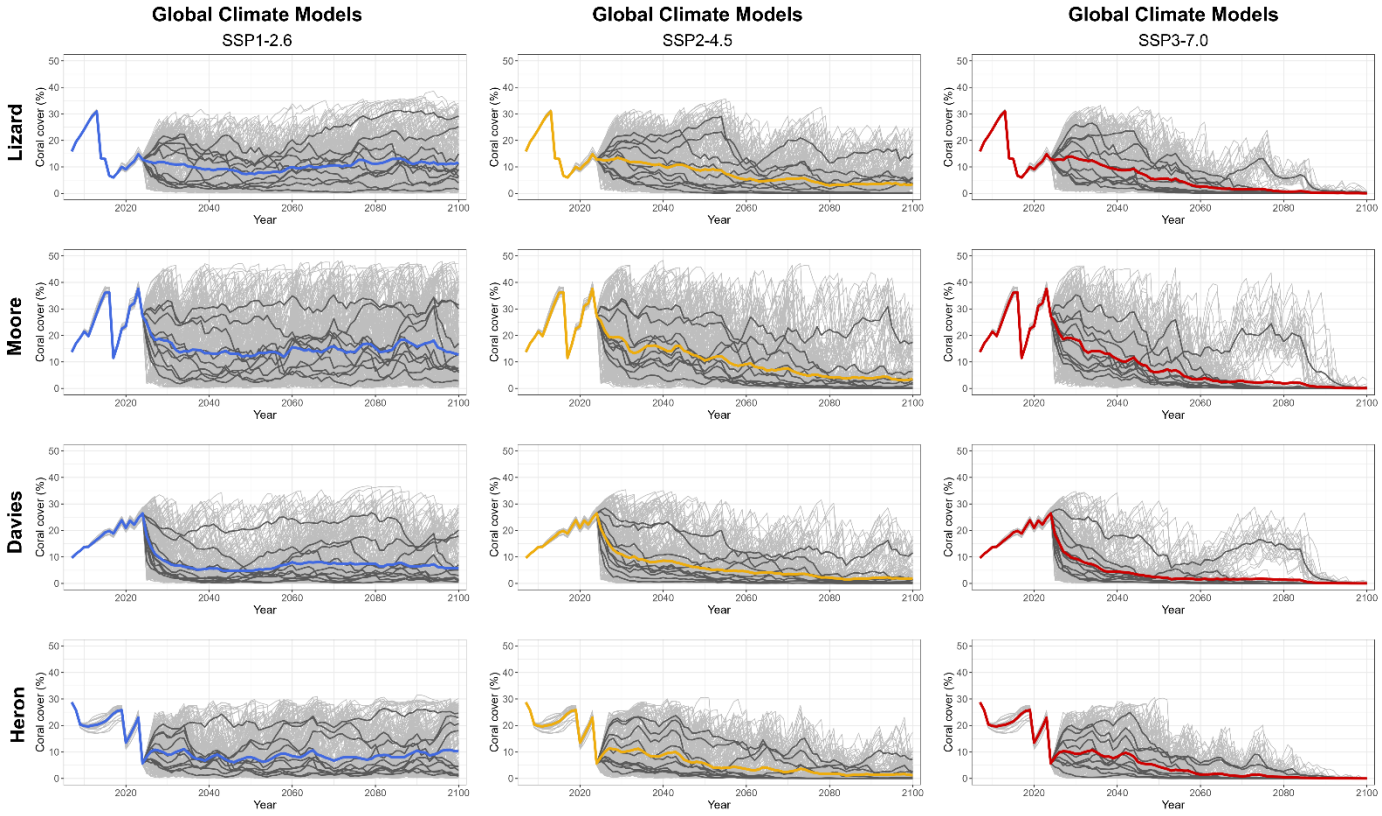


*Fig S 22.* ***Total coral-cover trajectories as projected by the C~scape modelling framework for the four case studies*** *(as rows: Lizard Island Cluster, Moore Reef Cluster (both North region), Davies Reef Cluster (Central) and Heron Island Cluster (South)). 200 future climate scenarios which stem from 10 Global Climate Models (GCMs) for Shared Socioeconomic Pathways of SSP1-2.6, SSP2-4.5, SSP3-7.0, downscaled to the reefs within the case study. Each of the 10 GCMs have variation in the exact timing of acute disturbances under 20 different realisations. The mean of each GCM is show in dark grey lines while the mean of all GCM realisations is shown by coloured line.*

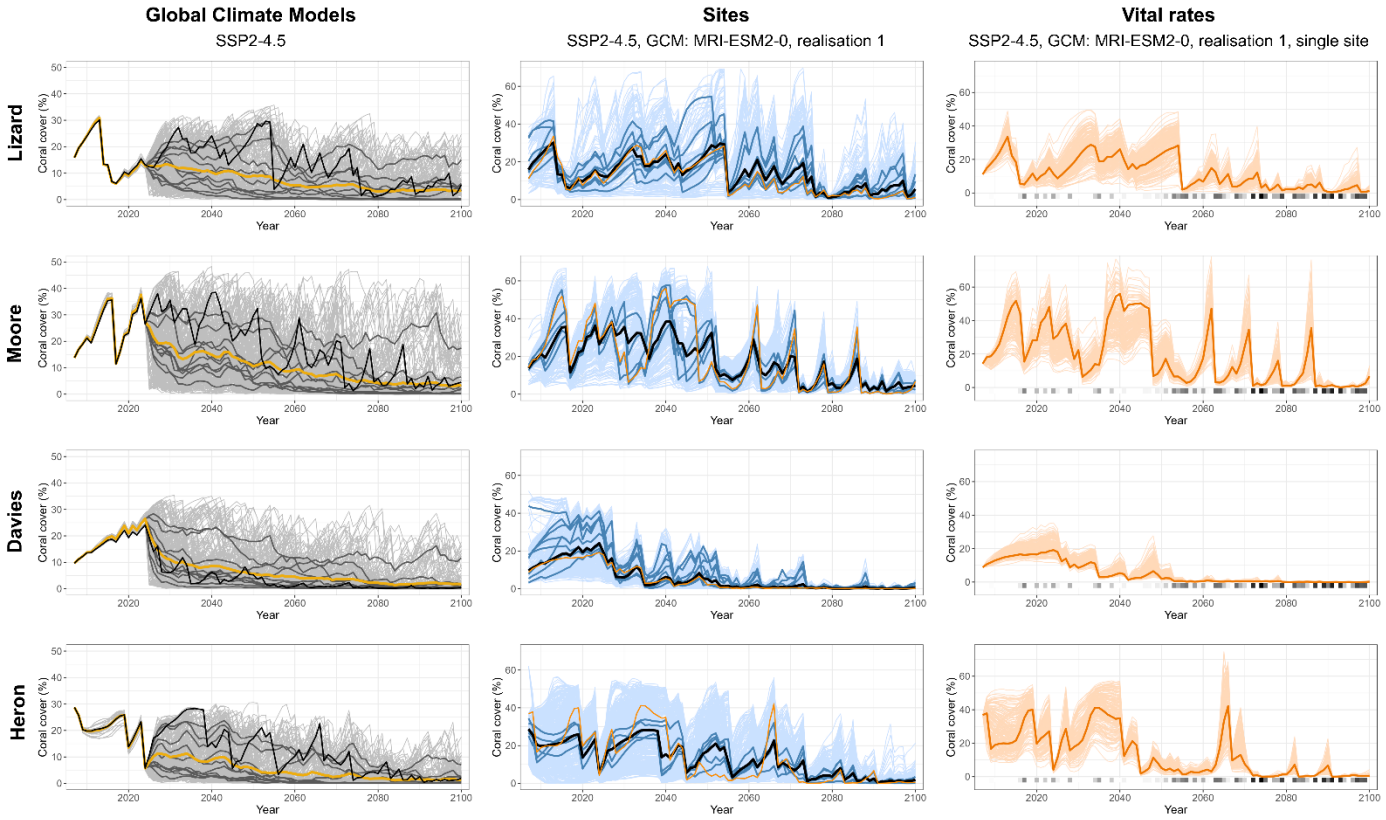


*Fig S 23. Total coral-cover trajectories as projected by the C~scape modelling framework for the four case studies (as rows: Lizard Island Cluster, Moore Reef Cluster (both North region), Davies Reef Cluster (Central) and Heron Island Cluster (South)). The first column shows 200 future climate scenarios which stems from 10 Global Climate Models (GCMs) for a Shared Socioeconomic Pathway (IPCC 2022) of SSP2-4.5, downscaled to the reefs within the case study. Each of the 10 GCMs have variation in the exact timing of acute disturbances under 20 different realisations. The mean of each GCM is show in dark grey lines while the mean of all GCM realisations shown in black. The orange line is a single climate future from GCM MRI-ESM2-0 that was selected to examine in more detail. In the second column GCM MRI-ESM2-0 is shown in black as the average projections of all sites within the case studies, while light blue lines show the trajectories of each of these sites. Dark blue lines show the mean across sites for each reef within the cluster. The orange line shows a single site that was closest to the median of all other sites. In the final column the same orange-coloured site is shown, with the light orange lines showing the trajectories resulting from 200 individual posterior draws (of a total possible 8000 for which the dark orange line was simulated) from the growth and survival regressions.*

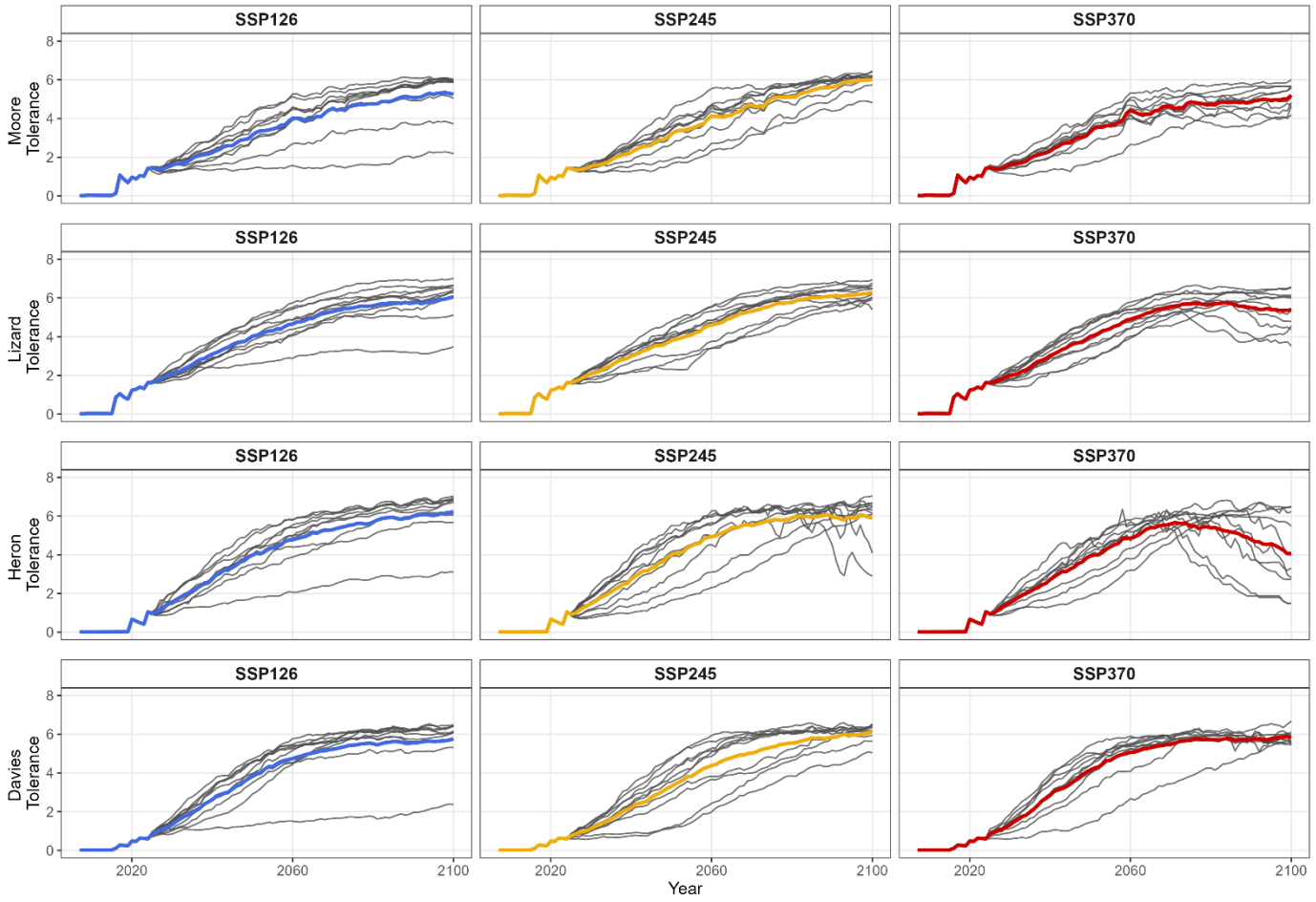


*Fig S 24.* ***Community-level mean thermal tolerance trajectories*** *as projected by the C~scape modelling framework for the four case studies (rows: Moore Reef Cluster, Lizard Island Cluster, Heron Island Cluster, and Davies Reef Cluster). Results represent the community-weighted mean of 14 thermal tolerance classes (ranging from -5 to +8) across 600 future climate scenarios per cluster. These scenarios originate from 10 Global Climate Models (GCMs) for three Shared Socioeconomic Pathways (SSP1-2.6, SSP2-4.5, and SSP3-7.0), downscaled to individual reefs. The mean of each GCM is shown as dark grey lines, while the ensemble mean of all GCM realisations for each SSP is indicated by the bold coloured line.*

*Table S 8.* ***Summary of variance partitioning for coral-cover projections.*** *Variability is presented across three metrics: (a) standard deviation in coral-cover units, (b) raw variance components, and (c) the relative percentage of total variance explained by each driver. The pooled analysis represents a nested mixed-effects model capturing the average variability structure across the entire simulation century and all Shared Socioeconomic Pathways (SSPs). Temporal snapshot rows provide the variance structure at specific milestones (2023, 2050, and 2099) for each SSP, derived from SSP x Year models.*

| **Standard deviation in coral cover (%)** | | | | | | | | |
|---|---|---|---|---|---|---|---|---|
| Analysis | SSP | Year | GCM | Realisation | Region | Reef | Site | Residual |
| Global (2008-2100) | 3.4 | 2.7 | 4.5 | 0.5 | 2.9 | 2.3 | 2.8 | 8.5 |
| Temporal | SSP126 | 2023 | 0 | 0.5 | 9.5 | 5 | 9.1 | 1.9 |
| Temporal | SSP126 | 2050 | 6.2 | 3.1 | 2.3 | 2.5 | 3.6 | 7.3 |
| Temporal | SSP126 | 2099 | 8.1 | 2.6 | 1.9 | 3.4 | 4.5 | 8.7 |
| Temporal | SSP245 | 2023 | 0 | 0.5 | 9.5 | 5 | 9.1 | 1.9 |
| Temporal | SSP245 | 2050 | 5.7 | 3.2 | 2 | 2.4 | 3 | 7.4 |
| Temporal | SSP245 | 2099 | 3.5 | 1.3 | 0.7 | 1.3 | 1.1 | 4.1 |
| Temporal | SSP370 | 2023 | 0 | 0.5 | 9.5 | 5 | 9.1 | 1.9 |
| Temporal | SSP370 | 2050 | 3.5 | 3 | 1.2 | 1.5 | 2.2 | 6.1 |
| Temporal | SSP370 | 2099 | 0.1 | 0.1 | 0 | 0 | 0.1 | 0.3 |
| **Magnitude of Variance Components** | | | | | | | | |
| Analysis | SSP | Year | GCM | Realisation | Region | Reef | Site | Residual |
| Global (2008-2100) | 11.9 | 7.5 | 20 | 0.3 | 8.4 | 5.3 | 8.1 | 71.9 |
| Temporal | SSP126 | 2023 | 0 | 0.4 | 98.9 | 26.5 | 115.6 | 5.2 |
| Temporal | SSP126 | 2050 | 39.4 | 9.9 | 4.6 | 6.1 | 13.2 | 53.8 |
| Temporal | SSP126 | 2099 | 63.3 | 7.3 | 3.2 | 11.8 | 20 | 75.7 |
| Temporal | SSP245 | 2023 | 0 | 0.4 | 98.9 | 26.5 | 115.6 | 5.2 |
| Temporal | SSP245 | 2050 | 34.2 | 10.9 | 3.4 | 5.5 | 9.2 | 55.5 |
| Temporal | SSP245 | 2099 | 11.1 | 1.6 | 0.4 | 1.7 | 1.3 | 15.2 |
| Temporal | SSP370 | 2023 | 0 | 0.4 | 98.9 | 26.5 | 115.6 | 5.2 |
| Temporal | SSP370 | 2050 | 11.4 | 9.3 | 1.1 | 2.4 | 4.6 | 37.5 |
| Temporal | SSP370 | 2099 | 0 | 0 | 0 | 0 | 0 | 0.1 |
| **Percentage of Total Variance Explained** | | | | | | | | |
| Analysis | SSP | Year | GCM | Realisation | Region | Reef | Site | Residual |
| Global (2008-2100) | 8.9 | 5.6 | 15 | 0.2 | 6.3 | 4 | 6.1 | 53.9 |
| Temporal | SSP126 | 2023 | 0 | 0.1 | 40.1 | 10.8 | 46.9 | 2.1 |
| Temporal | SSP126 | 2050 | 31 | 7.8 | 3.6 | 4.8 | 10.4 | 42.4 |
| Temporal | SSP126 | 2099 | 34.9 | 4 | 1.8 | 6.5 | 11 | 41.7 |
| Temporal | SSP245 | 2023 | 0 | 0.1 | 40.1 | 10.8 | 46.9 | 2.1 |
| Temporal | SSP245 | 2050 | 28.8 | 9.2 | 2.8 | 4.6 | 7.8 | 46.8 |
| Temporal | SSP245 | 2099 | 35.3 | 5.1 | 1.4 | 5.5 | 4.1 | 48.5 |
| Temporal | SSP370 | 2023 | 0 | 0.1 | 40.1 | 10.8 | 46.9 | 2.1 |
| Temporal | SSP370 | 2050 | 17.2 | 14 | 1.7 | 3.6 | 7 | 56.5 |
| Temporal | SSP370 | 2099 | 5.7 | 6.8 | 0.8 | 1.6 | 2.8 | 82.2 |

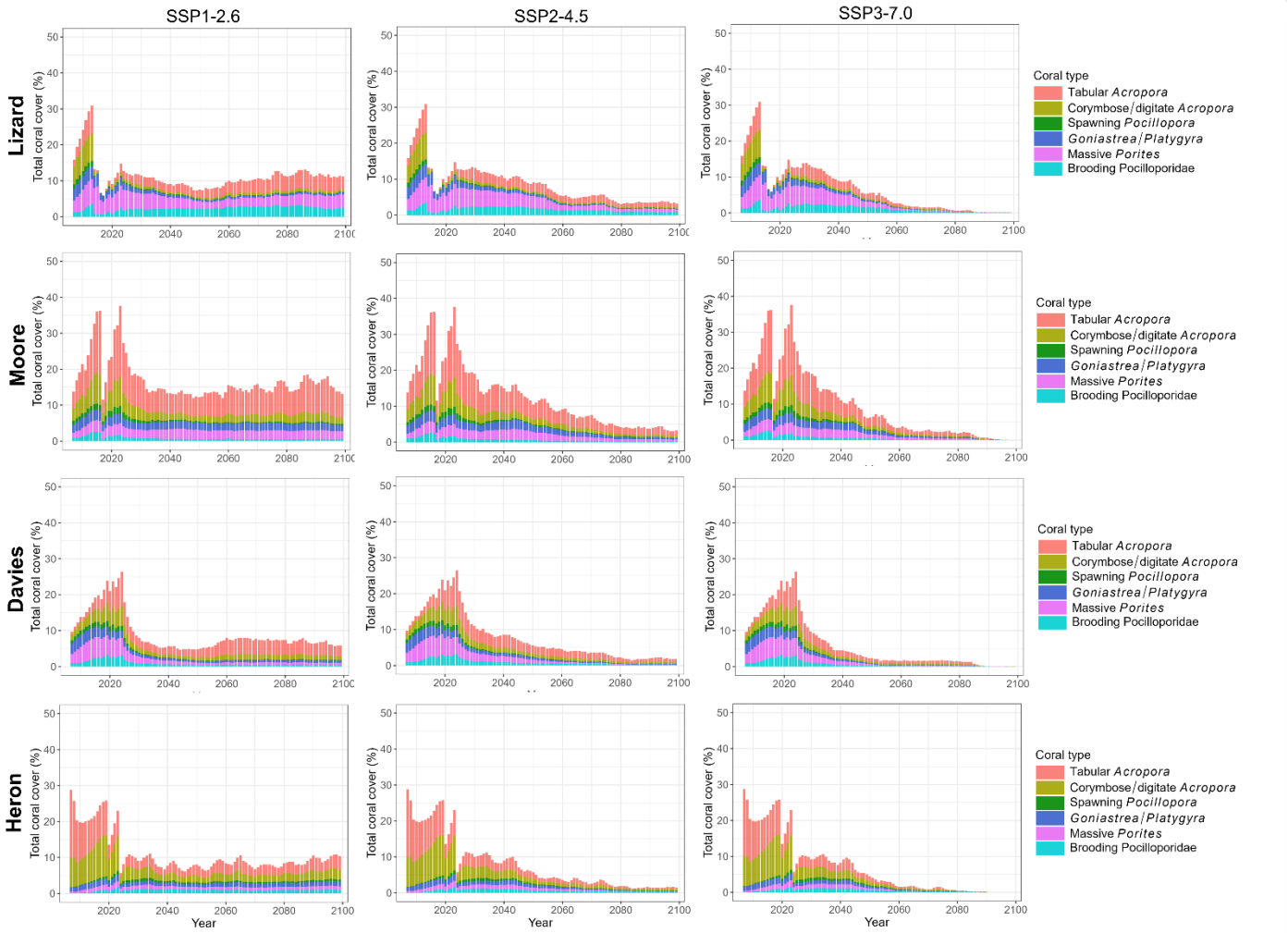


*Fig S 25.* ***Average total coral-cover trajectories as projected by the C~scape modelling framework across four case studies.*** *Each panel displays the projected trajectories of six coral taxa (see legend) for each of the three SSPs (columns) and GBR case studies (rows). Projections were made across the 200 future climate scenarios derived from 10 Global Climate Models (GCMs) per SSP.*

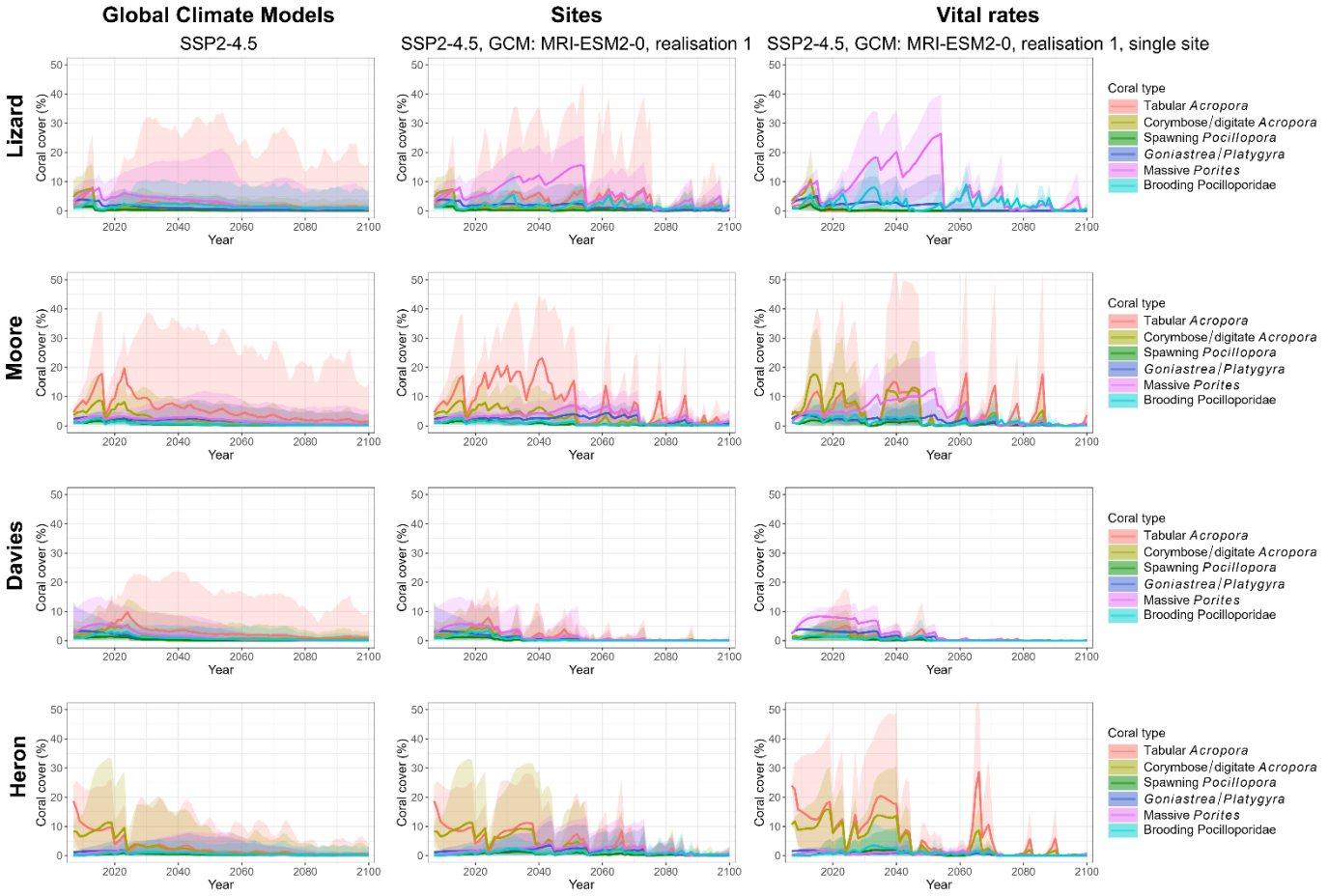


*Fig S 26.* ***Total coral-cover trajectories as projected by the C~scape modelling framework across four case studies.*** *Each panel displays the projected trajectories of six coral taxa (see legend) showing the mean (solid lines) and the 95% confidence interval (shaded ribbons). Predictions were made across the 200 future climate scenarios derived from 10 Global Climate Models (GCMs) under the SSP2-4.5 Shared Socioeconomic Pathway (IPCC 2022) (first column), across sites under a single realisation of the MRI-ESM2-0 climate future (second column), and across 200 individual posterior draws—sampled from a total possible 8000 from the growth and survival regressions—for a single site (third column).*

# APPENDIX 4. Supporting Information on the *C~scape* framework

## 4.1. *C~scape* overview

The *C~scape* modelling framework combines coral demography with information on the major processes that vary spatially within reefs and influence coral population growth and mortality to simulate coral metacommunity dynamics (Fig S 27).

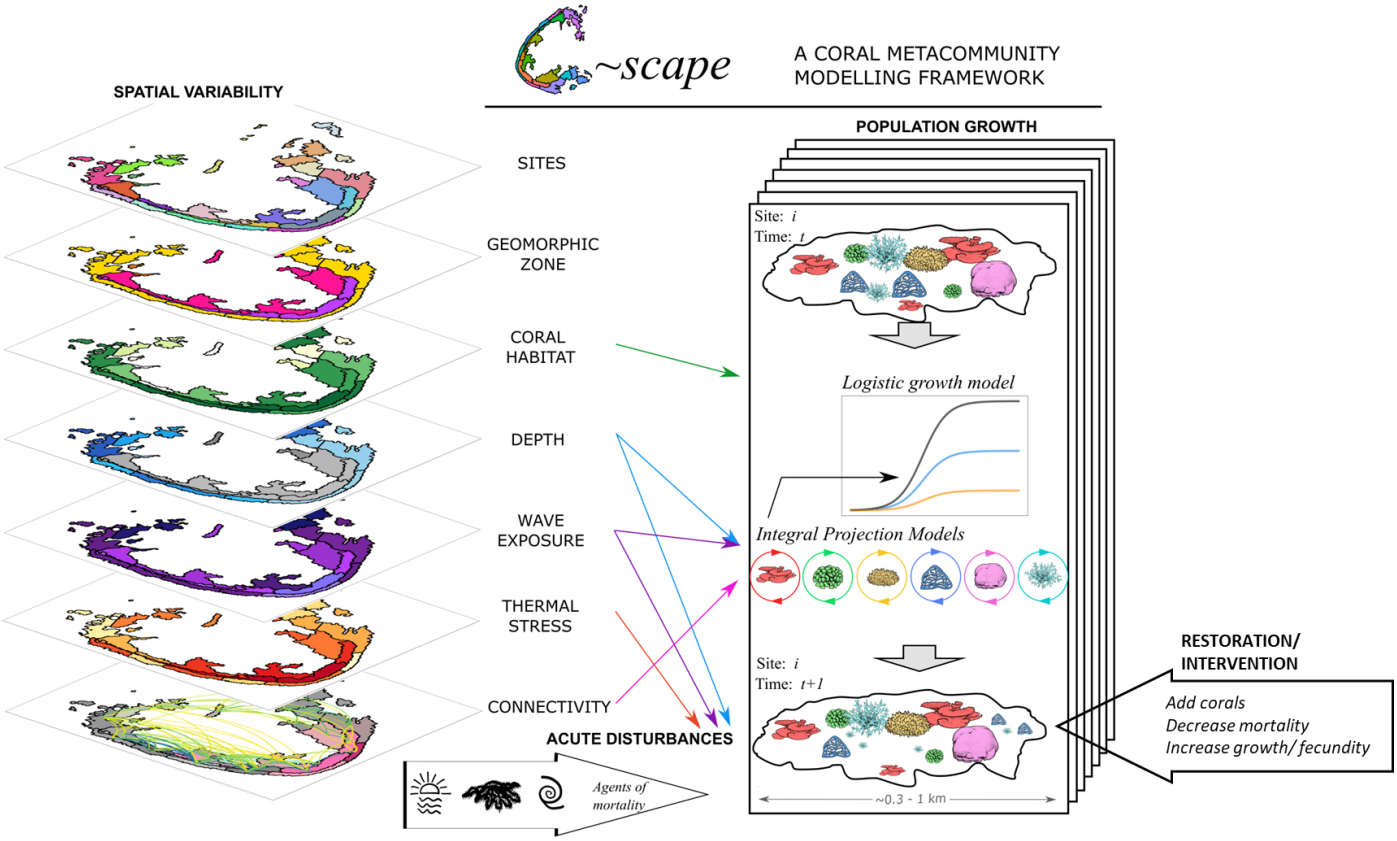


*Fig S 27. Schematic representation of the C~scape modelling framework. C~scape is applied to a reef or cluster of reefs. A reef is divided into multiple spatial units referred to as 'sites'. A 'population' for each distinct coral type is modelled discretely at each site. Populations are connected as metapopulations with a connectivity matrix describing the probability of coral larvae moving among sites. Intrinsic population growth rates are determined for each coral type from integral projection models (IPMs) that describe the coral life cycle, enabling the projection of changes in each population of corals over an annual period from time t to time t+1. The IPMs contain discrete life states for coral eggs, larvae and settlers, as well as a continuous state across the size range of each coral type captured by 100 size classes. Sites have different depths, influencing the populations' exposure to temperature stress. Sites are assigned a value for the 'coral habitat', which specifies the maximum percentage total coral cover in a site; this value modulates community growth as the maximum is approached. Acute disturbances (temperature stress, cyclones and crown-of-thorns starfish outbreaks) affect coral populations by killing individuals as function of disturbance intensity.*

## 4.2. Disturbance inputs and disturbance-mortality functions

Temperature stress, cyclones, and Acanthaster Crown-of-Thorns starfish (COTS) outbreaks are implemented as acute disturbances that may occur in any given year and kill a proportion of the corals. Three disturbance-mortality functions are used, where mortality (as proportional change in the coral cover) is simulated to occur in annual timesteps as a function of the disturbance magnitude at each site in each year.

### 4.2.1. Cyclones

*Table S 9. Cyclone categories and their associated wind speeds, as defined by the Bureau of Meteorology, were used to convert cyclone category to wind speed for the cyclone-mortality function (Fig S 28).*

| Cyclone category | Windspeed |
|---|---|
| 1 | 24.5 m/s |
| 2 | 32.5 m/s |
| 3 | 44.2 m/s |
| 4 | 55.3 m/s |
| 5 | 65 m/s |

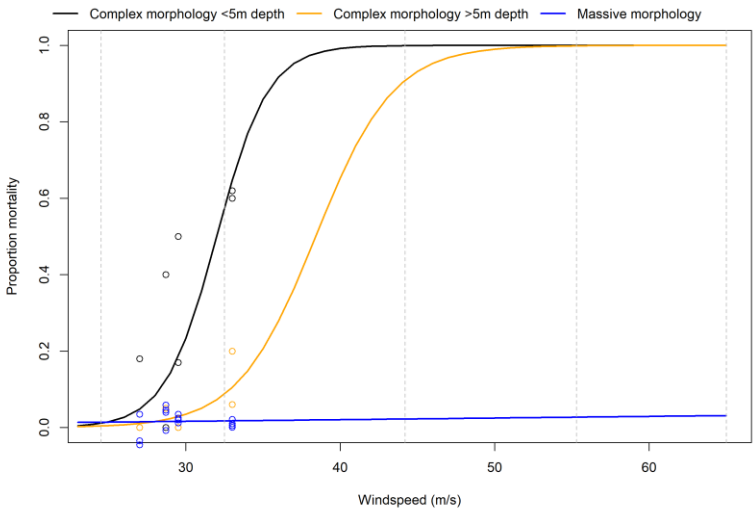


*Fig S 28. Windspeed and the predicted proportion of mortality which is applied to the coral cover of each coral type. Dashed vertical lines indicate cyclone categories 1-5 from left to right (see Table S 9).*

### 4.2.2. Crown-of-Thorns (COTS) starfish outbreaks

To account for the fact that coral consumption scales significantly with starfish diameter, we disaggregated total adult densities ((ind. ha-1, which were obtained from output from ReefMod-GBR) into four size-cohorts (10, 15, 25, and 45 cm). This disaggregation was based on empirical data provided by GBRMPA COTS Control Program cull data cluster proportions, which allowed the model to reflect regional differences in starfish demography (Miller et al. 2018). These proportions were filtered to reflect a representative background population structure. Any reefs surveyed by the COTS Control Program that matched those within the GBR case studies were examined to calculate a mean proportional frequency for each size class and each case study (Table 1).Site-level abundance in any given timestep was determined by multiplying the total ReefMod adult density by these cluster-specific proportions. The resulting cohort densities were then scaled to the physical area of individual reef sites.

*Table S 10. Proportions derived from filtered GBRMPA COTS Control Program cull data*

| GBR case study | Cohort 1 (10 cm) | Cohort 2 (15 cm) | Cohort 3 (25 cm) | Cohort 4 (45 cm) |
|---|---|---|---|---|
| **Davies Reef** | 0.06 | 0.28 | 0.42 | 0.24 |
| **Lizard Island** | 0.08 | 0.36 | 0.4 | 0.15 |
| **Moore Reef** | 0.45 | 0.32 | 0.16 | 0.07 |
| **Heron Reef** | 0.01 | 0.04 | 0.24 | 0.67 |

We estimated annual coral consumption by fitting a linear model to empirical feeding data in (Keesing and Lucas 1992), which related starfish size to the daily area of coral killed ($cm^2$ $day^{-1}$). The yearly consumption for each cohort was calculated as:

$$M_{COTS} = 365 \times (10.76 * size - 192.69)$$

The total annual potential coral consumption at a site was calculated by summing the consumption of all four COTS size-cohorts based on their specific abundances:

$$M_{total_{COTS}} = \sum_{cohort_s=1}^{4} (COTS_{cohort} \times (10.76 \times cohort_s - 192.69) \times 365$$

Where $COTS_{cohort}$ is the abundance of COTS in size-cohort $cohort_s$. The feeding rate for the smallest cohort (10 cm) was manually set to zero reflects biological observations that starfish of this size have not yet transitioned from a diet of crustose coralline algae to a significant coral diet (Engelhardt et al. 1999).

Total predation was allocated across coral functional types using a susceptibility-weighted selection ratio, which considers both the inherent preference for a coral type and its current availability. Following De'ath and Moran (1998), susceptibility values (Odds) were assigned to each functional type (Table S 1). For each site, a selection ratio (SR) is calculated by multiplying the inherent preference (Odds) by the proportional cover of that coral type. This ensures that COTS predation shifts dynamically as different coral groups become more or less abundant.

$$SR_{ft} = \frac{Odds_{ft} \times Cover_{ft}}{\sum Odds \times Cover}$$

The resulting proportion of total coral area removed was applied as a uniform proportional mortality across the coral size structure. To prevent local extinction within a single time step, total annual mortality was capped at 95%.

### 4.2.3. Heat stress

Heat stress mortality is modelled as a function of site depth, coral type and the maximum DHW assigned to that site:

$$m_{init_{ft_{site}}} = w_{site} \cdot s_{ft} \cdot \left((e^{0.17+0.35 \cdot DHW_{site}}) - 1\right)/100$$

with $w_{site}$ being the depth coefficient and $s_{ft}$ being the bleaching sensitivity of a coral type (Table S 1)

The depth coefficient was calculated as:

$$w_{site} = e^{-0.07551(sitedepth-2)}$$

Annual mortality ($M$) was then calculated as described in the main text to give (Fig S 29)

$$M_{ft_{site}} = \begin{cases} 0 & \text{if } \mathrm{DHW_{site}} < 3 \\ 1 - \left(1 - m_{init_{ft_{site}}}\right)^6 & \text{if } \mathrm{DHW_{site}} > 0 \end{cases}$$

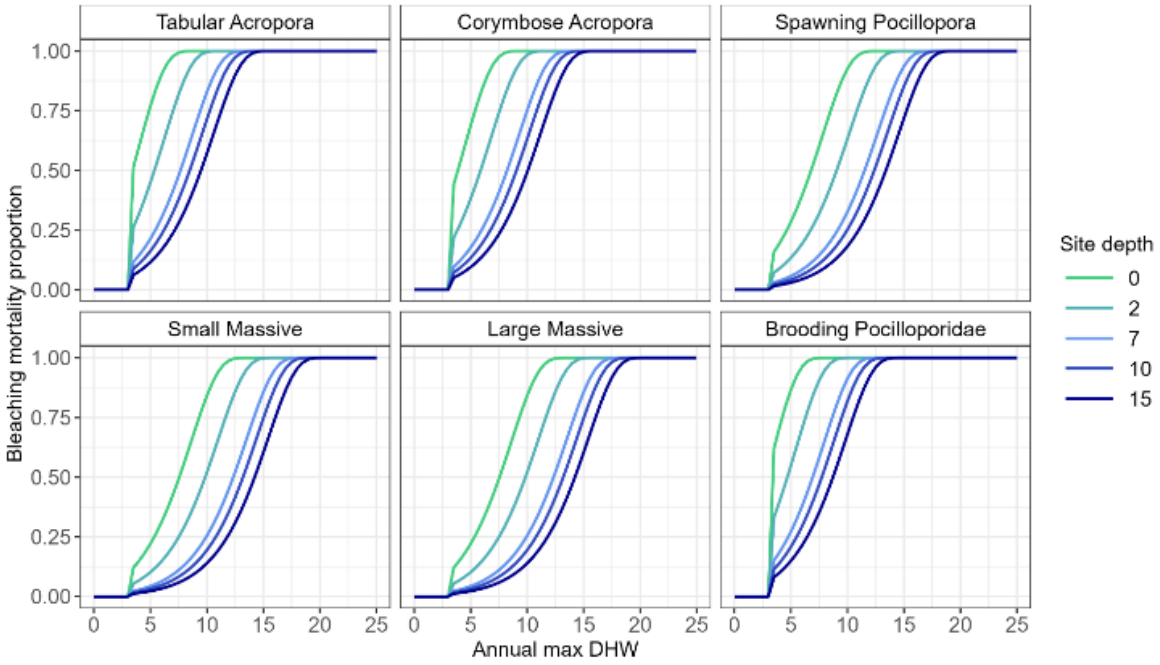


*Fig S 29. Bleaching mortality probability as a function of the maximum Degree Heating Weeks at a site shown for the six coral types at five depths. Coral types are parameterised with a relative bleaching susceptibility (see Table S 1) based on the approach used in (Ortiz et al. 2014) with information from (Hughes et al. 2018) and Crossman et al (In review).*

### 4.3. Cross-generational heritability of thermal tolerance

Natural selection and adaptation are modelled using phenotypic variance rather than a gene-based approach, due to the challenges of linking complex genetic models to demographic frameworks (Van de Walle et al. 2025), and the limited availability of specific genetic parameters for corals (Bairos-Novak et al. 2021). To achieve this, the *C~scape* framework was updated so that, in addition to tracking the total abundance individual corals in each of 100 size classes, the abundance was also tracked across a set of thermal tolerance classes.

Previously, the model used a vector, $\overrightarrow{N_{ft,i,t}}$ (Cresswell et al. 2024), representing the number of corals of type *ft* across 100 size classes at site *i* and time *t*. We expanded this into a two-dimensional matrix, allowing the model to track the number of corals across early life stages (egg, larvae, settler) and size classes alongside thermal tolerance classes.

Thermal tolerance was incorporated as a deviation from the population's mean bleaching mortality response. To parameterise the distribution of corals across thermal tolerance classes, we used data from (Humanes et al. 2024) to extrapolate bleaching mortality index (BMI) curves, which were a function of DHW, to 100% mortality—the point at which BMI and the mortality curves used in *C~scape* were comparable (see Fig. S31). This resulted in a normal distribution with a mean of 0 and a standard deviation of $sd = 1.91$ which was used for initialising the coral populations in *C~scape*. As infinite thermal tolerance is not realistic, we truncated the normal distribution to -8 and +8DHW. Within this range we defined thermal tolerance classes as $\Delta DHW$ from the mean, here utilising 14 discrete bins: $\Delta DHW = \{-5, -4 \ldots, 8\}$.

We incorporated tolerance class, $\Delta DHW$, into the bleaching mortality function (Bozec et al. 2022), which effectively shifted the bleaching mortality curve along the x-axis, where positive values ($\Delta DHW > 0$) equate to higher resistance (reduced mortality) and negative values ($\Delta DHW < 0$) higher susceptibility (increased mortality) (Fig. S31).

$$m_{init_{ft\_site}} = w_{site} \cdot s_{ft} \cdot ((e^{0.17+0.35\cdot(DHW_{site}-\Delta DHW)}) - 1)/100$$

In practice, this means that when a population within a given site and timestep experiences thermal stress (as DHW), the corals in each thermal tolerance class will have differing mortality probabilities.

Corals within each thermal tolerance class retain the same $\Delta DHW$ throughout their life cycle. To allow for cross-generational selection the transmission of this phenotypic trait to the next generation was modelled by applying the Breeder's equation (Lynch and Walsh 1998). The Breeder's equation predicts the selection differential (the difference between the mean of the parental population and the mean of the breeding individuals) of a given trait over one generation after selection based on a parameter the trait's 'narrow-sense heritability' (Postma 2014, de Villemereuil et al. 2018). We generalise this principle over multiple generations.

Larvae are allocated to tolerance classes via a vector, $\overrightarrow{L_{ft,i,t}}$ , which describes the proportion of total larvae of coral type *ft*, at site *i* and year *t* within each class. This is calculated as

$$\overrightarrow{L_{ft,i,t}} = \overrightarrow{L_{ft,i,t-1}} + \vec{R}$$

With $\vec{R}$ being the transgenerational response to selection, analogous to the Breeder's equation (Falkner and Mackay 1996, Lynch and Walsh 1998). We adjusted the Breeder's equation such that we could use the actual frequency distribution of the offspring's thermal tolerance, rather than calculating only the mean of a presumed normal distribution. This allowed us to retain the true distribution of thermal tolerance independent of normality and avoided making assumptions about the variance around the mean across multiple generations under selection. Therefore, in our implementation, $\vec{R}$ is expressed as a vector rather than a single value containing the proportion of larvae in each thermal tolerance class.

The generational response is defined as:

$$\vec{R} = \mathrm{h}^2\vec{S}$$

where $h^2$ is the narrow-sense heritability and $\vec{S}$ is the selection differential vector.

Narrow-sense heritability expresses how much of the trait is inherited by the offspring and ranges from 0 (no trait transfer between parent and offspring) to 1 (100% of the trait is transferred). Narrow-sense heritability ($h^2$) has been investigated in many populations of organisms and found to tend towards $h^2$=0.3 for polygenic traits that are non-morphological and related to fitness (Moore et al 2019). This fits within the available reports (Bairos-Novak et al. 2021) for corals so we used this value for all model simulations in the present study.

The selection differential, $\vec{S}$, is calculated as the difference in the distribution of thermal tolerances before and after selection pressure is applied (i.e. at the beginning and end of an annual timestep):

$$\vec{S} = \overrightarrow{L_{ft,\iota,t+1}} - \overrightarrow{L_{ft,\iota,t}}$$

where $\overrightarrow{L_{ft,\iota,t}}$ is the larval thermal distribution in the case thermal stress was not applied (initial state), and $\overrightarrow{L_{ft,\iota,t+1}}$ is the provisional thermal tolerance distribution of the larvae that would be generated by this year's surviving adult population after all selection events have occurred ($\overrightarrow{N_{ft,\iota,t+1}}$), assuming perfect heritability ($h^2 = 1$ ). Utilising the selection differential in this fashion allows there to be a carry-on effect of the initial thermal tolerance distribution beyond the first year, slowing down selection and accounting for multiple generations.

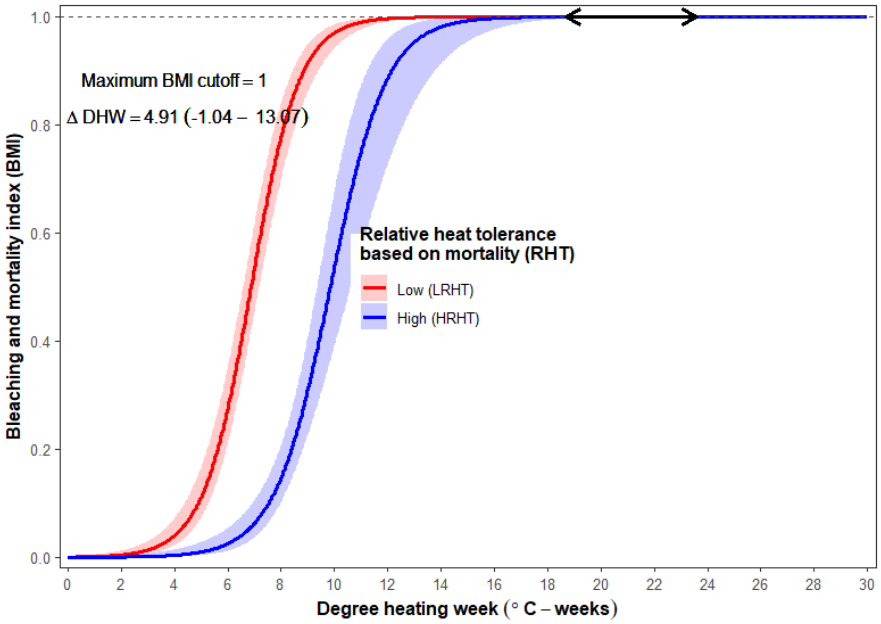


*Fig S 30. Bleaching Mortality Index as per (Humanes et al. 2022) extrapolated to BMI=1 based on the C~scape implementation of heat tolerance on the bleaching mortality curve. (Humanes et al. 2022) exposed 102 healthy adult colonies to a 30-day temperature stress experiment. Here we show the results for the mortality response of the 10% least heat tolerant corals (red, ΔDHW ± 95% confidence intervals) and the response for the 10% most heat tolerant corals (blue, ΔDHW ± 95% confidence intervals).The difference between the two responses ΔDHW=4.91 reflects the intrapopulation variability used to determine the thermal tolerance.*

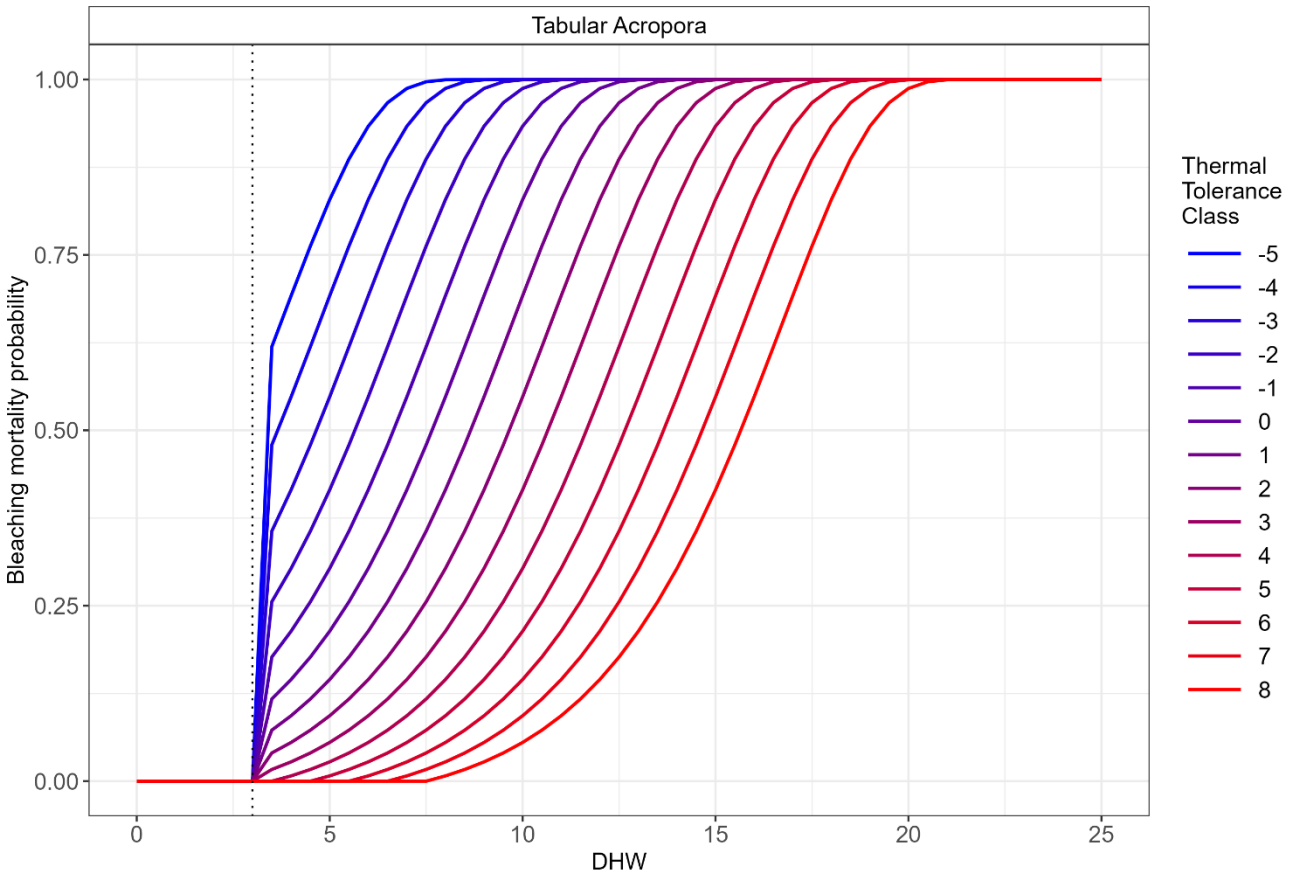


*Fig S 31. Thermal stress (Degree Heating Weeks) mortality curve for tabular Acropora for a site depth of 7 metres showing the mortality that would result for a coral in each of the 14 thermal tolerance classes which describe a shift from the original thermal tolerance where the thermal tolerance class is zero.*

# APPENDIX 5. *C~scape* model assumptions and limitations

Any model of a complex system is constrained by the available knowledge and the data that can be gathered across space and time. Table S1 details the key assumptions, omissions and limitations of the current modelling efforts. The authors judged whether each factor would likely lead to an over- or underestimation in the projected coral cover values, or whether it creates uncertainty or imprecision for which it is not possible to judge the likely direction of influence.

Of the factors where the direction of influence was assessed, the majority resulted in an overestimation; this suggests our projections may be overall optimistic regarding the future coral cover of the Great Barrier Reef.

*Table S 11. Summary of key assumptions and limitations in the C~scape modelling framework as applied in the present study. Rows are grouped into three categories of uncertainty: parametric uncertainty (reducible with more data), structural assumptions (fixed model design choices and omissions), and scenario uncertainty (arising from choice of climate forcing). Grey shading indicates factors likely to introduce additional variability or uncertainty in a direction that is difficult to predict. Purple shading indicates factors likely to cause overestimation of coral-cover projections; orange text indicates factors likely to cause underestimation.*

| Factor | Description and importance of factor | Parameterisation / assumptions in the *C~scape* framework |
|---|---|---|
| ***Parametric uncertainty*** | | |
| **Vital rate data** | Growth, survival, and early life history parameters define population growth, maintenance, and recovery. | **Uncertainty:** Parameterised from only one year of monitoring data. Multi-year data would better disentangle individual and spatial variability from interannual variability.<br>**Uncertainty:** Growth follows a logistic assumption as space becomes limiting, though survival and the true shape of this relationship may vary. We assume survival is not directly affected by space limitation. |
| **Thermal tolerance distribution** | Quantifying baseline variability in heat tolerance is critical for predicting how a population might shift or adapt under selection. | **Uncertainty:** Natural selection and adaptation are modelled based on phenotypic variance rather than a gene-based model. Thermal tolerance of individuals is defined relative to the mean bleaching susceptibility of the group at initialisation. Thermal tolerance phenotypes follow a single Acropora population (*A. digitifera*) from Palau.<br>**Underestimation risk:** A conservative upper limit to thermal tolerance (+8DHW relative to contemporary level) is assumed. Greater adaptation may be possible, but empirical data on the upper limit remain limited. |
| **Heritability** | Corals can inherit phenotypes from their parents, but rarely is this transferred fully. | **Uncertainty**: Modelled corals have an individual heat tolerance that is partially inherited from the coral's parents, with parameter $h^2 = 0.3$, allowing for the simulation of natural selection and adaptation over time. This parameter is likely variable across species or locations. Heritability has not been validated across multiple consecutive generations. |
| **Trade-offs with increasing heat tolerance** | Selection for thermal tolerance may involve energetic trade-offs, potentially impacting other life-history traits like growth and reproduction. | **Uncertainty**: Modelled based on phenotypic variance rather than gene-based models. Does not account for other critical traits (e.g., colony growth, fecundity) or potential trade-offs (e.g., reduced growth) that may accompany enhanced heat tolerance. |
| **DHW-mortality relationship** | The relationship between degree heating weeks and coral mortality is complex, varying with depth, prior thermal exposure, local conditions, and repeated stress. | **Underestimation risk:** The function predicts near 100% mortality for DHW >10 which likely results in an overestimation of mortality, and thus an underestimation in coral-cover projections.<br>**Uncertainty:** Limited empirical data exists for very high DHW events (>16), which are projected to become more common. |
| **Connectivity** | Connectivity is variable, difficult to parameterise, and may change in future oceans (Maciejewski and Cumming 2016, McManus et al. 2021, Mason et al. 2025) The are strong differences in the capacity for connectivity between coral species. | **Uncertainty:** Future connectivity is inferred from three years of hindcast modelling.<br><br>**Uncertainty:** Modelling currently assumes the same biological parameters for all spawning coral types. |
| **Depth** | Influences mortality during acute disturbance and vital rates of growth and survival. | **Uncertainty:** Depth is included in the DHW-mortality function, but only at the resolution of median depth of sites (~300x300m).<br>Finer-scale variability is omitted, meaning realised trajectories are likely more variable in space than modelled. |
| ***Structural assumptions*** | | |
| **Coral types** | Species are not modelled explicitly, making it difficult to model factors such as fertilisation | **Uncertainty:** Species with distinctions in growth, survival, or reproduction (e.g. digitate and corymbose Acropora) are grouped together, which may mask species-specific demographics.<br>**Overestimation risk:** Species are not modelled explicitly, and it is assumed that all coral individuals within a coral type can reproduce. This would create an overestimation in fertilisation rates.<br>**Uncertainty:** High species diversity offers potential for community shifts toward heat-tolerant assemblages of species, in addition to shifts among individuals within a species.<br>**Uncertainty:** Staghorn acroporids, foliose corals and other groups were excluded as they form thickets and did not align well with the individual-based Integral Projection Modelling framework. |
| **Early life history** | Processes such as fecundity, fertilisation, and settlement are likely variable with environment. | **Uncertainty:** Environment-dependent influences on fecundity, fertilisation, and settlement were not modelled due to limited data availability. Vital rates of growth and survival were allowed to vary with environment, but early life history rates were held constant. |
| **Non-lethal effects of acute heat stress** | Coral vital rates are known to vary in non-linear, taxa-dependent ways under acute disturbances (Hall et al. 2021, Morais et al. 2021, Speare et al. 2022, Stratford et al. 2025), for example decreased fecundity and growth, or increased partial mortality. | **Overestimation risk**: Not captured in the current modelling framework. Would cause overestimation of coral cover. |

914 Table S 10 contined

| Factor | Description and importance of factor | Parameterisation / assumptions in the *C~scape* framework |
|---|---|---|
| ***Structural assumptions*** | | |
| **Chronic changes to temperature** | Rates of coral growth (Álvarez-Noriega et al. 2023) and fecundity may change with chronic warming (Edmunds 2024) or result from non-lethal effects of heat stress. | **Uncertainty:** The base rates of growth, survival and fecundity are assumed constant throughout the century.<br>**Overestimation risk:** Non-lethal effects (presumably negative), such as reduced fecundity or growth following acute stress, are not captured in the current framework. |
| **Fertilisation** | Low coral cover is associated with low coral densities which leads to reduced fertilisation success (Allee effect) (Ricardo et al. 2025) | **Uncertainty:** Information to parameterise fertilisation was limited and variable across taxa and studies.<br>**Overestimation risk:** The model assumes fertilisation success is not affected by diminishing coral density, |
| **Link to regional-scale modelling** | Integrating *C~scape* with a regional-scale model (ReefMod-GBR) introduces interface assumptions at the boundaries of the modelled domain, including larval influx from external reefs. | **Uncertainty:** Two coral community models were run in parallel, most notably to account for the larval influx from reefs outside the simulated domain of the *C~scape* cluster. Although they have similarities, differences exist in parameterisation and architecture meaning that assumptions are necessary at the interface, for example thermal tolerance distributions for external larvae are assigned based on the within cluster tolerances, and the parameterisation of coral types does not match exactly. This means the demographic rates of growth and survival in *C~scape* are different from the parameterisations in ReefMod-GBR, which are structured around different size classes, but comparable in capturing the major differences in growth and survival between functional types. |
| **Black swan events** | "Black swan" events are high-impact, rare events that are difficult to predict (Bray and Wang 2020) | **Overestimation risk:** Beyond the scope of the modelling. Examples include severe disease outbreaks, invasive species, or systemic collapses such as the breakdown of the Atlantic Meridional Overturning Circulation (AMOC). |
| **Reef representation** | High variability exists across GBR reef; for example, inshore reefs are exposed to multiple additional stressors including poor water quality, sedimentation, and nutrient loading. | **Overestimation risk:** This study modelled select clusters of offshore reef only, omitting the full range of stressors for inshore reefs. |
| **Phase shifts** | Ecological shifts (e.g., coral to turf/algae) can inhibit coral recovery processes. | **Overestimation risk:** Alternative stable states (i.e. a shift from coral to another benthic organism) arising from phase shifts are not captured and are difficult to predict. |
| **Ocean acidification** | High CO2 levels negatively impact coral growth, recruitment, and wave damage resistance. May also impact calcifying algae abundance (Klein et al. 2022) | **Overestimation risk:** Not captured in the modelling framework. Including ocean acidification would likely result in lower coral resilience and reef condition. |
| ***Scenario uncertainty*** | | |
| **DHW downscaling** | Future frequency and intensity of marine heatwaves are driven by downscaled temperature projections. | **Underestimation risk**: Downscaled projections for 2014–2023 tend to predict more severe heat stress than observed in satellite data. Predicted coral over the next 1–2 decades may be underestimated (Bozec et al. 2025). |
| **SSPs** | Shared Socioeconomic Pathways are considered the most robust way to represent a range of plausible future greenhouse gas emission trajectories and societal development pathways. | **Uncertainty:** We chose three SSPs for this study: SSP1-2.6, SSP2-4.5, SSP3-7.0. SSP1-1.9 (limiting warming to 1.5°C) was not included as this pathway is now considered very unlikely (Olhoff et al. 2024). SSP5-8.5 was excluded as the scale of societal impacts at >4°C warming would erode capacity for meaningful reef management. |
| **Global Climate Models** | An ensemble of coupled atmosphere-ocean general circulation models (GCMs) are available via the CMIP6 database (Eyring et al. 2016). These simulate a set of alternative scenarios of societal and economic development leading to different trajectories of atmospheric carbon concentrations. | **Underestimation risk:** We selected 10 GCMS to cover a range of equilibrium climate sensitivity (ECS) values (2.6 – 5.3 °C), but caution has been raised over the selection of models associated to unrealistically high ECS (Tokarska et al. 2020, Hausfather et al. 2022). Equilibrium climate sensitivity is very likely (90% probability) to lie between 2.3–4.7 °C (Sherwood et al. 2020), yet a significant number of CMIP6 models have an ECS value above this range (Tokarska et al. 2020). |
| **Realisations** | While the GCMs provide projections of future temperature, the uncertainty and stochasticity in these was not available but we acknowledge that it is impossible to predict the exact year of marine heatwaves in future decades. | **Uncertainty:** DHW timing within decades was shuffled across realisations to represent stochasticity in thermal stress events (Bozec et al. 2025). This approach captures one dimension of temporal uncertainty; alternative methods of representing DHW stochasticity exist and may yield different results. |

915

916

# References


Althaus, F., N. Hill, R. Ferrari, L. Edwards, R. Przeslawski, C. H. Schönberg, R. Stuart-Smith, N. Barrett, G. Edgar, and J. Colquhoun. 2015. A standardised vocabulary for identifying benthic biota and substrata from underwater imagery: the CATAMI classification scheme. PloS one 10:e0141039.

Álvarez-Noriega, M., A. H. Baird, M. Dornelas, J. S. Madin, V. R. Cumbo, and S. R. Connolly. 2016a. Fecundity and the demographic strategies of coral morphologies. Ecology 97:3485–3493.

Álvarez-Noriega, M., A. H. Baird, M. Dornelas, J. S. Madin, V. R. Cumbo, and S. R. Connolly. 2016b. Fecundity and the demographic strategies of coral morphologies. Ecology 97:3485–3493.

Álvarez-Noriega, M., I. Marrable, S. H. C. Noonan, D. R. Barneche, and J. C. Ortiz. 2023. Highly conserved thermal performance strategies may limit adaptive potential in corals. Proceedings of the Royal Society B: Biological Sciences 290:20221703.

Álvarez-Noriega, M., J. C. Ortiz, D. M. Ceccarelli, M. J. Emslie, K. E. Fabricius, M. J. Jonker, M. Puotinen, B. J. Robson, C. M. Roelfsema, T. H. Sinclair-Taylor, and R. Ferrari. 2024. Spatial Variation in Upper Limits of Coral Cover on the Great Barrier Reef. Global Ecology and Biogeography 33:e13928.

Babcock, R., and C. Mundy. 1996. Coral recruitment: Consequences of settlement choice for early growth and survivorship in two scleractinians. Journal of Experimental Marine Biology and Ecology 206:179–201.

Bairos-Novak, K. R., M. O. Hoogenboom, M. J. van Oppen, and S. R. Connolly. 2021. Coral adaptation to climate change: Meta-analysis reveals high heritability across multiple traits. Global Change Biology 27:5694–5710.

Bozec, Y.-M., A. A. S. Adam, B. A. Nava, A. K. Cresswell, V. Haller-Bull, T. Iwanaga, L. Lachs, S. A. Matthews, J. K. McWhorter, K. R. N. Anthony, S. A. Condie, P. R. Halloran, J.-C. Ortiz, C. Riginos, and P. J. Mumby. 2025, January 25. A rapidly closing window for coral persistence under global warming. Ecology.

Bozec, Y.-M., K. Hock, R. A. B. Mason, M. E. Baird, C. Castro-Sanguino, S. A. Condie, M. Puotinen, A. Thompson, and P. J. Mumby. 2022. Cumulative impacts across Australia's Great Barrier Reef: a mechanistic evaluation. Ecological Monographs 92:e01494.

Bray, S. R., and B. Wang. 2020. Forecasting unprecedented ecological fluctuations. PLoS computational biology 16:e1008021.

Callaghan, D. P., J. X. Leon, and M. I. Saunders. 2015. Wave modelling as a proxy for seagrass ecological modelling: Comparing fetch and process-based predictions for a bay and reef lagoon. Estuarine, Coastal and Shelf Science 153:108–120.

Castro-Sanguino, C., J. C. Ortiz, A. Thompson, N. H. Wolff, R. Ferrari, B. Robson, M. M. Magno-Canto, M. Puotinen, K. E. Fabricius, and S. Uthicke. 2021. Reef state and performance as indicators of cumulative impacts on coral reefs. Ecological Indicators 123:107335.

Connolly, S. R., and A. H. Baird. 2010. Estimating dispersal potential for marine larvae: dynamic models applied to scleractinian corals. Ecology 91:3572–3583.

Cooley, D., and R. Shao. 2023. h3r.

Cresswell, A. K., V. Haller-Bull, M. Gonzalez-Rivero, J. P. Gilmour, Y.-M. Bozec, D. R. Barneche, B. Robson, K. R. N. Anthony, C. Doropoulos, C. Roelfsema, M. Lyons, P. J. Mumby, S. Condie, V. Lago, and J.-C. Ortiz. 2024. Capturing fine-scale coral dynamics with a metacommunity modelling framework. Scientific Reports 14:24733.

De'ath, G., and P. J. Moran. 1998. Factors affecting the behaviour of crown-of-thorns starfish (Acanthaster planci L.) on the Great Barrier Reef:: 2: Feeding preferences. Journal of Experimental Marine Biology and Ecology 220:107–126.

Dela Cruz, D. W., and P. L. Harrison. 2020. Enhancing coral recruitment through assisted mass settlement of cultured coral larvae. PLoS ONE 15:e0242847.

Delandmeter, P., and E. Van Sebille. 2019. The Parcels v2. 0 Lagrangian framework: new field interpolation schemes. Geoscientific Model Development 12:3571–3584.

Doropoulos, C., M. Alvarez-Noriega, K. Fabricius, R. Ferrari, P. J. Mumby, S. H. C. Noonan, M. Orr, and K. Salee. 2025a. Impact of environmental gradients on juvenile coral demography across the Great Barrier Reef and Torres Strait. Coral Reefs.

Doropoulos, C., M. Alvarez-Noriega, K. Fabricius, R. Ferrari, P. J. Mumby, S. H. Noonan, M. Orr, and K. Salee. 2025b, August 1. Impact of environmental gradients on juvenile coral demography across the Great Barrier Reef and Torres Strait. In Review.

Doropoulos, C., J. Elzinga, R. ter Hofstede, M. van Koningsveld, and R. C. Babcock. 2019. Optimizing industrial-scale coral reef restoration: comparing harvesting wild coral spawn slicks and transplanting gravid adult colonies. Restoration Ecology 27:758–767.

Doropoulos, C., L. A. Gómez-Lemos, K. Salee, M. J. McLaughlin, J. Tebben, M. Van Koningsveld, M. Feng, and R. C. Babcock. 2022. Limitations to coral recovery along an environmental stress gradient. Ecological Applications 32:e2558.

Doropoulos, C., G. Roff, Y.-M. Bozec, M. Zupan, J. Werminghausen, and P. J. Mumby. 2016. Characterizing the ecological trade-offs throughout the early ontogeny of coral recruitment. Ecological Monographs 86:20–44.

Edmunds, P. J. 2024. Decadal-scale time series highlight the role of chronic disturbances in driving ecosystem collapse in the Anthropocene. Ecology 105:e4360.

Eyring, V., S. Bony, G. A. Meehl, C. A. Senior, B. Stevens, R. J. Stouffer, and K. E. Taylor. 2016. Overview of the Coupled Model Intercomparison Project Phase 6 (CMIP6) experimental design and organization. Geoscientific Model Development 9:1937–1958.

Fabricius, K. E., G. De'Ath, M. L. Puotinen, T. Done, T. F. Cooper, and S. C. Burgess. 2008. Disturbance gradients on inshore and offshore coral reefs caused by a severe tropical cyclone. Limnology and oceanography 53:690–704.

Ferrari, R., W. F. Figueira, M. S. Pratchett, T. Boube, A. Adam, T. Kobelkowsky-Vidrio, S. S. Doo, T. B. Atwood, and M. Byrne. 2017. 3D photogrammetry quantifies growth and external erosion of individual coral colonies and skeletons. Scientific Reports 7:16737.

Gelman, A., and D. B. Rubin. 1992. Inference from Iterative Simulation Using Multiple Sequences. Statistical Science 7:457–472.

Gilmour, J. P., L. D. Smith, and R. M. Brinkman. 2009. Biannual spawning, rapid larval development and evidence of self-seeding for scleractinian corals at an isolated system of reefs. Marine Biology 156:1297–1309.

Gordon, S., E. Aston, M. Lechene, J. Harianto, P. Bray, W. Figueira, M. Gonzalez Rivero, and L. Ferrari. 2023. Field photogrammetry in 4D. Reef restoration and adaption program (EcoRRAP). Standard operational procedure number 1: overview and in-field workflow. Australian Institute of Marine Science, Townsville 62.

Hall, T. E., A. S. Freedman, A. M. De Roos, P. J. Edmunds, R. C. Carpenter, and K. Gross. 2021. Stony coral populations are more sensitive to changes in vital rates in disturbed environments. Ecological Applications 31:e02234.

Hausfather, Z., K. Marvel, G. A. Schmidt, J. W. Nielsen-Gammon, and M. Zelinka. 2022. Climate simulations: recognize the 'hot model'problem. Nature 605:26–29.

Heyward, A., L. Smith, M. Rees, and S. Field. 2002. Enhancement of coral recruitment by in situ mass culture of coral larvae. Marine Ecology Progress Series 230:113–118.

Hughes, T. P. 1984. Population dynamics based on individual size rather than age: a general model with a reef coral example. The American Naturalist 123:778–795.

Hughes, T. P., J. T. Kerry, A. H. Baird, S. R. Connolly, A. Dietzel, C. M. Eakin, S. F. Heron, A. S. Hoey, M. O. Hoogenboom, G. Liu, M. J. McWilliam, R. J. Pears, M. S. Pratchett, W. J. Skirving, J. S. Stella, and G. Torda. 2018. Global warming transforms coral reef assemblages. Nature 556:492–496.

Humanes, A., L. Lachs, E. A. Beauchamp, J. C. Bythell, A. J. Edwards, Y. Golbuu, H. M. Martinez, P. Palmowski, A. Treumann, E. van der Steeg, R. van Hooidonk, and J. R. Guest. 2022. Within-population variability in coral heat tolerance indicates climate adaptation potential. Proceedings of the Royal Society B: Biological Sciences 289:20220872.

Humanes, A., L. Lachs, E. Beauchamp, L. Bukurou, D. Buzzoni, J. Bythell, J. R. Craggs, R. de la Torre Cerro, A. J. Edwards, and Y. Golbuu. 2024. Selective breeding enhances coral heat tolerance to marine heatwaves. Nature Communications 15:8703.

Klein, S. G., N. R. Geraldi, A. Anton, S. Schmidt-Roach, M. Ziegler, M. J. Cziesielski, C. Martin, N. Rädecker, T. L. Frölicher, and P. J. Mumby. 2022. Projecting coral responses to intensifying marine heatwaves under ocean acidification. Global change biology 28:1753–1765.

Levitan, D. R., W. Boudreau, J. Jara, and N. Knowlton. 2014. Long-term reduced spawning in Orbicella coral species due to temperature stress. Mar Ecol Prog Ser 515:1–10.

Lynch, M., and B. Walsh. 1998. Genetics and analysis of quantitative traits. Sinauer Sunderland, MA.

Maciejewski, K., and G. Cumming. 2016. Multi-scale network analysis shows scale-dependency of significance of individual protected areas for connectivity. Landscape Ecology 31.

Madin, J. S., K. D. Anderson, M. H. Andreasen, T. C. Bridge, S. D. Cairns, S. R. Connolly, E. S. Darling, M. Diaz, D. S. Falster, and E. C. Franklin. 2016. The Coral Trait Database, a curated database of trait information for coral species from the global oceans. Scientific Data 3:1–22.

Madin, J. S., A. H. Baird, S. R. Connolly, M. A. Dornelas, M. Álvarez-Noriega, M. J. McWilliam, M. Barbosa, S. A. Blowes, P. Cetina-Heredia, A. P. Christie, V. R. Cumbo, M. Diaz, M. A. Emms, E. Graham, D. Hansen, M. Hisano, E. Howells, C.-Y. Kuo, C. Palmer, J. T. C. Hong, T. Zhi En Teo, and R. M. Woods. 2023. Six years of demography data for 11 reef coral species. Ecology 104:e4017.

Mason, R. A. B., C. Langlais, J. Uribe-Palomino, M. Tonks, F. Coman, S. Choukroun, J. Porobic, and C. Doropoulos. 2025. Reef-scale variation in larval supply and settlement: validating Lagrangian dispersal predictions with observations of coral larvae. Estuarine, Coastal and Shelf Science 326:109506.

McManus, L. C., E. W. Tekwa, D. E. Schindler, T. E. Walsworth, M. A. Colton, M. M. Webster, T. E. Essington, D. L. Forrest, S. R. Palumbi, and P. J. Mumby. 2021. Evolution reverses the effect of network structure on metapopulation persistence. Ecology 102:e03381.

McWhorter, J. K., P. R. Halloran, G. Roff, W. J. Skirving, C. T. Perry, and P. J. Mumby. 2022. The importance of 1.5° C warming for the Great Barrier Reef. Global Change Biology 28:1332–1341.

Miller, I. R., M. Jonker, and G. Coleman. 2018. Crown-of-thorns starfish and coral surveys using the manta tow technique. Australian Institute of Marine Science, Townsville, Australia.

Morais, J., R. A. Morais, S. B. Tebbett, M. S. Pratchett, and D. R. Bellwood. 2021. Dangerous demographics in post-bleach corals reveal boom-bust versus protracted declines. Scientific Reports 11:18787.

Mulla, A. J., V. Denis, C. Lin, C. Fong, J. Shiu, and Y. Nozawa. 2024. Natural coral recovery despite negative population growth. Ecology 105:e4368.

Mumby, P. J., G. Sartori, E. Buccheri, C. Alessi, H. Allan, C. Doropoulos, G. Rengiil, and G. Ricardo. 2024. Allee effects limit coral fertilization success. Proceedings of the National Academy of Sciences 121:e2418314121.

Olhoff, A., J. Christensen, W. F. Lamb, M. Pathak, T. Kuramochi, T. Fransen, J. Rogelj, M. den Elzen, J. Portugal-Pereira, and N. Grant. 2024. Emissions Gap Report 2024: No more hot air… please! With a massive gap between rhetoric and reality, countries draft new climate commitments.

Ortiz, J. C., Y.-M. Bozec, N. H. Wolff, C. Doropoulos, and P. J. Mumby. 2014. Global disparity in the ecological benefits of reducing carbon emissions for coral reefs. Nature Climate Change 4:1090–1094.

Postma, E. 2014. Four decades of estimating heritabilities in wild vertebrate populations: improved methods, more data, better estimates. Quantitative genetics in the wild 16:33.

Pratchett, M. S., K. D. Anderson, M. O. Hoogenboom, E. Widman, A. H. Baird, J. M. Pandolfi, P. J. Edmunds, and J. M. Lough. 2015. Spatial, temporal and taxonomic variation in coral growth—implications for the structure and function of coral reef ecosystems. Oceanography and marine biology: an annual review 53:215–295.

Randall, C. J., C. Giuliano, K. Allen, A. Bickel, M. Miller, and A. P. Negri. 2023. Site mediates performance in a coral-seeding trial. Restoration Ecology 31:e13745.

Randall, C. J., C. Giuliano, A. J. Heyward, and A. P. Negri. 2021. Enhancing Coral Survival on Deployment Devices With Microrefugia. Frontiers in Marine Science 8:662263.

Randall, C. J., C. Giuliano, B. Stephenson, T. N. Whitman, C. A. Page, E. A. Treml, M. Logan, and A. P. Negri. 2024. Larval precompetency and settlement behaviour in 25 Indo-Pacific coral species. Communications Biology 7:142.

Rapuano, H., T. Shlesinger, L. Roth, O. Bronstein, and Y. Loya. 2023. Coming of age: Annual onset of coral reproduction is determined by age rather than size. iScience 26:106533.

Raymundo, L. J., and A. P. Maypa. 2004. GETTING BIGGER FASTER: MEDIATION OF SIZE-SPECIFIC MORTALITY VIA FUSION IN JUVENILE CORAL TRANSPLANTS. Ecological Applications 14:281–295.

Ricardo, G., C. Doropoulos, R. C. Babcock, E. Buccheri, A. Khalil, and P. J. Mumby. 2025. Critical thresholds of adult patch density and spacing during coral fertilization. Nature Ecology & Evolution.

Roelfsema, C. M., E. M. Kovacs, J. C. Ortiz, D. P. Callaghan, K. Hock, M. Mongin, K. Johansen, P. J. Mumby, M. Wettle, M. Ronan, P. Lundgren, E. V. Kennedy, and S. R. Phinn. 2020. Habitat maps to enhance monitoring and management of the Great Barrier Reef. Coral Reefs 39:1039–1054.

Sato, M. 1985. Mortality and growth of juvenile coral Pocillopora damicornis (Linnaeus). Coral Reefs 4:27–33.

Sherwood, S. C., M. J. Webb, J. D. Annan, K. C. Armour, P. M. Forster, J. C. Hargreaves, G. Hegerl, S. A. Klein, K. D. Marvel, and E. J. Rohling. 2020. An assessment of Earth's climate sensitivity using multiple lines of evidence. Reviews of geophysics 58:e2019RG000678.

Speare, K. E., T. C. Adam, E. M. Winslow, H. S. Lenihan, and D. E. Burkepile. 2022. Size-dependent mortality of corals during marine heatwave erodes recovery capacity of a coral reef. Global Change Biology 28:1342–1358.

Steven, A. D. L., M. E. Baird, R. Brinkman, N. J. Car, S. J. Cox, M. Herzfeld, J. Hodge, E. Jones, E. King, N. Margvelashvili, C. Robillot, B. Robson, T. Schroeder, J. Skerratt, S. Tickell, N. Tuteja, K. Wild-Allen, and J. Yu. 2019. eReefs: An operational information system for managing the Great Barrier Reef. Journal of Operational Oceanography 12:S12–S28.

Stratford, J. E., A. O. M. Mogg, H. J. Koldewey, L. Lachs, R. Ferrari, J. Guest, and D. T. I. Bayley. 2025. Fate-tracking early coral recruits following bleaching in a remote reef ecosystem. Coral Reefs 44:1651–1667.

Suzuki, G., S. Tashiro, Y. Fujikura, I. Tanita, Y. Suhara, W. Fujiie, Y. Yonezawa, T. Kanyama, and A. Suto. 2024. Settlement success and post-settlement survival of Acropora sp. aff. tenuis spat within a small bay in Japan. Marine Ecology Progress Series 728:15–24.

Tokarska, K. B., G. C. Hegerl, A. P. Schurer, P. M. Forster, and K. Marvel. 2020. Observational constraints on the effective climate sensitivity from the historical period. Environmental Research Letters 15:034043.

Toor, M., M. Lechene, M. Becker, T. Remmers, S. Gordon, R. Ferrari Legorreta, and J. Stratford. 2025. Field photogrammetry in 4D: Digitisation and 2D metric extraction Reef Restoration and Adaption Program (EcoRRAP) Standard Operational Procedure Number 17 (No. 3 of series).

Tsounis, G., and P. J. Edmunds. 2016. The potential for self-seeding by the coral Pocillopora spp. in Moorea, French Polynesia. PeerJ 4:e2544.

Turner, S. D., V. Nagraj, M. Scholz, S. Jessa, C. Acevedo, J. Ge, A. E. Woerner, and B. Budowle. 2022. skater: an R package for SNP-based kinship analysis, testing, and evaluation. F1000Research 11:18.

Van de Walle, J., J. Garnier, T. Bonnet, and S. Jenouvrier. 2025. Toward a unified approach to modelling adaptation among demographers and evolutionary ecologists. Methods in Ecology and Evolution 1644–1657.

Van der Meer, L., L. Abad, A. Gilardi, and R. Lovelace. 2024. sfnetworks: tidy geospatial networks. R package version 0.6. 5.

Vehtari, A., A. Gelman, J. Gabry, and Y. Yao. 2021. Package 'loo.' Efficient leave-one-out cross-validation and WAIC for Bayesian models.

de Villemereuil, P., M. B. Morrissey, S. Nakagawa, and H. Schielzeth. 2018. Fixed-effect variance and the estimation of repeatabilities and heritabilities: issues and solutions. Journal of Evolutionary Biology 31:621–632.